FINAL REPORT

POSSIBLE METHODOLOGY FOR PROBABILISTIC ASSESSMENT OF BRIDGE SAFETY AGAINST COLLISIONS

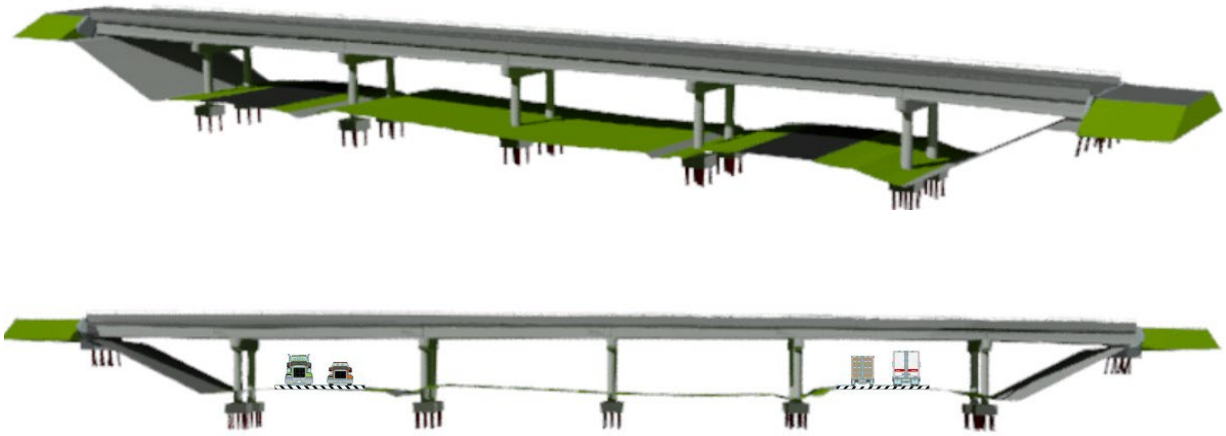

Pedro F. Silva
Pan Dong
Samer H. Hamdar
Sameh S. Badie

Department of Civil and Environmental Engineering
The George Washington University

EXECUTIVE SUMMARY

The objective of this research is to develop a possible stochastic methodology for quantifying the probability of bridge failure against heavy truck collisions. This methodology will account for the stochastic nature of the following variables:

- Individual weight and speed of heavy trucks circulating in traffic flows.
- Frequency of heavy truck collisions at a given bridge location and its direct impact on bridge safety.
- Parametric impulse loading functions associated with the intensity of collisions between heavy trucks and bridge piers/girders.
- Strain rate effects on material properties from the resulting impact loads.

A literature review outlined mechanisms that contributed to the disproportionate collapse of bridges. Review of these collapse mechanisms confirm a reduction in the resiliency and safety of code conforming bridges from either frontal pier or overhead girder collisions. Furthermore, research in the last decade have identified uncertainties involved in both estimating collisions and system response that can cause the collapse of bridges. To meet the research objective and to expand the knowledge of bridge safety against collisions, two main limitations remain to be addressed:

- Lack of modeling methodologies that jointly consider uncertainty in bridge failure modes and traffic dynamics involving speed, vehicular type, and collision distributions as a function of space and time.
- Unavailable bridge data in the National Bridge Inventory (NBI) such as number of pier elements, pier protection elements and condition of individual elements deterioration, along with data to model heavy truck collisions taking place under a bridge site. Collection of these data will feed into evaluation models for prediction and mitigation of collisions.

This report illustrates these limitations by reviewing current design practice of bridges to resist heavy truck collisions. A literature review was extended to include review of experimental and analytical research and risk analysis relating to the vulnerability of bridges against these collisions. The AASHTO LRFD Bridge Design Specifications (BDS) and the Eurocode Actions on Structures both include specific information on the design of bridge piers against heavy truck frontal collisions. Information on design forces for overhead collisions on bridge girders is only present in the Eurocode Actions on Structures. This report highlights sections of the AASHTO LRFD BDS for calculating the probability of failure of a bridge system subjected to heavy truck collisions. This report presents research findings that may interest members of the bridge design and research engineering community as well as personnel from bridge programs at the Federal, and State and local agencies. The research findings can complement the AASHTO LRFD BDS to assess the vulnerability and mitigation of bridge components and bridge systems subjected to the impact of vehicles.

ACKNOWLEDGMENTS

The original maps on page 8, pages 34 to 49, and pages 63 to 84 are the copyright property of Google® Earth™ and can be accessed from https://www.google.com/earth.

As indicated in the figures some of the original maps are the copyright property of © 2022 TomTom. The use of these TomTom maps is subject to the terms of license agreements and can be accessed from https://www.tomtom.com/en_us/thirdpartyproductterms/eula/.

TECHNICAL REPORT DOCUMENTATION PAGE

1. Report No. GW-01-2024	**2. Government Accession No.**	**3. Recipient's Catalog No.**
4. Title and Subtitle Possible Methodology for Probabilistic Assessment of Bridge Safety Against Collisions		**5. Report Date** April 2024 **6. Performing Organization Code:**
7. Author(s) Silva, P.F. (0000-0002-4562-9844), Dong, P., Hamdar, S.H., Badie, S.S., Chong, C., Chiarito, V. P.		**8. Performing Organization Report No.**
9. Performing Organization Name and Address The George Washington University 1922 F Street NW, 4th Floor, Washington, DC, 20052-0001		**10. Work Unit No.** **11. Contract or Grant No.** 693JJ321C000031
12. Sponsoring Agency Name and Address Office of Bridges and Structures Federal Highway Administration 1200 New Jersey Ave SE Washington, DC 20590		**13. Type of Report and Period** **14. Sponsoring Agency Code**
15. Supplementary Notes		

16. Abstract

This report presents a possible stochastic methodology that can be used in identifying bridges with greater probability of failure from vehicular collisions. To meet this objective, this report first outlines the design of bridges against these collisions in the United States and compares against the Eurocode design methodology. Existing experimental studies and data on heavy truck collisions with bridge systems were also reviewed and analyzed to develop safety metrics and quantify the probabilistic bridge failure.

In 2021, the National Bridge Inventory (NBI) had over 618,456 bridges and culverts registered in its U.S. bridge database, of which 13,963 bridges and culverts are in Virginia. Data shows that 93,000 bridges in the United States and 2,689 bridges in Virginia have one or more traffic lanes under the structure. Data for the Virginia bridges were collected and analyzed within a methodology for classifying bridges most vulnerable to heavy truck collisions and the resulting structural failures. Given the on-site availability of the three specified data types, 17 bridges were selected from the commonwealth of Virginia to form a test-bed study site. Finally, stochastic models were formulated for estimating the probability of bridge failure. Research findings may interest those connected to bridge programs at the Federal, State, and local agencies.

17. Key Words Stochastic Models, Bridge Collisions, Annual Frequency of Bridge Failure	**18. Distribution Statement** No restrictions. This document is available to the public through the National Technical Information Service, Springfield, VA 22161. http://www.ntis.gov		
19. Security Classif. (of this report) Unclassified	20. Security Classif. (of this page) Unclassified	21. No. of Pages 159	22. Price

Form DOT F 1700.7 (8-72) Reproduction of completed page authorized.

SI* (MODERN METRIC) CONVERSION FACTORS

APPROXIMATE CONVERSIONS TO SI UNITS

Symbol	When You Know	Multiply By	To Find	Symbol
		LENGTH		
in	inches	25.4	millimeters	mm
ft	feet	0.305	meters	m
yd	yards	0.914	meters	m
mi	miles	1.61	kilometers	km
		AREA		
in^2	square inches	645.2	square millimeters	mm^2
ft^2	square feet	0.093	square meters	m^2
yd^2	square yard	0.836	square meters	m^2
ac	acres	0.405	hectares	ha
mi^2	square miles	2.59	square kilometers	km^2
		VOLUME		
fl oz	fluid ounces	29.57	milliliters	mL
gal	gallons	3.785	liters	L
ft^3	cubic feet	0.028	cubic meters	m^3
yd^3	cubic yards	0.765	cubic meters	m^3
		NOTE: volumes greater than 1000 L shall be shown in m^3		
		MASS		
oz	ounces	28.35	grams	g
lb	pounds	0.454	kilograms	kg
T	short tons (2000 lb)	0.907	megagrams (or "metric ton")	Mg (or "t")
		TEMPERATURE (exact degrees)		
°F	Fahrenheit	5 (F-32)/9 or (F-32)/1.8	Celsius	°C
		ILLUMINATION		
fc	foot-candles	10.76	lux	lx
fl	foot-Lamberts	3.426	candela/m^2	cd/m^2
		FORCE and PRESSURE or STRESS		
lbf	poundforce	4.45	newtons	N
lbf/in^2	poundforce per square inch	6.89	kilopascals	kPa

APPROXIMATE CONVERSIONS FROM SI UNITS

Symbol	When You Know	Multiply By	To Find	Symbol
		LENGTH		
mm	millimeters	0.039	inches	in
m	meters	3.28	feet	ft
m	meters	1.09	yards	yd
km	kilometers	0.621	miles	mi
		AREA		
mm^2	square millimeters	0.0016	square inches	in^2
m^2	square meters	10.764	square feet	ft^2
m^2	square meters	1.195	square yards	yd^2
ha	hectares	2.47	acres	ac
km^2	square kilometers	0.386	square miles	mi^2
		VOLUME		
mL	milliliters	0.034	fluid ounces	fl oz
L	liters	0.264	gallons	gal
m^3	cubic meters	35.314	cubic feet	ft^3
m^3	cubic meters	1.307	cubic yards	yd^3
		MASS		
g	grams	0.035	ounces	oz
kg	kilograms	2.202	pounds	lb
Mg (or "t")	megagrams (or "metric ton")	1.103	short tons (2000 lb)	T
		TEMPERATURE (exact degrees)		
°C	Celsius	1.8C+32	Fahrenheit	°F
		ILLUMINATION		
lx	lux	0.0929	foot-candles	fc
cd/m^2	candela/m^2	0.2919	foot-Lamberts	fl
		FORCE and PRESSURE or STRESS		
N	newtons	0.225	poundforce	lbf
kPa	kilopascals	0.145	poundforce per square inch	lbf/in^2

TABLE OF CONTENTS

LIST OF FIGURES

LIST OF TABLES

LIST OF ABBREVIATIONS

AASHTO	American Association of State Highway and Transportation Officials
ADT	average daily traffic
ADTT	average daily truck traffic
AI	artificial intelligence
API	application programming interface
ASCE	American Society of Civil Engineers
AXL	axial load ratio
BAC	blood alcohol concentration
BDS	Bridge Design Specifications
BDM	Bridge Design Manual
BTS	Bureau of Transportation Statistics
Caltrans	California Department of Transportation
CFR	Code of Federal Regulations
CRSS	Crash Report Sampling System
CT	collision traffic (vehicular collision)
DIF	dynamic increase factor
DOT	Department of Transportation
EN	Eurocode
ESF	equivalent static force
FARS	Fatality Analysis Reporting System
FHWA	Federal Highway Administration
FMCSA	Federal Motor Carrier Safety Administration
GDP	gross domestic product
GVWR	gross vehicle weight rating
HRC	horizontal roadside clearance
HSIS	Highway Safety Info System
LRFD	Load and Resistance Factor Design
LTBP	Long-Term Bridge Performance
MAIS	Maximum Abbreviated Injury Scale
MASH	Manual for Assessing Safety Hardware
MCMIS	Motor Carrier Management Information System
MCS	Monte Carlo simulation
NASS GES	National Automobile Sampling System General Estimates System
NBI	National Bridge Inventory
NCHRP	National Cooperative Highways Research Program
NHS	National Highway System
NHTSA	National Highway Traffic Safety Administration
NSC	National Safety Council
NYC	New York City
PDF	probability distribution function
Peak-DF	peak dynamic force
VDOT	Virginia Department of Transportation
VMT	vehicle miles traveled
WIM	weigh-in-motion

LIST OF NOTATIONS

This section provides a list of notations used in this report.

f_c'	concrete compressive design strength
ρ_s	reinforcing steel reinforcement ratio
Φ_T	truck-related collision involvement rate
$\widehat{N}_i$	number of truck-related collisions occurring on link i
$\widetilde{N_i}$	random variable nominal/design value
$\widehat{V}_i$	volume of trucks traversing link i
$\dot{\varepsilon_c}$	concrete average strain rate
$\dot{\varepsilon_s}$	reinforcing steel average strain rate
E_s	reinforcing steel modulus
$E(X)$	expected value
L_i	length of link i in miles
N_i	site-specific adjustment factor
Q_{CT}	worst-case collision force (kip)
R_{CPC}	critical pier component capacity
T_{eff}	performance limit State effective period
$\widehat{V}$	annual truck volume traversing under the bridge
W_b	denotes the width of bridge in feet
f_{yd}	dynamic reinforcing Steel yield strength
$\hat{\lambda}$	random variable bias factor
ξ_{eff}	performance limit state effective damping ratio
ω_{eff}	performance limit state effective frequency
b	pier width or diameter
f_y	reinforcing steel yield strength
r	Spearman's rank correlation coefficient
t_E	time gap from first impact to peak response
W	truck weight
AF_{BC}	annual frequency of bridge collapse
HVE_i	heavy vehicle base encroachment frequency
KE	truck kinetic energy
$P(Q_{CT} > R_{CPC}\|C)$	the probability of the worst-case collision force, Q_{CT}, exceeding the critical pier component capacity R_{CPC}
$P(C\|HVE_i)$	probability of a collision given a heavy vehicle encroachment
$Pr(Q\|C)$	probability of bridge failure due to a specific truck-related collision
V	truck velocity
X	number of truck-related collisions
Ω	random variable coefficient of variation
β	distribution beta factor
λ	expected annual number of truck-related collisions
μ	distribution mean value

CHAPTER 1 - INTRODUCTION

1.1. BACKGROUND

Bridge failures' causes can include two general categories of natural and non-natural hazards. Human-made hazards, such as vehicular collisions, can be classified as intentional. Data extracted from the National Highway Traffic Safety Administration (NHTSA) database (2021), shows that since 2013, vehicular collisions involving bridges in the United States have occurred at an average annual rate of approximately 15,000 (Dunne and Thorkildsen 2020). Therefore, assessing the vulnerability of bridges, improving the resiliency of bridges, developing effective mitigation strategies, and continuously improving design approaches against heavy truck collisions comprise some of the critical components to support protection and ensuring safety of the U.S. transportation network system. This report outlines a review of published work across research, design, construction, and field performance.

A literature review focused mainly on design and construction of bridges against heavy truck collisions and the severity of traffic collisions. Many bridges around the United States have collapsed or suffered significant damage mainly due to hydraulic events, which include flooding and scour events (Wardhana and Hadipriono 2003; Cook et al. 2015). The next two main causes of bridge failures were attributed to vehicular collisions or vehicles crossing a bridge in violation of posted weight limits (Wardhana and Hadipriono 2003; Lee et al. 2013, Cook et al. 2015). Studies by Cao et al. (2020) have demonstrated that vehicular collisions produce large shear forces and bending moment demands on bridge elements. If not properly accounted for in design, these actions can cause damage to bridge piers or other structural elements and eventually catastrophic bridge failure.

This report presents a direct comparison between design practice according to the American Association of State Highway and Transportation Officials (AASHTO) Load and Resistance Factor (LRFD) Bridge Design Specifications (BDS) and the Eurocode Actions on Structures. The AASHTO LRFD BDS, 8th Edition[1] provides three scenarios that engineers may consider when designing bridges piers against vehicular collisions (AASHTO 2017) (23 CFR 625.4(d)(1)(v)). In the first scenario, engineers may consider options for redirecting or absorbing the collision load by placing a structurally independent barrier between the traffic and the bridge pier. In the second scenario, engineers design the bridge pier resistance to withstand the collision force. Finally, Owners may approve exemptions for these two scenarios based on the annual frequency of heavy truck collisions (AASHTO 2017) (23 CFR 625.4(d)(1)(v)). Eurocode 1: Actions on Structures – Part 1-7[2]: General Actions – Accidental Actions (EN 1991-1-7, 2006) only considers the first two options: designing the bridge pier resistance to withstand the collision force and providing protective measures to reduce the probability of damage to the structure. The EN 1991-1-7[2] provides equivalent static design forces for overhead collisions on

[1] AASHTO LRFD Bridge Design Specifications, 8th Edition (2017) is incorporated by reference at 23 CFR 625.4(d)(1)(v).

[2] Eurocode 1: Actions on Structures is not a Federal requirement.

bridge girders. Unlike EN 1991-1-7[2], the AASHTO LRFD BDS, 8th Edition[1] does not include specific design criteria for collisions on bridge girders (AASHTO 2017) (23 CFR 625.4(d)(1)(v)).

This report presents the results of data mining on the Federal Highway Administration (FHWA) Long-Term Bridge Performance (LTBP) InfoBridge™, National Bridge Inventory (NBI), and NHTSA databases. According to the 2019 Traffic Safety Facts Annual Report distributed by NHTSA (2021), there were 6,756,000 police-reported crashes in the United States in 2019. This marks the second highest in the 2010s. Among these crashes, less than 1 percent (33,244 collisions) were fatal, 28 percent (1,916,000) resulted in a non-fatal injury, and 71 percent (4,806,000) were classified as property-damage only with no reported injuries. The 2019 report by NHTSA presents the following national fatality and injury rates due to motor vehicle crashes:

- 1.11 fatalities and 84 injured persons per 100 million vehicle miles traveled.
- 12.06 fatalities and 916 injured persons per 100,000 registered vehicles
- 15.78 fatalities and 1,198 injured persons per 100,000 licensed drivers.

Since 1966, crash, fatality and injury rates consistently decreased until the 2010s. During the 2010s, these rates either decreased slightly or remained nearly constant regardless the countermeasures deployed.

Few studies have evaluated the impact of collisions on roadway infrastructure and the resulting losses. As the number of motor vehicles increases, the frequency of vehicle collisions with bridge systems increases (Chen et al. 2021). Hong et al. (2007) reviewed the work by Mallet et al. (2005) and concluded truck travel will also continue to increase in the future with an expected increase of 60 to 70 percent between 2001 and 2020. The work of Mallet et al. (2005) was based on the Highway Statistics series reported in FHWA (2006). Within this same period, Hong et al. (2007) concluded that international shipments are expected to increase by 85 percent. As truck travel and accidents continue to increase the need to protect more bridge structures against heavy traffic collisions will continue to increase.

The literature review also covered other critical bridge safety elements. References covering experimental and analytical research and risk analysis were reviewed to identify data for evaluating the vulnerability of bridge piers and girders against heavy truck collisions. NHTSA's Traffic Safety Facts Annual Reports indicate that between 2011 and 2020, the annual average of vehicular collisions with bridges was approximately 15,000 (Dunne and Thorkildsen 2020). As shown in Table 1-1 and Table 1-2, this specific type of collision accounts for 0.2 percent to 0.3 percent of total collisions, and 0.5 percent to 0.7 percent of fatal collisions in the United States. This illustrates the severity of vehicle collisions with bridges. Research indicates that heavy traffic collisions have resulted in the disproportionate collapse or reduction in the resiliency and safety of bridges.

In 2021, the National Bridge Inventory listed 618,456 bridges and culverts in the United States (NBI 2021), of which 13,963 are in Virginia. Data mining of the LTBP InfoBridge™ (FHWA-LTBP 2021) shows that 2,689 bridges in Virginia have traffic lanes underneath. Data presented

in this report was collected and analyzed using a methodology for classifying bridges most vulnerable to heavy truck collisions and the resulting structural failures for these 2,689 Virginia bridges. From this classification of vulnerable bridges in Virginia, 17 bridges were selected to form a test-bed study site.

Table 1-1. Number of collisions with bridges from 2010 to 2014.

Crash Severity [1,2]	2010	2011	2012	2013	2014
Fatal	216 (0.7)	219 (0.7)	204 (0.7)	193 (0.6)	201 (0.7)
Injury	2,937 (0.2)	4,902 (0.3)	4,493 (0.3)	3,675 (0.2)	3,580 (0.2)
Property damage	11,437 (0.3)	11,454 (0.3)	10,935 (0.3)	14,181 (0.3)	10,159 (0.2)
Total	14,590 (0.3)	16,575 (0.3)	15,632 (0.3)	18,049 (0.3)	13,940 (0.2)

[1] Numbers in parentheses denote the percentages of collisions with bridges as a subset of the total number of collisions at the corresponding severity levels.
[2] Data was extracted from NHTSA *Traffic Safety Facts Annual Report Tables from 2010 to 2014* (NHTSA 2021).

Table 1-2. Number of collisions with bridges from 2015 to 2019.

Crash Severity [1, 2]	2015	2016	2017	2018	2019
Fatal	196 (0.6)	231 (0.7)	193 (0.6)	181 (0.5)	187 (0.6)
Injury	3,443 (0.2)	5,079 (0.2)	4,940 (0.3)	2,413 (0.1)	3,050 (0.2)
Property damage	12,698 (0.3)	9,796 (0.2)	9,576 (0.2)	10,154 (0.2)	7,908 (0.2)
Total	16,337 (0.3)	15,106 (0.2)	14,709 (0.2)	12,748 (0.2)	11,144 (0.2)

[1] Numbers in parentheses denote the percentages of collisions with bridges as a subset of the total number of collisions at the corresponding severity levels.
[2] Data was extracted from NHTSA *Traffic Safety Facts Annual Report Tables from 2015 to 2019* (NHTSA 2021).

The test-bed study site for the 17 bridges focuses on developing and validating stochastic models for estimating the probability of bridge failure due to collisions involving trucks. To develop the stochastic models, the following parameters need further evaluation:

- Modeling methodologies that can jointly consider uncertainty in structural failure modes, traffic dynamics involving speed and vehicular type, and collision distributions as a function of space and time.

- Comprehensive bridge data including number of pier elements, pier protection elements and condition of individual elements deterioration. Other relevant data to this project are heavy truck collision data near a bridge site. Combination of these data types will feed into predictive models for prediction and mitigation of collisions.

1.2. RESEARCH OBJECTIVES

The objective of this research is to develop a stochastic methodology for quantifying the probabilistic failure of a bridge subjected to heavy truck collisions. This methodology will include the need to further evaluate the stochastic nature of vehicular collisions and its ensuing impact on the safety of bridges. Although extensive research had been conducted investigating the dynamic interaction when heavy trucks collide with bridge elements, there still is the need to account for the stochastic nature of the following variables:

- Individual weight and speed of heavy trucks circulating in traffic flows.
- Frequency of heavy truck collisions at a given bridge location and its direct impact on bridge performance.
- Parametric impulse loading functions associated with the intensity of the collisions between heavy trucks and bridge piers or girders.
- Strain rate effects on material properties from the resulting impact loads.

The work presented in this report leverages knowledge from both the transportation engineering and structural engineering domains. This knowledge includes the stochastic nature of truck weight and speed distributions, and the expected frequency of truck-related collisions. To evaluate the stochastic nature of these variables, data was obtained from available traffic detector and collision data. Traffic and collision data were used jointly to develop Poisson-based probability functions for evaluating the probability of bridge failure. The suggested methodology can calculate the probability of failure over a one-year period, or during any selected period. The established Poisson-based probability functions will support estimating the likelihood of failure using stochastic models to assess the vulnerability and mitigation of bridge elements and systems subjected to the impact of heavy vehicles. This work may supplement the AASHTO LRFD BDS concerning bridge systems subjected to heavy truck collisions.

The stochastic methodology will help identify strategic solutions for prioritizing the replacement or significant rehabilitation of higher risk bridges from vehicular collisions. This work can also supplement the AASHTO LRFD BDS and potentially increase the safety of bridges according to the following target objectives:

- Evaluate the resiliency of bridge girders against overhead collisions. Research by Harries et al. (2012) highlights examples of impacted bridge girders resulting from overhead truck collisions. Harries et al. (2012) also reports on the severity of damage and the repair methods employed in recovering bridges to full service.
- Evaluate the resiliency of bridges from frontal collisions on bridge piers. Research by Wehbe et al (2017) highlights many examples of previous truck collisions with bridge piers and the ensuing bridge damage. Wehbe et al. (2017) and Cao et al. (2020) also report on disproportionate collapse of bridges resulting from vehicular collisions.

- Evaluate the resiliency of bridges against fires resulting from collisions. A typical example of bridge failure resulting from fires was the collapse of the two spans of the MacArthur Maze interchange in California (AASHTO 2008; Wright et al. 2013). This bridge suffered extensive damage after a fire erupted following a tanker truck overturn on the bridge.

- Evaluate potential cascading effects and disproportionate collapse resulting from heavy truck collisions. Develop simplified analytical tools for assessing the vulnerability and improving the resiliency and safety of bridges.

- Estimate the likelihood of a collision involving flammable fuel or cargo that detonates or combusts and then results in a fire event with high consequences.

- Develop a stochastic methodology for quantifying the probability of failure of bridges subjected to heavy truck collisions as a means for assessing the vulnerability of bridges using analytical and/or experimental methods.

CHAPTER 2 - LITERATURE REVIEW

This chapter presents a literature of current design practice of bridges to resist heavy truck collisions. A literature review was extended to include review of experimental and analytical research and risk analysis relating to the vulnerability of bridges against these collisions. The AASHTO LRFD BDS and Eurocode 1: Actions on Structures[2] (EN 1991) both include specific information on the design of bridge piers against heavy truck frontal collisions. Information on design forces for overhead collisions on bridge girders is only present in the Eurocode Actions on Structures[2]. This chapter highlights sections of the AASHTO LRFD BDS for calculating the probability of failure of a bridge system subjected to heavy truck collisions.

2.1. STATE OF DESIGN PRACTICE – VEHICLE COLLISIONS ON BRIDGE PIERS

2.1.1. AASHTO LRFD Bridge Design Specifications

In the AASHTO LRFD BDS, 8th Edition[1] (AASHTO 2017) (23 CFR 625.4(d)(1)(v)) and the AASHTO LRFD BDS, 9th Edition[3] (AASHTO 2020), Extreme Event II load combinations are considered events with a long return period. When designing for these load combinations the following applies (AASHTO Section C3.4.1) (AASHTO 2017) (23 CFR 625.4(d)(1)(v))):

- The recurrence period of extreme events is larger than the design life of the bridge.
- The joint probability with other extreme events is extremely low and are specified to be applied separately.

AASHTO LRFD BDS, 8th Edition[1] Article 3.6.5.1 states that bridge owners can assess site conditions and determine if an evaluation of abutments and bridge piers located within 30.0 ft from the edge of the roadway for vehicular collisions should be included (AASHTO 2017) (23 CFR 625.4(d)(1)(v)). An example of an edge of roadside clearance is presented in Figure 2-1. In general, abutment walls are backfilled with soil. Therefore, State Departments of Transportation (State DOTs) in the United States do not include an evaluation of abutments for vehicular collisions (Caltrans BDM, 2014; WSDOT, 2020). For example, the Texas DOT specifies that abutment and retaining walls do not need an evaluation for collision forces because the soil behind the abutment and retaining walls acts to dissipate the collision force (Texas BDM, 2020).

AASHTO LRFD BDS, 8th Edition[1] Article 3.6.5.1 states three alternatives to consider when investigating vehicular collisions including exemption for protection based on site conditions; protection of bridge piers and abutments with roadside barriers; and structural resistance of piers and abutments (AASHTO 2017) (23 CFR 625.4(d)(1)(v)).

[3] Use of AASHTO LRFD Bridge Design Specifications, 9th Edition (2020) is not a Federal requirement.

Note: horizontal roadside clearance (HRC). Original Photo: © 2022 Google® (see Acknowledgments page)

Figure 2-1. Photo. Example of a horizontal roadside clearance.

2.1.1.1. Exemption for protection based on site conditions

AASHTO LRFD BDS, 8th Edition[1], Article 3.6.5.1 indicates that Owners may approve exemptions for pier protection based on the annual frequency of heavy truck collisions (AASHTO 2017) (23 CFR 625.4(d)(1)(v)). When making this judgment, AASHTO LRFD BDS, 8th Edition[1], Article C3.6.5.1, suggests that owners seek input from highway or safety engineers and structural engineers. AASHTO LRFD BDS, 8th Edition[1], Article C3.6.5.1 specifies that site conditions may qualify for exemptions provided the annual frequency of impact from heavy vehicles, AF_{HBP}, for critical or essential bridges and typical bridges is less than 0.0001 or 0.001, respectively. Equation C3.6.5.1-1 in combination with Table C3.6.5.1-1 are used in calculating AF_{HBP} (AASHTO 2017) (23 CFR 625.4(d)(1)(v)):

$$AF_{HBP} = 2 \times ADTT \times P_{HBP} \times 365 \quad \textbf{(2-1)}$$

In this equation AF_{BHP} is the annual frequency of impact from heavy vehicles, $ADTT$ is the number of trucks per day in one direction and is evaluated using AASHTO Table C3.6.1.4.2-1, and P_{HBP} is the annual probability for a bridge pier to be hit by a heavy vehicle. In AASHTO Table C3.6.1.4.2-1 the average daily traffic (ADT), including all vehicles (i.e., cars and trucks) is obtained from available data and can be used in estimating the $ADTT$.

AASHTO (2017) (23 CFR 625.4(d)(1)(v)) provides information for estimating P_{HBP} based on Equation (2-2) (AASHTO 2017).

$P_{HBP} = 3.457 \text{ x } 10^{-9}$	Undivided roadways in tangent and horizontally curved sections	
$P_{HBP} = 1.090 \text{ x } 10^{-9}$	Divided roadways in tangent sections	**(2-2)**
$P_{HBP} = 2.184 \text{ x } 10^{-9}$	Divided roadways in horizontally curved sections	

In the AASHTO LRFD BDS, 9th Edition3, Article C3.6.5.1 site conditions also qualify for exemption from protection. However, the exemption is based on the annual frequency of bridge collapse from vehicle collisions, AF_{BC}. For critical or essential bridges and typical bridges the limits for AF_{BC} are less than 0.0001 and 0.001, respectively. Equation C3.6.5.1-1 is used in evaluating AF_{BC} (AASHTO 2020):

$$AF_{BC} = \sum_{i=1}^{m} [N_i \times HVE_i \times P(C|HVE_i) \times P(Q_{CT} > R_{CPC}|C)] \quad \textbf{(2-3)}$$

In this equation AF_{BC} is the expected annual frequency of bridge collapse, and other variables are as follows:

- When protective barriers are placed alongside the roadway, each approach direction is identified from *i* to *m* for a pier component at risk of an impact from approaching traffic.
- N_i is the site-specific variable from AASHTO LRFD BDS, 9th Edition3 Table C3.6.5.1-1.
- HVE_i is the heavy vehicle base encroachment frequency from AASHTO LRFD BDS, 9th Edition3 Table C3.6.5.1-2.
- $P(C|HVE_i)$ is the probability of a collision given a heavy vehicle encroachment from AASHTO LRFD BDS, 9th Edition3 Table C3.6.5.1-3.
- $P(Q_{CT} > R_{CPC}|C)$ is the probability of the worst-case collision force, Q_{CT}, exceeding the critical pier component capacity, $R_{CPC}|C$, obtained from AASHTO LRFD BDS, 9th Edition3 Table C3.6.5.1-4.

2.1.1.2. Protection of bridge piers and abutments with roadside barriers

AASHTO LRFD BDS, 8th Edition[1] Article 3.6.5.1 provides a design choice for resisting vehicular collisions by redirecting or absorbing the collision load with a protective system. In this case, protection consists of one of the following (AASHTO 2017) (23 CFR 625.4(d)(1)(v)):

- An embankment.
- A structurally independent, crashworthy ground-mounted 54-inch-high barrier, located within 10 feet from the structural component being protected.
- A 42-inch-high barrier located at more than 10 feet from the component being protected.

AASHTO LRFD BDS, 8th Edition[1] Article 3.6.5.1 states that any barriers used in the protection of bridge piers or other elements shall be structurally and geometrically capable of surviving a Test Level 5 (i.e., MASH TL-5) crash. Article 3.6.5.2 of the AASHTO LRFD BDS, 8th Edition[1] requires that the use of the provisions in Section 13 to select, design, and construct traffic railings. AASHTO LRFD BDS, 8th Edition[1], Article 13.7.2, Table 13.7.2-1, provides bridge railing test levels and crash test criteria (AASHTO 2017) (23 CFR 625.4(d)(1)(v)).

For crash tests on barriers, AASHTO LRFD BDS, 8th Edition[1] specifies six different test levels (AASHTO 2017) (23 CFR 625.4(d)(1)(v)). These six test levels are in AASHTO's Manual for Assessing Safety Hardware and based on NCHRP Report 350, "Recommended Procedures for the Safety Performance Evaluation of Highway Features" (Ross et al., 1993). The crash test criteria for the various bridge railing test levels and vehicular collision forces are presented in AASHTO LRFD BDS, 8th Edition[1] Article 13.7.2 (AASHTO 2017) (23 CFR 625.4(d)(1)(v)):

1. Test Level One (TL-1) — Generally acceptable for work zones with low posted speeds and very low volume, low speed local streets.
2. Test Level Two (TL-2) — Generally acceptable for work zones and most local and collector roads with favorable site conditions as well as where a small number of heavy vehicles is expected and posted speeds are reduced.
3. Test Level Three (TL-3) — Generally acceptable for a wide range of high-speed arterial highways with very low mixtures of heavy vehicles and with favorable site conditions.
4. Test Level Four (TL-4) — Generally acceptable for most applications on high-speed highways, freeways, expressways, and interstate highways with a mixture of trucks and heavy vehicles.
5. Test Level Five (TL-5) — Generally acceptable for the same applications as TL-4 and where large trucks make up a significant portion of the average daily traffic or when unfavorable site conditions justify a higher level of rail resistance.

6. Test Level Six (TL-6) — Generally acceptable for applications where tanker-type trucks or similar high center-of-gravity vehicles are anticipated, particularly along with unfavorable site conditions.

Since January 1, 2011, all new roadside hardware must be tested using MASH crash test criteria to receive Federal-aid eligibility (FHWA 2015). In January 2016, the FHWA and AASHTO entered a Joint Implementation Agreement for the AASHTO Manual for Assessing Safety Hardware (MASH 2016), documented in FHWA memorandum (FHWA 2016). The agreement was executed to fully implement MASH for the crash testing of safety hardware devices for use on the National Highway System (NHS). MASH replaced NCHRP Report 350. All new testing is done following MASH evaluation techniques. However, hardware accepted under NCHRP Report 350 is appropriate for replacement and new installation without retesting (FHWA 2015).

2.1.1.3. Structural resistance of piers and abutments

Research by Buth et al. (2010) reviewed heavy truck collisions with bridge piers and reports on a collision that has occurred on the Chatfield Road Bridge, I-45, Navarro County, Texas in 2007. This crash event illustrates the pier column adequately resisted the collision. Buth et al. (2010) highlights the heavy truck collision that occurred in Tancahua Street Bridge over I-37, Corpus Christi, Texas. For this crash event the bridge pier column capacity did not adequately resist the collision forces. However, the collision did not result in disproportionate collapse (Dusenberry 2022) and overall structural failure of the bridge.

Providing structural resistance in piers has been incorporated in design of bridges by bridge owner. For example, when considering the design of bridge piers to resist vehicular collisions, Section 4.3.14A of the New Hampshire DOT (2016) Bridge Design Manual states that providing structural resistance in the pier may lead to more economical design options. An embankment or barrier as the protection mechanism may not provide an economical design option.

AASHTO LRFD BDS, 8th Edition[1], Article 3.6.5.1, describes design requirements to resist vehicular collisions based on structural resistance to bridge elements (AASHTO 2017) (23 CFR 625.4(d)(1)(v)). AASHTO LRFD BDS, 8th Edition[1] Article 3.6.5.1 specifies designing bridge piers or abutments to resist an equivalent static force of 600 kips, applied in a horizontal plane at 5.0 ft above the ground level, and acting in a direction of 0 degrees to 15 degrees with the edge of the pavement in a horizontal plane (AASHTO 2017) (23 CFR 625.4(d)(1)(v)). A schematic for the application of this equivalent static force is depicted in Figure 2-2.

The equivalent static force was assessed by Buth et al. (2010, 2011) using full-scale 80-kip tractor-trailers travelling at speeds of 50 mph crash tests against rigid columns. Buth et al. (2010, 2011) further refined and validated results from these full-scale crash test simulations. This was done by conducting high-fidelity finite element simulations on bridge pier elements with varying diameters and reinforcement details and simulating these 80-kip tractor-trailers striking the piers. More recently, Zhou et al. (2017) also confirmed that the AASHTO equivalent static force of 600.0 kips can be mathematically represented by an impact weight of 80.0 kips travelling at 50.0 mph.

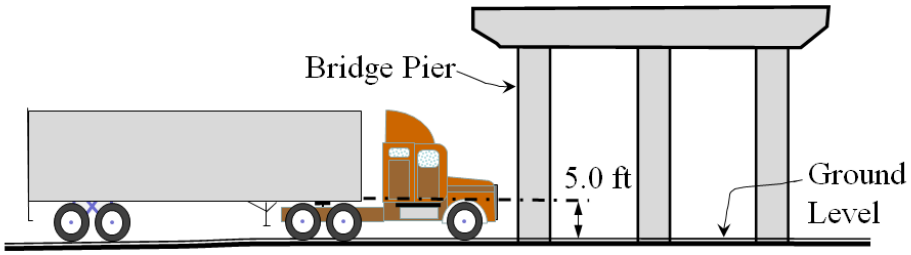

A. Truck collision above the ground level

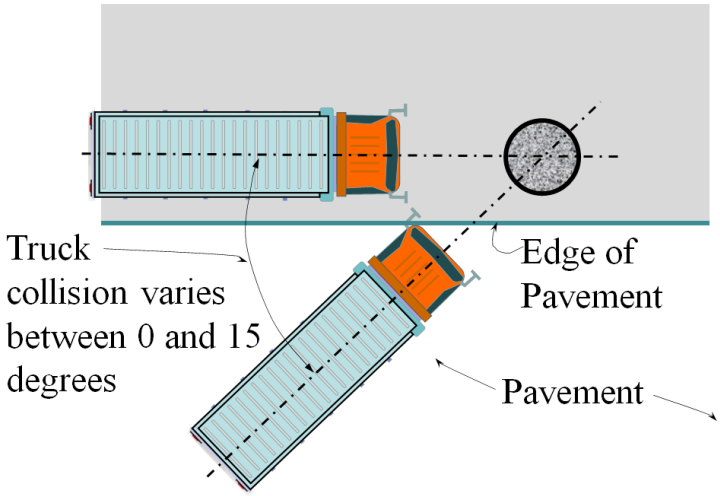

B. Truck collision in the horizontal plane

Figure 2-2. Illustration. Position of equivalent static force.

AASHTO LRFD BDS, 9th Edition[3], Article 3.6.5.1 provides the same forces used when designing bridge piers or abutments to provide structural resistance. However, Article C3.6.5.1 additionally notes that two peak load impact cases, including the engine striking the pier at a height of 2.0 ft and the back of the cab or the front of the trailer striking the pier at a height of 5.0 ft, should be analyzed for critical shear and moment in the pier component and its connections to the foundation or pier cap (AASHTO 2020).

There is another difference between the two editions under the same article. AASHTO LRFD BDS, 8th Edition[1], Article 3.6.5.1 (AASHTO 2017) does not specify a criterion to design substructure components against vehicular collisions. AASHTO LRFD BDS, 9th Edition[3], Article 3.6.5.1 does identify the following four substructure components considered to have adequate structural capacity to resist bridge collapse from vehicular impacts (AASHTO 2020):

- Substructure components, such as an abutment wall, that are backed by soil, will absorb the vehicular collision without serious consequences of affecting the integrity of the bridge superstructure.

- Reinforced concrete (RC) pier columns that are at least 3.0 ft in diameter or 3.0 ft thick and have a concrete cross-sectional area of 30.0 ft² or larger have adequate capacity in resisting vehicular collisions. This area should be satisfied in all horizontal plane from the top of the pier foundation to a height of at least 5.0 ft above the grade. Studies by Buth et al. (2010, 2011) support the same conclusion.

- Bridge piers that can be evaluated by the designer and can validate that sufficient resistance for the superstructure exists against collapse. Evaluating the collapse can include removing any column in the pier system while the superstructure is subjected to the load combination of the full dead load with a load factor of 1.1 and a live load in the permanent travel lanes with a load factor of 1.0.

- Pier walls and multi-column piers that have struts between columns and were designed and detailed as MASH TL-5 longitudinal traffic barriers according to Section 13 (AASHTO 2020).

In either the AASHTO LRFD BDS, 8th Edition[1], Article 3.6.5.1 or the AASHTO LRFD BDS, 9th Edition[3], Article 3.6.5.1 the design force of 600 kip is based on an equivalent static force. Cao et al. (2020) evaluated these equivalent static forces based on the dynamic interaction that occurs between the colliding truck and the bridge pier at the time of bumper, engine, and trailer impact. Based on their work, Agrawal et al. (2018) proposed a general shape of the pulse function for frontal collisions which accounts for the dynamic interaction that occurs between the colliding vehicle and the bridge structure and recognizes the effects of vehicle characteristics on the equivalent static force.

2.1.2. Eurocode 1 - Actions on Structures Impact on Substructure

This section outlines the design of structures against accidental collisions according to the Eurocode[2] (EN 1991-1-7). This section provides a direct comparison with design guidelines of the AASHTO LRFD BDS, 8th Edition[1] (AASHTO 2017). EN 1991-1-7[2] is used by multiple European countries when assessing accidental actions on buildings and bridges including impact forces from vehicles, rail traffic, ships, helicopters, explosions, etc. According to EN 1991-1-7[2], determining design actions due to vehicular collisions may use two approaches: (1) dynamic analysis or, (2) equivalent static force analysis (EN 1991-1-7, 2006). These two approaches are discussed next.

2.1.2.1. Dynamic analysis

Sections 1.5.5 and 4.2 of the EN 1991-1-7[2] (2006), outlines how to determine actions due to impact by a dynamic analysis or represented by an equivalent static force. Section 4.2 of the EN 1991-1-7[2] (2006) outlines that when considering dynamic analysis, the designer should include the following variables:

- Impact velocity of the collision vehicle.

- Mass distribution of the bridge pier.

- Deformation behavior and damping characteristics of both the collision vehicle and the structure.

- Other factors such as the angle of impact, the construction of the impacting object and movement of the impacting object after collision may also be relevant.

- The capacity of the impacting body to absorb all the energy. In general, this assumption results in conservative design.

- The material properties of the impacting object and the structure. To determine these properties and where relevant, upper or lower characteristic values should be used. This should include strain rate effects on the material properties of the resisting structure.

2.1.2.2. Equivalent static force for accidental actions caused by road vehicles

Section 4.3 of the EN 1991-1-7[2] (2006) outlines the design of bridge piers against vehicle collisions based on the equivalent static force shown in Table 2-1. This table is from EN 1991-1-7[2], Table 4.1 - Indicative equivalent static design forces due to vehicular impact on members supporting structures over or adjacent to roadways (EN 1991-1-7, 2006). The design procedure resembles the design approach in AASHTO LRFD BDS, 8th Edition[1]. For comparison, the AASHTO LRFD BDS, 8th Edition[1] (AASHTO 2017) specifies piers to resist an equivalent static force of 600.0 kips and the Eurocode[2] stipulates that the equivalent static force is 224.8 kips or 1000.0 N (EN 1991-1-7, 2006).

Table 2-1. Eurocode equivalent static forces for bridge piers.

Note: Table data from EN 1991-1-7[2] Table 4.1 - Indicative equivalent static design forces due to vehicular impact on members supporting structures over or adjacent to roadways. (EN 1991-1-7, 2006)

Category of traffic	Static Force (kip) X-direction [a)]	Static Force (kip) Y-direction [b)]
Motorways and country national and main roads	224.8	112.4
Country roads in rural area	168.6	84.3
Roads in urban area	112.4	56.2
Courtyards and parking garages with access to Cars	11.2	5.6
Courtyards and parking garages with access to Lorries [c)]	33.7	16.9

Note: X-direction is the normal travel direction, Y-direction is perpendicular to the normal travel direction. The term "lorries" refers to vehicles with maximum gross weight greater than 3.5 tonnes.

For structural design, an equivalent static force may represent the impact that produces the same structural response. This simplified model may be used for verifying static equilibrium and adequate strength capacities, and for determining acceptable deformations of the impacted structure. For structures designed to absorb impact energy by elastic-plastic deformations of members (i.e., soft impact), the equivalent static loads may be determined by accounting for both plastic strength and the deformation capacity of such members. In structures for which the energy is mainly dissipated by the impacting body (i.e., hard impact), the equivalent static forces may be determined from Sections 4.3 to 4.7 of the EN 1991-1-7[2] (2006).

The collision force is applied at 1.64 ft to 4.92 ft above the level of the carriageway. The suggested application area for the collision force is 9.8 inches (height) by 60.0 inches (width) or the member width, whichever is smaller.

2.2. STATE OF DESIGN PRACTICE –VEHICLE COLLISIONS ON BRIDGE GIRDERS

2.2.1. AASHTO Policy on Geometric Design of Highways and Streets

AASHTO LRFD BDS, 8th Edition[1] (AASHTO 2017) (23 CFR 625.4(d)(1)(v)) does not address vehicular collisions in the design of superstructures or bridge girders. The AASHTO GDHS-7, A Policy on Geometric Design of Highways and Streets, known as the Green Book provides minimum vertical clearances for bridge clearances at under crossings (AASHTO Green Book 2018) (23 CFR 625.4(d)(1)(i)). Vertical clearance in most highway bridges in the United States is 16 feet. This clearance corresponds to the largest legal vehicle travelling without a permit.

Low vertical clearance bridges over roadways are vulnerable to overheight vehicle collision damage. Collisions can cause driver and passenger injuries and fatalities, cause property loss to the vehicle and bridge owners, and jeopardize the bridge structural capacity. Many State DOTs measure vertical clearances using a single, minimum value under each bridge. However, accurate measurements of bridge vertical clearance can vary, especially when height differentials occur either from site topography, a superelevated bridge deck, or changes in pavement thickness along the bridge footprint. Maghiar et al. (2017) reports on the specific systems/products currently used by State DOTs to measure vertical clearances and prevent collisions with roadway bridge girders.

States DOTs in the United States report regularly that bridge girders incur damage from overheight vehicular collisions. A study by Wipf et al. 2004 as reported that in Iowa on average 5 to 6 significant overheight vehicular collisions occur on bridge superstructures each year. Minor impact damage is repaired each year, much of which local entities and DOTs may not report. Wipf et al. (2004) notes that on average 50 percent of recorded impacts originate from vehicles travelling with the necessary permit or were hauling loads that did not require a permit. Furthermore, a large portion of vehicular collisions at bridges were caused by construction equipment being hauled on flatbed trailers (Wipf et al. 2004).

Research by Harries et al. (2012) highlights examples of typical impacted bridge girders resulting from overhead truck collisions. A wide range of variables can affect the type and magnitude of damage that is commonly associated with an overhead strike or impact by an overheight vehicle with bridge girders.

2.2.2. Eurocode 1 – Actions on Structures Impact on Superstructures

As outlined in Table 2-2, the Eurocode[2] (EN 1991-1-7, 2006) specifies design forces from vehicular collisions at under crossings. As stated in the Eurocode[2] (EN 1991-1-7, 2006), in addition to the required bridge vertical clearances, impact forces should also be considered in the design of overhead structures. These design forces can be either determined by a dynamic analysis or by the equivalent static forces indicated in Table 2-2. The Eurocode[2] suggests ranges of adequate clearance, excluding future resurfacing of the roadway under the bridge, is from 16.4 ft to 19.7 ft. Waiving the suggested range of adequate clearance is possible provided there exists suitable protection measures to avoid impact on girders.

Table 2-2. Eurocode vehicular collision equivalent static forces for design of bridge girders.

Note: Table data provided in Eurocode[2] Table 4.2 – Indicative equivalent static design forces due to vehicular impact on bridge girders. (EN 1991-1-7, 2006)

Category of traffic	Static Force (kip) X-direction [a)]
Motorways and country national and main roads	112.4
Country roads in rural area	84.3
Roads in urban area	56.2
Courtyards and parking garages	16.9

a) X-direction is the normal travel direction

2.3. STUDIES ON HEAVY TRUCK COLLISIONS WITH BRIDGES

2.3.1. Bridge Failure Rates Due to Vehicular Collisions in the United States

Wardhana and Hadipriono (2003) conducted a study on bridge failure data from the New York Department of Transportation (NYDOT) bridge database. This study summarized data between 1989 and 2000. Wardhana and Hadipriono (2003) concluded that the natural and human hazards, noted in Figure 2-3A, were the main factors in causing failure or distress to the 503 bridges identified in their study. In this figure, the natural hazards leading to distress and/or collapse of bridges include flood, scour, earthquake, and others such as landslides, debris flow, hurricane, typhoon, and wind. Human hazards noted in the figure include vehicular collisions, fire, and vehicle overloading. In addition, "Other" causes stated in the figure include faulty design, lack of inspection and maintenance, and material defects. Figure 2-3A indicates that nearly 15 percent of total bridge failures resulted from vehicle collisions and fires. The frequency of collisions are almost six times that of earthquakes.

Figure 2-3A is inconclusive in determining the different factors that have led to bridge failures from exposure to fire events. Other reports have identified severe cascading effects that can result from tanker truck collisions on bridge piers (Garlock et al. 2012; Wright et al. 2013; Peris-Sayol et al. 2016). These researchers and others acknowledge deficiencies presented in the Wardhana and Hadipriono (2003) dataset may not contain data of many other bridge failures. Their conclusion highlights the need to conduct a similar study from 2000 to the present.

Other researchers have used the data from Wardhana and Hadipriono (2003) and compiled bridge failure rates as a function of bridge types and are outlined in Figure 2-3B (Deng et al. 2016). These researchers summarize that nearly 33 percent of the total bridge failures include steel girder systems and nearly 60 percent of other frequent failures consist of either cast-in-place or pre-stressed concrete girder and concrete slab bridge systems.

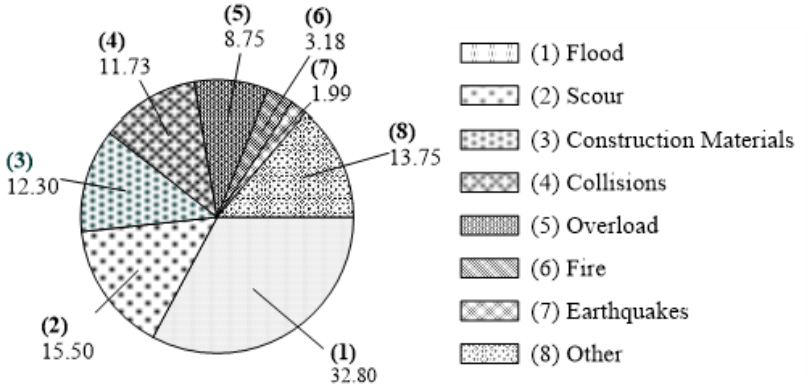

A. Factors causing failure of bridges.

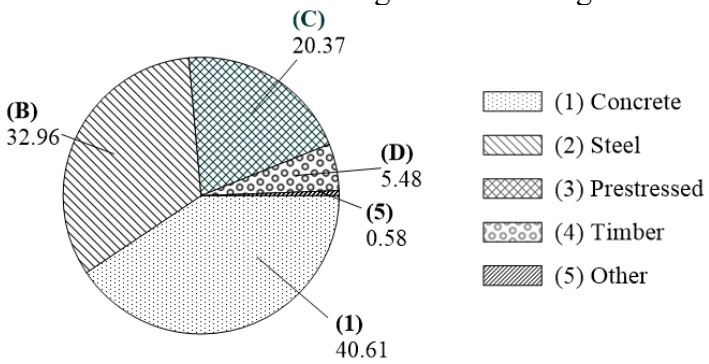

B. Bridge failures grouped by NBI Element *Main Span Material*.

Note: Original data source Wardhana and Hadipriono (2003)

Figure 2-3. Charts. Bridge failures between 1989 and 2000.

Data from the 2020 LTBP InfoBridge™ database (FHWA- LTBP 2021) shows a total of 620,377 bridges with the following distributions grouped by *Main Span Material*:

- 25.40 percent (157,557) are steel bridges, which consists of either continuous or simply supported systems.
- 21.12 percent (131,053) are concrete bridges, which consists of either continuous or simply supported systems.
- 27.22 percent (168,844) are prestressed concrete bridges, which consists of either continuous or simply supported systems.
- 23.13 percent (143,478) are either concrete or steel culverts.
- 3.13 percent (19,445) bridges with other main span materials such as timber/wood, aluminum, or masonry.

2.3.2. Studies conducted in United States

2.3.2.1. Collisions with Bridge Piers

Buth et al. (2010, 2011) investigated the validity of the 400.0 kip design load that was stipulated in the AASHTO LRFD BDS, 8th Edition[1] (AASHTO 2017) (23 CFR 625.4(d)(1)(v)) for collision with abutments and piers located within 30.0 feet of the edge of the roadway, or within 50 feet of the centerline of a railway track. In the first phase of the investigation (Buth et al. 2010), nineteen crashes involving trucks colliding with bridge columns were investigated and reported. Several crashes resulted in partial or complete structural failure to the pier and bridge. Failure mechanisms consisted of two shear failure planes – one extending upward from the applied load at approximately 45 degrees and the other extending downward at approximately 45 degrees.

Finite element analyses of trucks colliding with bridge pier columns were performed. Parameters investigated included type of truck (65-kip single-unit truck, and 80-kip tractor-trailer), type of cargo (deformable and rigid), impact speed (40, 50, and 60 mph), and diameter of pier columns (24, 36, and 48 inches). The investigation found that collision forces generated based on an assumed rigid bridge pier column analysis are directly dependent on the structural body of the vehicle and properties of the payload. The investigation was conducted based on a collision of a truck traveling at a usual highway speed.

Finite element results from simulations show that the dynamic forces averaged over a 50-millisecond time interval ranged from 480 to 580 kips for the engine block impact and 1,000 to 2,490 kips for the ballast impact. These results show that for typical trucks with soft, deformable payloads, forces generated are less than forces generated by more rigid payloads. As expected, higher impact speeds generate higher impact forces. Conversely, the pier diameter influenced the magnitude of force less.

The shear resistance was estimated for the 24-, 36-, and 48-inch diameter columns. Research results show that although large bending moments were transferred to the pier column, shear was the critical failure mechanism in the pier column.

Buth et al. (2010) developed a crash risk analysis methodology for estimating the risk of a heavy vehicle leaving the roadway and colliding with a bridge pier column. The crash risk analysis showed that undivided highway segments have higher risk for bridge pier collisions than for divided highway segments. Likewise, horizontally curved roadway sections have higher risk of bridge pier collisions than tangent roadway sections. The methodology focused on segment-based analysis coupled with the theoretical principles of a Bernoulli random variable distribution. The methodology by Buth et al. (2010) focused on estimating the risk of a heavy vehicle hitting a bridge pier column using the conditional probability of a heavy vehicle leaving the roadway and then hitting a bridge pier column. Based on this methodology, Buth et al. (2010) provided formulas to determine the annual frequency of a collision with a bridge pier column in a given roadway segment.

In the second phase of the investigation, Buth et al. (2011) conducted two full-scale crash tests and used the results to verify and validate numerical simulations. Based on the results obtained

from the full-scale crash tests and the corresponding numerical simulations, the following suggestions for the AASHTO LRFD BDS were made (Buth et al. 2011): (1) change height of force from 4 ft above ground to 5 ft above ground (see Figure 2-4), and (2) change direction of force from "any direction" to "zero to 15 degrees with the edge of pavement", and (3) change equivalent static force from 400 kips to 600 kips (see Figure 2-5).

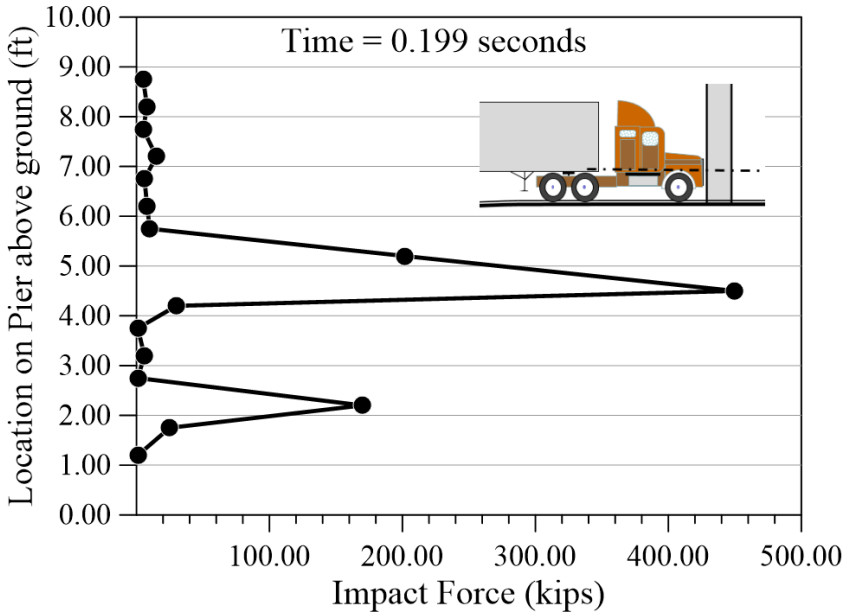

Note: Original Data Source Buth et al. (2010)

Figure 2-4. Graph. Full-scale crash test numerical simulation.

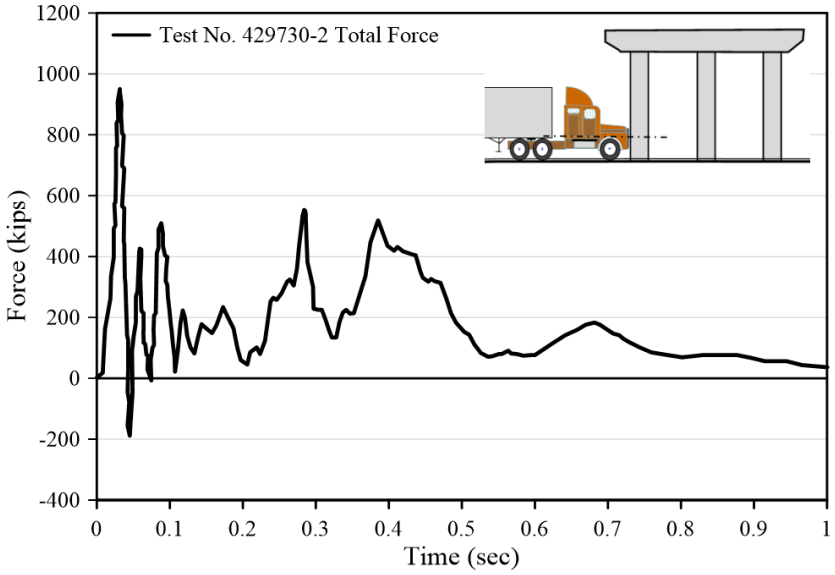

Note: Original Data Source Buth et al. (2010)

Figure 2-5. Graph. Full-scale crash test force-time relationship.

2.3.2.2. Collisions from Overheight Vehicles

Many research studies conducted by highway authorities in the United States showed that most collisions on bridge girders are related to overheight vehicles and inadequate vertical clearance of bridges. The following listed items summarizes some of these studies.

- A study by Hilton (1973) investigated crashes involving highway bridges in Virginia. "Inadequate vertical clearance" was listed as a key contributing factor in 4 percent and 6 percent of the total bridges cited by police officers and highway engineers, respectively.

- Shanafelt and Horn (1980) reported on damage evaluation and repair methods for prestressed concrete bridge members. As part of the study, a survey was conducted to collect information on prestressed concrete bridge damage around the country. In response to the survey, state bridge engineers listed overheight loads as the leading cause of damage (81 percent) to prestressed concrete bridges (other causes were overweight loads, fire, salt, and water freezing).

- Shanafelt and Horn (1984) released a similar report on damage to steel bridge members. Their research identified that 815 steel bridges were damaged over a 5-year period and 94 percent of these bridges suffered damage due to overheight vehicles. From these bridges, 767 were repaired, and the other 48 bridges were either replaced or were never repaired. However, their report did not include the exact number of bridges that had been replaced.

- Harik et al. (1990) analyzed U.S. bridge failures over a 38-year period (1951-1988). Each collapse was classified by its cause. Of the 79 bridge failures considered in the study, 11 were caused by truck collisions (14 percent). However, the classification did not differentiate between superstructure and substructure collisions, so the percentage of failures caused by overheight vehicles may be less.

- Some U.S. states have recorded a rise in the frequency of bridges hit by overheight loads. For example, in 1988 the Michigan Department of Transportation reported a yearly increase of 36 percent in overheight collisions (MRC, 1988). Many overheight collisions in the state of Michigan have been attributed to the fact that although the legal height of trucks allowed on Michigan highways is only 13 feet and 6 inches, permits are often issued for overheight loads of up to 15 feet (MRC, 1988).

- Hanchey and Exley (1990) reported that the Mississippi State Highway Department installed overheight warning systems on some rural bridges after an increase in bridge damage by overheight logging trucks.

- In a study conducted by the Texas Department of Transportation, Feldman et al. (1992) reported a rise in the occurrence of overheight impact damage to prestressed concrete bridges.

- Fu (2001) reported that in April 2000, the Maryland Department of Transportation installed overheight detector systems at the West Friendship Weigh Station on I-70 and at

the exits to five terminals at the Port of Baltimore. The data revealed that from May to July 2001, 20 overheight vehicles were detected at the West Friendship Weigh Station. Only five trucks had overheight permits (25 percent). From the period of January 2001 to June 2001, 1,584 overheight vehicles were detected at exits of the Port of Baltimore, where only 227 had overheight permits (14 percent).

Analysis of the Maryland Automated Accident Reporting System conducted by Fu (2001), showed that from 1995 to 2000, police reported 116 overheight collisions in Maryland. Over this period, the annual number of crashes increased by 81 percent. These crashes involved 19 injuries and one fatality. The analysis also revealed that overheight crashes in Baltimore City involved 36 percent box trailers, 31 percent flatbed trailers, 16 percent dump trucks, and 17 percent other. Overheight crashes as function of the vehicle type are reported in Figure 2-6. At least 16 percent of these crashes occurred at railroad bridges.

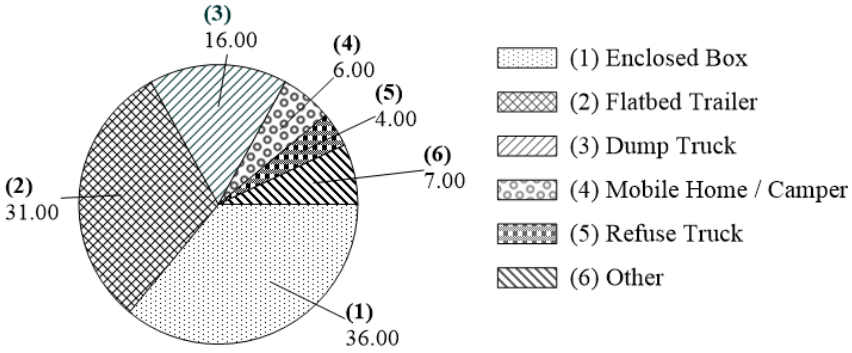

Note: Original Data Source Fu (2001)

Figure 2-6. Chart. Vehicle types involved in overheight crashes.

Fu (2001) analyzed bridge inspection reports from the state of Maryland, and concluded the following:

- 1,496 bridges cross roadways or have overhead members are susceptible to impact by overheight vehicles. Figure 2-7 and Figure 2-8 highlight the range of bridges vertical clearance analyzed in this study.

- 309 of these bridges (20 percent) have sustained some damage from overheight vehicles, where these damaged bridges are clustered around metropolitan areas.

- 34 percent of the damaged bridges cross over interstate highways.

- Of the 309 bridges struck, 47 percent had scrapes only, 34 percent had minor damage, and 19 percent required repairs.

- Of the 1496 impact-susceptible bridges, 79 percent have no observable damage, 10 percent received scrapes only, 7 percent sustained minor damage, and 4 percent have required repairs.

- Figure 2-7 shows that 51, 63 and 87 bridges were struck, respectively, at the vertical clearance of 14.5, 16.0 and 16.5 feet.

- Figure 2-8 shows that nearly 33 percent, 27 percent, and 17 percent, of bridges in the state of Maryland with clearances of 16.0 ft, 16.5 ft, and 17.0 ft, respectively, have been struck by overheight vehicles.

Number of bridges struck in Maryland by overheight vehicles are summarized in Figure 2-7. The dashed line in this figure outlines the percentage of bridges struck at the specified vertical clearance. Figure 2-7 shows more bridge overhead collisions between vertical clearances of 14.5 to 16.5 feet. The percentage of collisions decreases significantly for vertical clearances over 16.5 feet. The severity of bridge damage resulting from overheight crashes is shown in Figure 2-8. This figure indicates that at the vertical clearance of 16.5 feet nearly 17 bridges had major damage requiring major repair. This is about 20 percent of the total number of bridges that were struck at the vertical clearance of 16.5 ft. At this vertical clearance, 27 bridges or 31 percent of bridges that were hit required minor repairs. Likewise, Figure 2-8 indicates that 43 bridges had scrapes only with minor superficial damage and did not require repairs. This is about 49 percent of the total number of bridges that were struck at the vertical clearance of 16.5 ft.

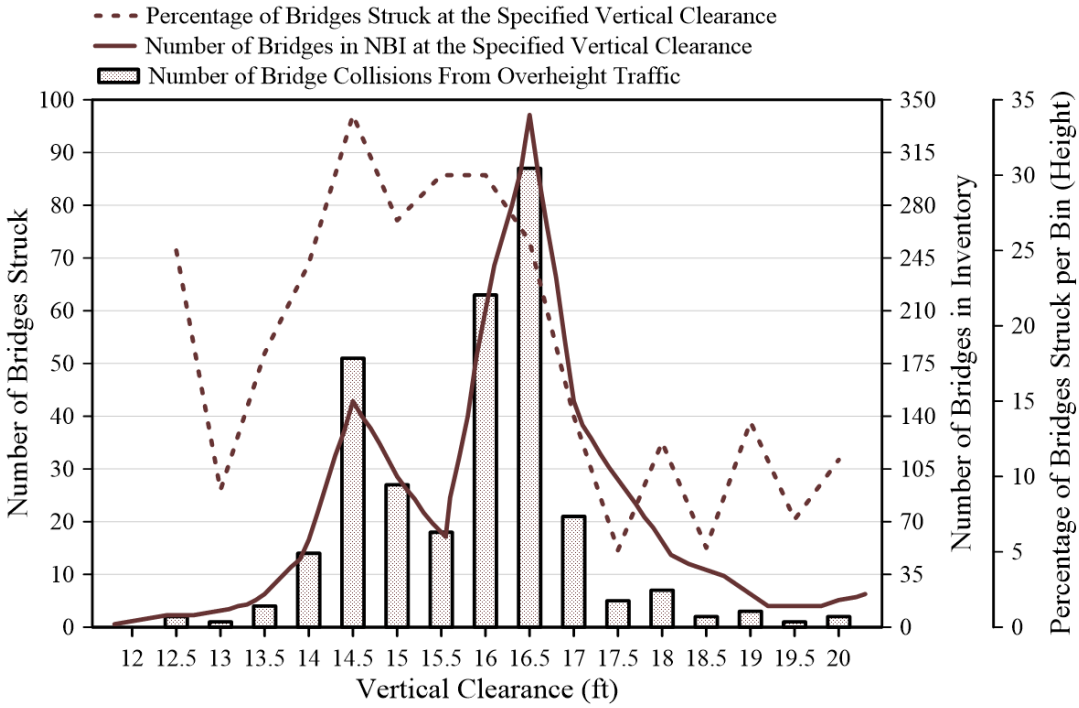

Note: Original Data Source Fu (2001)

Figure 2-7. Graph. Vertical clearance relation to bridge collisions.

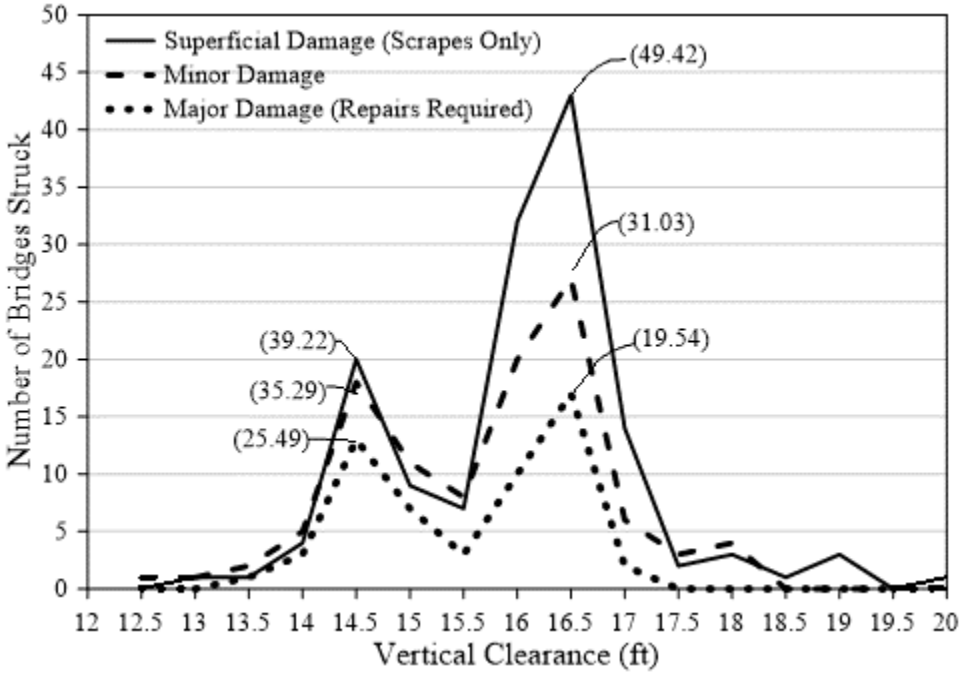

Note: The numbers in parenthesis indicate percentage of bridges classified by severity of damage at the bins of 14.5 ft and 16.5 ft. Original Data Source Fu (2001)

Figure 2-8. Graph. Vertical clearance classified by severity of damage.

Fu (2001) conducted a national survey with response from 29 States. The results showed:

- Most states report bridge clearances ranging from 16.0 ft to 17.0 ft on interstates and freeways. For bridges in other arterials, collectors and local routes states report clearances ranging from 14.0 ft to 17.0 ft.

- Some states post the actual vertical clearance on warning signs, while other states under-report the clearance by up to six inches.

- Most states allow vehicle heights up to 13.5 ft without a permit; a few states allow up to 14.5 ft.

- Over half of the states reported using automatic overheight detection systems. Twelve states provided statistics on overheight collisions. The average annual number of collisions increased by 1.3 percent per year from 1995 to 1999. During the same period, the annual number of truck accidents in these States decreased by 1.7 percent per year.

- Most States were not able to provide data on casualties or damage.

- Eighteen states or 62 percent of the states surveyed, responded that overheight collisions was a significant problem. The remaining states surveyed, or 11 states (38 percent), did not consider overheight collisions a problem.

- Seven states have proposed increasing the vertical clearance of existing overpasses to reduce the frequency of overheight collisions.

In the study by Fu (2001) concluded that increasing penalties for overheight violations would probably not significantly reduce overheight collisions. Instead, Fu (2001) suggested the following countermeasures to reduce overheight crashes:

- Automated overheight detection devices are effective in locations where authorities are present to take corrective action.
- Increasing vertical clearances whenever possible should reduce the incidence of overheight collisions.
- Add questions on overheight vehicles/loads to the Commercial Driver License (CDL) exam.
- New emerging technologies, including intelligent infrastructure and intelligent vehicles, can be employed to avert overheight collisions and reduce their effects.
- The combined crash and bridge database can be used to monitor changes in the frequency of overheight collisions and identify possible candidates for overheight warning systems or clearance improvements.

2.3.3. Overheight collision study conducted outside of the United States

Berton et al. (2020) carried a statistical analysis of vehicle-bridge collisions (VBC) that occurred in Quebec between 2000 and 2016. In their studies, Berton et al. (2020) analyzed a total of 2,344 overheight collisions. The analysis considered many factors such as vehicle's body type, bridge dimensions, prescribed speed limit, road configuration, road surface condition and lighting. The statistical analysis of the collected data showed that:

- As shown in Figure 2-9, most of the reported VBCs occurred on plate web-girder bridges.
- Most of the reported VBCs involved cars and light trucks and occurred on numbered roads where the posted speed limit equal to or less than 31.0 mph (see Figure 2-10).
- Approximately half of VBCs occurred on the Canadian highway system.
- VBCs do not correlate directly to a specific road configuration, surface, or lighting conditions.
- Bridges that were more affected by VBCs were those with lower vertical clearances, total bridge length greater than 131.0 ft, or bridges carrying less than 50,000 vehicles per day (see Figure 2-11). However, larger truck traffic flow did not directly correlate to an increased risk of a VBC occurrence (see Figure 2-12).

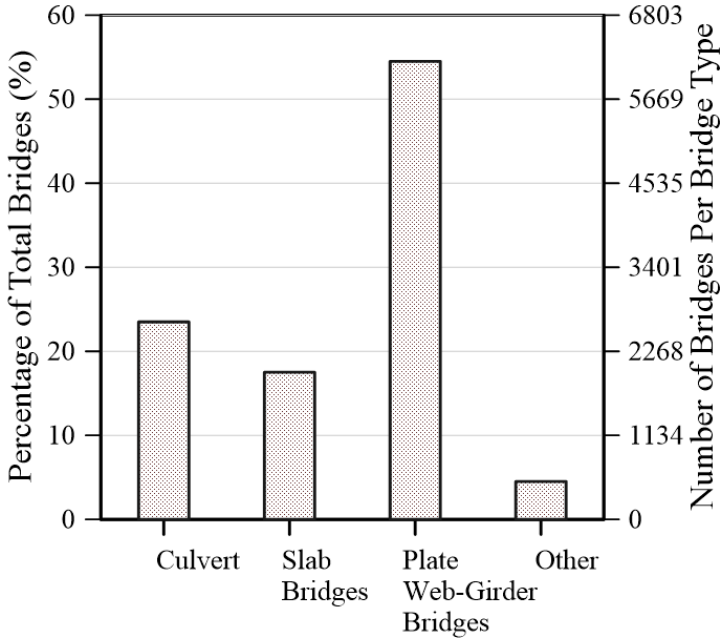

A. Number of bridges in Quebec, Canada.

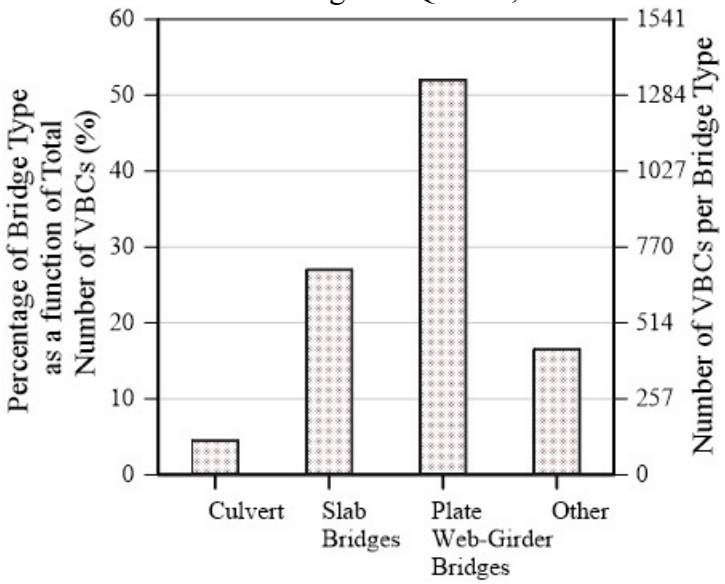

B. Number of VBCs in Quebec, Canada.

Note: Original Data Source Berton et al. (2020)

Figure 2-9. Charts. Overheight collisions per bridge type.

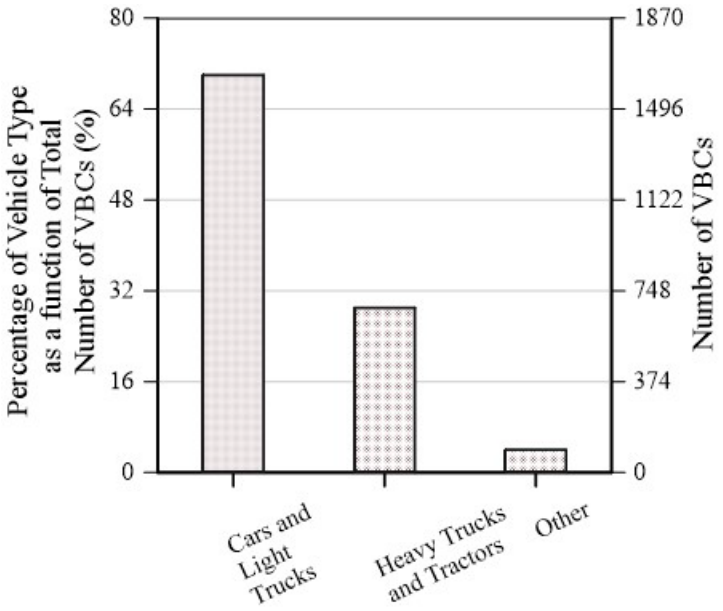

A. Vehicle Type.

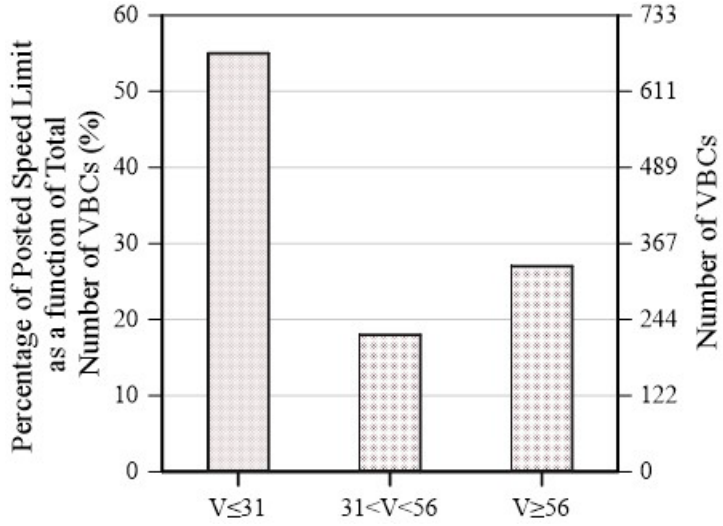

B. Posted Speed Limit, V (mph).

Note: Original Data Source Berton et al. (2020)

Figure 2-10. Charts. VBCs based on vehicle type and speed limit.

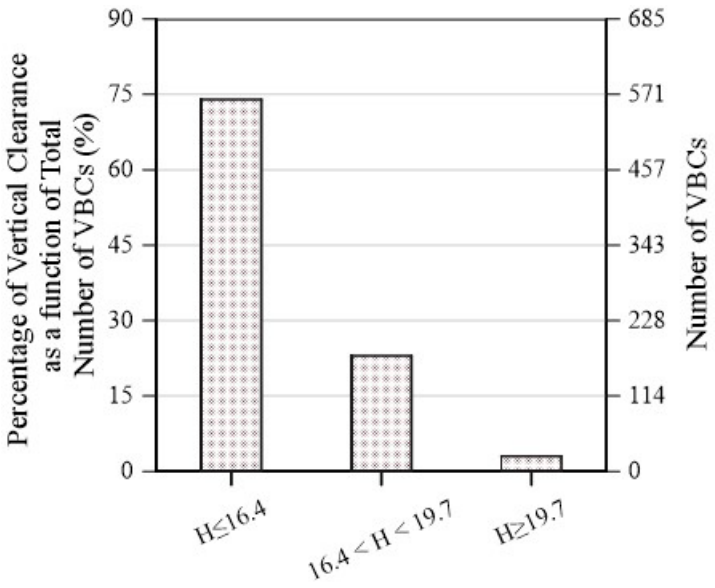

A. Vertical Clearance, H (ft).

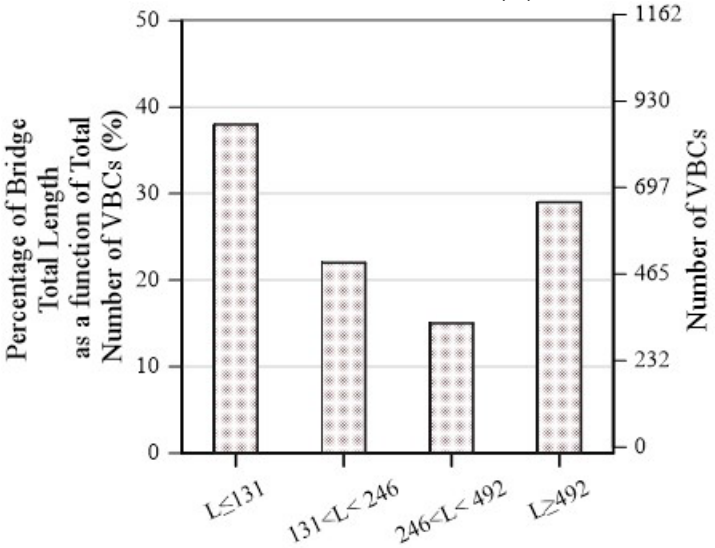

B. Bridge Total Length, L (ft).

Note: Original Data Source Berton et al. (2020)

Figure 2-11. Charts. VBCs based on vertical clearance and bridge total length.

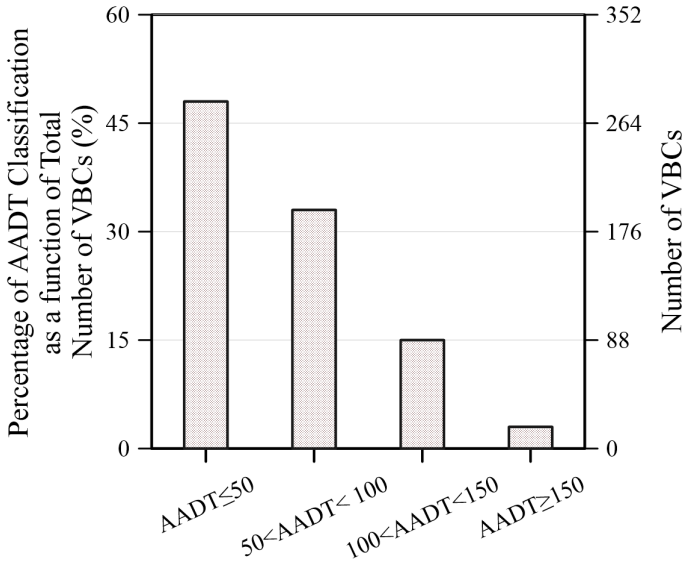

A. AADT (x1000).

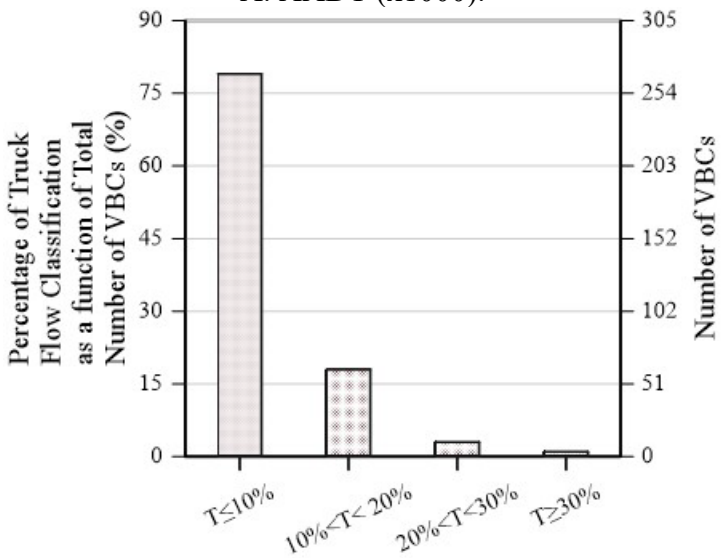

B. Truck Flow (percent).

Note: Original Data Source Berton et al. (2020)

Figure 2-12. Charts. VBCs based on ADTT and truck flow.

2.4. DATA REPOSITORIES AND STATISTICS ON BRIDGES AND COLLISIONS

The following sections outline statistical analyses performed on data queried from different U.S. databases associated with traffic collisions, mobility, and transportation roadway infrastructure. The statistics highlight the added value of these U.S. databases in understanding the problem of bridge exposure to failure due to heavy vehicle collisions.

2.4.1. National Bridge Inventory (NBI)

The FHWA National Bridge Inventory (NBI) database contains detailed information on more than 600,000 highway bridges and large culverts in the United States (NBI 2021). Researchers and engineers typically use this database to conduct diverse data mining protocols necessary for bridge assessment studies using the LTBP InfoBridge™ portal (FHWA- LTBP 2021). The LTBP InfoBridge™ portal is an online platform used for querying data available from the FHWA NBI. LTBP InfoBridge™ provides users with easy access to collect bridge data for in-depth data analyses. The in-depth analyses may develop a better understanding of bridge performance.

2.4.2. Bureau of Transportation Statistics (BTS)

The U.S. Department of Transportation's Bureau of Transportation Statistics (BTS 2023) was extensively used in this research as the preeminent source of statistics on the following data: number of trucks by weight, transportation crashes by mode, large heavy truck involvement in fatal crashes, average daily trucks carrying flammable fuels, and among many others the average daily weight of trucks (BTS 2021). Data from NBI along with the AADT data was used by Button and Reilly (2020) to estimate the release and fire incident rates for trucks in transit carrying dangerous goods. The AADT data is mainly used to consider the uncertainty associated with traffic variations in different locations. However, the temporal resolution in such variations is limited given the aggregation level in the average annual daily traffic data. The focus is mostly associated with the spatial variation of AADT per roadway location and the traffic levels on different roadway segments.

2.4.3. Highway Safety Information System (HSIS)

The FHWA Highway Safety Information System (HSIS) includes the NASS GES (National Automobile Sampling System General Estimates System) dataset and the FARS (Fatality Analysis Reporting System) dataset. Additional local state collision databases also provide data to study collision formation.

Accordingly, the HSIS database was used in linking existing infrastructure and safety data libraries with traffic detector, socio-demographic, and weather data repositories. Such linkage is possible given that all collisions are coded in these libraries with specific time of event and geographic locations.

2.4.4. General Crash Statistics

The National Highway Traffic Safety Administration (NHTSA) reported 33,244 fatal motor vehicle crashes in the United States in 2019 in which 36,096 deaths occurred (NHTSA 2021). This amounts to 11.0 deaths per 100,000 people and 1.11 deaths per 100 million miles traveled.

Statistics from FHWA reveal that vehicle miles traveled (VMT) in 2020 decreased by 359 billion over previous years, or about a 11.0 percent decrease (FHWA 2021). While Americans drove

less in 2020 due to the COVID pandemic, NHTSA's statistics (NHTSA 2022) show that 38,824 people died in motor vehicle traffic crashes. Compared to the 36,096 fatalities reported in 2019, this represents an increase of about 7.6 percent and the largest number of fatalities since 2007.

The fatality rate for 2020 was 1.34 fatalities per 100 million VMT, up from 1.11 fatalities per 100 million VMT in 2019. NHTSA's research (NHTSA 2021) suggests that throughout the national public health emergency and associated lockdowns, driving patterns and behaviors changed significantly, including more risky behavior such as speeding, failing to wear seat belts, and driving under the influence of drugs or alcohol.

Traffic data indicates that average speeds increased throughout the year, and examples of extreme speeds became more common, while the evidence also shows that fewer people involved in crashes used their seat belts. In the first three months of 2021, NHTSA estimates (NHTSA 2021, NHTSA 2022) that 8,730 people died in motor vehicle traffic crashes, a 10.5 percent increase from the 7,900 fatalities the agency projected for the first quarter of 2020.

These increases in fatalities come even as driving declined. Statistics from the Federal Highway Administration show that vehicle miles traveled (VMT) in the first three months of 2021 decreased by 2.1 percent over the previous months of 2020 (FHWA 2021). This decrease corresponds to nearly 14.9 billion miles compared to their respective projections in 2020 (NHTSA 2021b). The fatality rates for the first quarter of 2021 increased to 1.26 fatalities per 100 million VMT, up from the projected rate of 1.12 fatalities per 100 million VMT at the same time in 2020 (NHTSA 2022).

2.4.5. Truck Collisions with Bridges

Lee et al. (2013) demonstrated that vehicle collisions was the third cause of bridge failures after flood and scour in the United States between 1980 and 2012. Similarly, Cook, et al. (2015) reported that nearly 19 percent of bridge collapses between 1987 and 2011 (25 years) in New York were caused by vehicular collisions. The safety risks and costs imposed on society by truck-involved crashes shows the need to better understand the contributing factors and develop effective countermeasures to prevent or reduce the consequences of these crashes.

There is a wealth of literature associated with structural modeling of truck collisions with bridge, bridge failure risk and design standards. Collisions of vehicles with bridges have been studied using experimental, analytical, or computational simulations. In studying vehicle collisions with bridges, Deng and Cai (2010) and Wang et al. (2016) developed numerical models in their simulations for the HS-20 design truck in the AASHTO (2020) specifications.

Many simulation studies on truck to pier collisions were conducted using a Ford F800 truck model developed by the FHWA at the National Crash Analysis Center. In these studies, computational models simulated trucks crashing into models of single column, multi-column bents, or an entire bridge. The simulation results are typically used to either assess the demands associated with the collision or to evaluate the capacity of the columns to resist the impact demands. However, the 20,000 lb F800 truck used in this study is lighter than heavy trucks (tractor–semitrailers, 80.0-kip weight).

During a collision with a bridge pier, key elements of the colliding heavy truck will deliver different force intensities at different times. The bumper, engine block, and trailer cargo can deliver especially high forces to the pier because of their structural nature (bumper) or mass (in the case of the engine or trailer cargo). The bumper, engine, and trailer are not located at the same elevation, and therefore, representing their effect by a single load at a given height is an approximation. Moreover, the applied load is dynamic and depends on the truck weight, characteristics, and approach speed. These variables make the modeling and analysis of heavy truck crash impact on bridges complex.

Heng et al. (2021) and Hosseinzadeh et al. (2021) provided a list of literature that covers truck related crash data analysis and severity. Past studies have focused on specific types of crashes (e.g., rollover or rear end) or on specific injury severity levels (e.g., fatal crashes). There are limited studies that present comprehensive analysis of the severity of large-truck collisions with bridge pier elements. Some studies evaluated heavy vehicle (tractor-semitrailer) impacts on single piers under controlled experiments (Agrawal et al. 2018). However, there is a lack of information in the literature that can be used to quantify the stochasticity and the variations associated with the truck, bridge, and surrounding roadway characteristics that will impact the outcome of the heavy truck collisions on or near a bridge in terms of their frequency and severity.

This section underscores the need for using different data repositories and modeling techniques to account for the uncertainty associated with large-truck crashes near bridges. Understanding these events and their impact on bridge failures will be valuable in transportation policy, improvement of carrier operation, and incident-cost reduction.

2.5. STRUCTURAL RESPONSE UNDER IMPACT LOADS

2.5.1. Dynamic Impact Forces

AASHTO LRFD BDS, 8th Edition[1] Article 3.6.5.1 specifies that abutments and bridge piers located within 30.0 ft from the edge of the roadway are to be investigated for vehicular collisions (AASHTO 2017) (23 CFR 625.4(d)(1)(v)). AASHTO LRFD BDS, 8th Edition[1], Article 3.6.5.1, requires bridge piers to be designed using an equivalent static force of 600 kips when vehicular collisions are addressed by structural resistance, (AASHTO 2017) (23 CFR 625.4(d)(1)(v)). This force is applied at 5.0 feet above the ground level and is assumed to act from zero to 15 degrees. AASHTO LRFD BDS, 9th Edition3 states the same information (AASHTO 2020).

Researchers have performed high fidelity finite-element (FE) simulations of truck impact in bridge columns and have concluded that these suggestions will need further refinements (Agrawal et al. 2018). Figure 2-13 depicts parametric impulse loading functions proposed by Cao et al. (2020) for calculating the equivalent static force resulting from frontal collisions. These parametric impulse loading account for the dynamic interaction that occurs between the colliding truck and the bridge pier at the time of bumper, engine, and trailer impact. Numerical values for each of the time segments and dynamic forces are calculated as a function of the truck weight (W in tons) and velocity (V in mph), and the bridge pier (b in inches) width using Equations (2-4) to (2-14) (Agrawal et al. 2018). The parametric impulse loading functions

depicted in Figure 2-13 and calculated using Equations (2-4) to (2-14) are outlined in Agrawal et al. (2018).

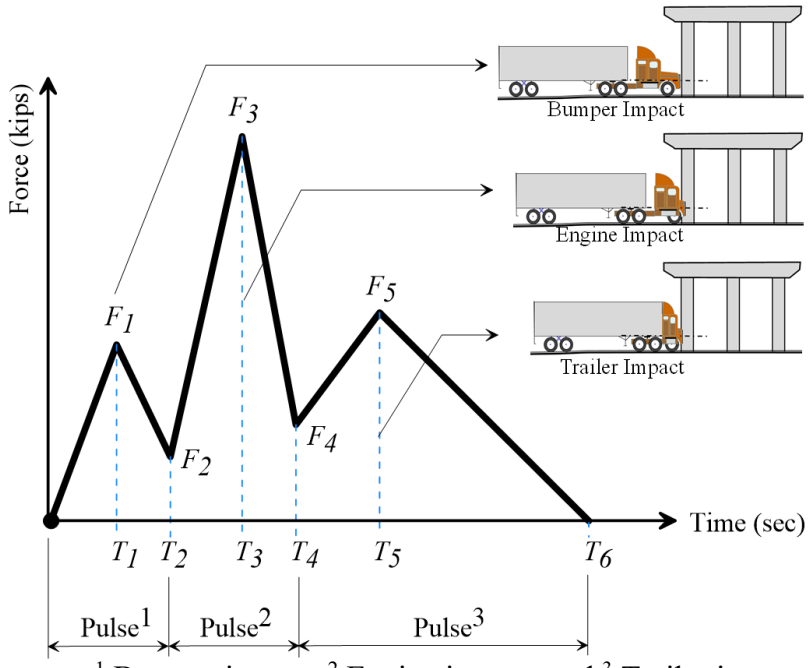

[1] Bumper impact, [2] Engine impact, and [3] Trailer impact.

Note: Original Chart Source Cao et al. (2020)

Figure 2-13. Chart. Parametric impulse loading functions for frontal collisions.

$$F_1 = 109\,V^{0.52}\left(\frac{b}{36}\right)^{0.33}\ (kips) \quad \textbf{(2-4)}$$

$$F_2 = 52\,V^{0.51}\left(\frac{b}{36}\right)^{-0.84}\ (kips) \quad \textbf{(2-5)}$$

$$F_3 = 30\,V^{0.95}(kips) \quad \textbf{(2-6)}$$

$$F_4 = 3\,V^{1.08}\left(\frac{b}{36}\right)^{-0.75}\ (kips) \quad \textbf{(2-7)}$$

$$F_5 = 0.05\,V^{1.77}W^{0.61}\left(\frac{b}{36}\right)^{1.14}\ (kips) \quad \textbf{(2-8)}$$

$$T_1 = 0.27\,V^{-0.86}\ (sec) \quad \textbf{(2-9)}$$

$$T_2 = 1.49\,V^{-1.09}\left(\frac{b}{36}\right)^{0.64}\ (sec) \quad \textbf{(2-10)}$$

$$T_3 = 1.04\,V^{-0.93}(sec) \quad \textbf{(2-11)}$$

$$T_4 = 2.96\,V^{-1.05}\left(\frac{b}{36}\right)^{-1.21}\ (sec) \quad \textbf{(2-12)}$$

$$T_5 = 0.22\ (sec) \quad \textbf{(2-13)}$$

$$T_6 = 0.80\ (sec) \quad \textbf{(2-14)}$$

2.6. CRASH INVESTIGATIONS IN THE UNITED STATES

Data on ten bridge crash sites investigated in Wehbe et al. (2017), Cao et al. (2020), and Buth et al. (2010) on truck collisions with bridge piers and the ensuing bridge damage are outlined in this section. Table 2-3 indicates that for most of these ten bridges the site-specific adjustment factor is at or near 1.00, indicating the site was not a significant factor in the collision. Bridge failures rates due to collisions are addressed in a later section, which is on Section 4.2.3 of this report.

Table 2-3. Site specific adjustment factor, *Ni*.

NBI Structure Number	Major Accesses	Lane Width	Horizontal Curve Radius	Lanes in One Direction	Posted Speed Limit	Grade	Ni
161780007406173	1.00	1.00	1.00	0.91	1.18	1.00	1.07
180710004804492	1.00	1.00	1.00	0.91	1.18	1.00	1.07
181750016601205	1.00	1.00	1.36	0.91	1.18	1.00	1.46
181750009206176	1.00	1.00	1.00	0.91	1.18	1.00	1.07
S080 10736	1.00	1.03	1.00	1.00	1.18	1.00	1.22
36	1.00	1.00	1.07	1.00	1.18	1.00	1.26
AXP	1.00	1.00	1.00	1.00	1.00	1.00	1.00
95I00400003	1.00	1.03	1.00	0.91	1.00	1.00	0.94
082210000606323	1.00	1.03	1.00	1.00	1.00	1.00	1.03
8309	1.00	1.00	1.00	1.00	1.18	1.00	1.18

2.6.1. Crash at Tancahua Street Bridge on I-37, Corpus Christi, Texas

This bridge is located at the following Latitude, Longitude: 27.7996587, -97.3984704.

A truck carrying approximately 72,000 lb of compressed gas collided with the eastern most pier column of a set of three center piers that supports the Tancahua Street Bridge. The collision occurred at nearly 9:00 am on May 14, 2004. The Tancahua Street Bridge allows traffic to flow over I-37 in downtown Corpus Christi. Reported by Buth et al. (2010), the vehicle was traveling at approximately 55 mph when it overturned upon merging onto I-37. The overturned vehicle then collided with one of the pier columns, which caused significant damage to the pier column but did not result in disproportionate collapse of the bridge system.

The pier column was 30 inches in diameter, and the reinforcement layout consisted of eight #9 reinforcing bars in the longitudinal direction and #2 stirrups for transverse reinforcement. Figure 2-14 shows a westbound approach of the Tancahua Street Bridge. This is the same direction the truck was travelling when the collision occurred. It is important to note that in Figure 2-14, there exists a concrete barrier between lane and the median. The posted speed limit for I-37 is 50 mph.

Original Photo: © 2022 Google® (see Acknowledgments page)

Figure 2-14. Photo. Street view of Tancahua Street bridge over I-37.

Figure 2-15 highlights the column that was struck in the collision as well as the direction of traffic. Based on Google Maps, an approximation into the width of the lanes was made at 12.37 ft. Standard lanes are between 9 and 15 feet wide. Figure 2-16 shows an expanded top view that shows a major access point to I-37. This distance was also approximated, using Google Maps, at 709.26 ft. Major access points distances, along with lane width distances are factors that go into determining the site-specific adjustment factor.

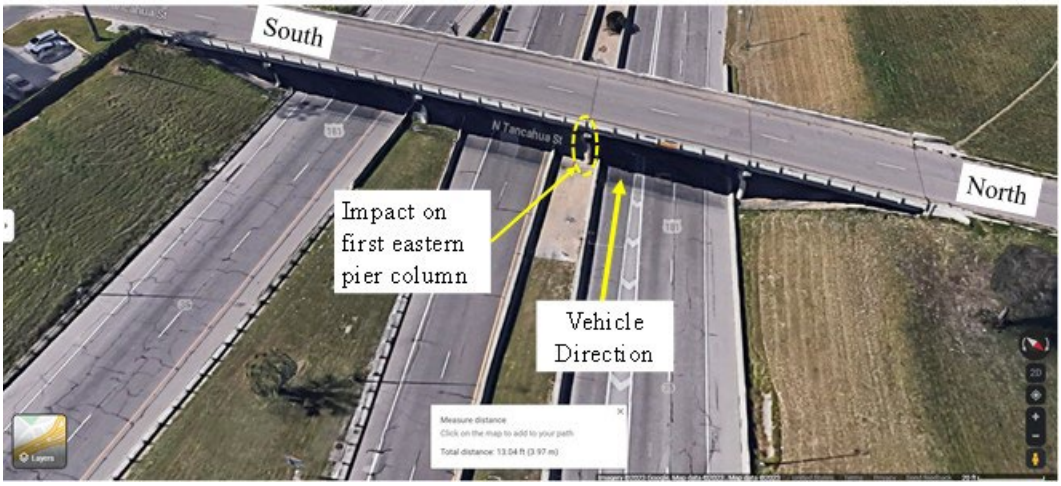

Original Photo: © 2022 Google® (see Acknowledgments page)

Figure 2-15. Photo. Aerial top view: Lane width 12.37ft.

Original Photo: © 2022 Google® (see Acknowledgments page)

Figure 2-16. Photo. Aerial top view: Major access point at 709.26 ft.

2.6.2. Crash at US-77 Bridge over I-35, Red Oak, Texas

This bridge is located at the following longitude and latitude: 32.497654, -96.8230088

On July 7, 2005, a semi-trailer truck collided with the northernmost pier column of the US-77 Bridge that carries traffic over I-35. Reports indicate the vehicle was exceeding 60 mph when the collision occurred. The accident caused the 30-inch diameter pier column to fail (Buth et al. 2010). The pier was designed with eight # 9 reinforcement bars longitudinally with #2 spiral stirrups for transverse reinforcement. The impact did not cause the bridge to collapse. Figure 2-17 shows the southbound approach of the current condition of US-77 Bridge passing over I-35. The posted speed limit on I-35 is 60 mph.

Original Photo: © 2022 Google® (see Acknowledgments page)

Figure 2-17. Photo. Street view of US-77 bridge over I-35.

Figure 2-18 shows a top view of I-35. The lane width measured using Google Maps was estimated to be 13.50 ft wide. Also shown highlighted here is the pier of the US-77 Bridge that was struck during the collision.

Figure 2-19 and Figure 2-20 show expanded top views with the nearest major access point to I 35. The distance was estimated using Google Maps measurements to be 1.14 miles between the access point and the bridge.

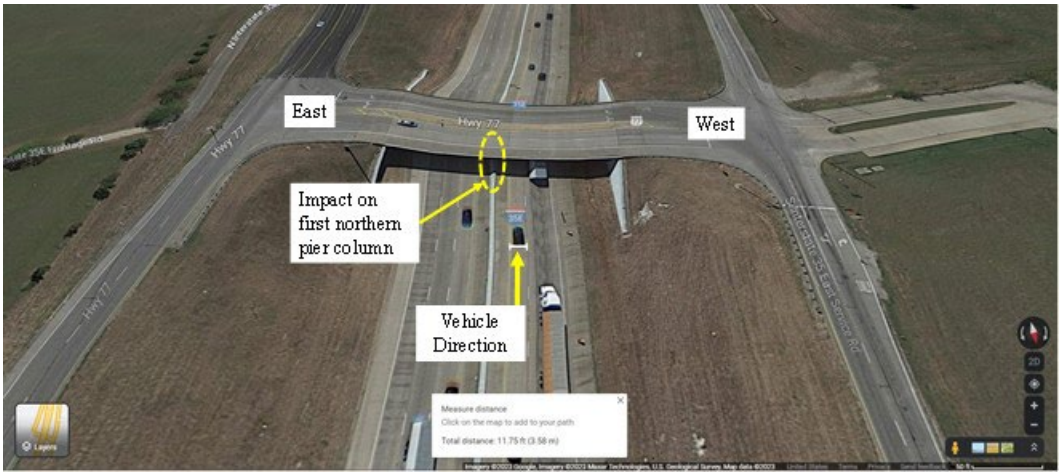

Original Photo: © 2022 Google® (see Acknowledgments page)

Figure 2-18. Photo. Aerial top view: Lane width 13.50 ft.

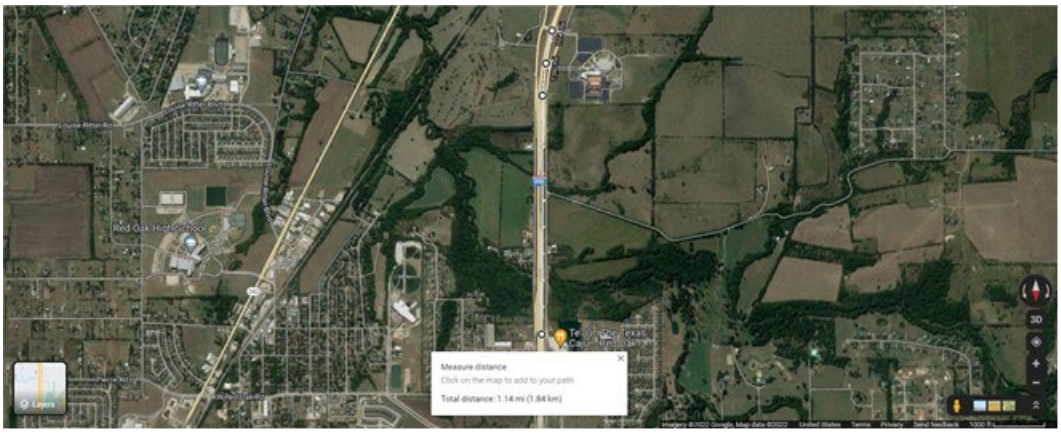

Original Photo: © 2022 Google® (see Acknowledgments page)

Figure 2-19. Photo. Google aerial view: Major access point 1.14 mi.

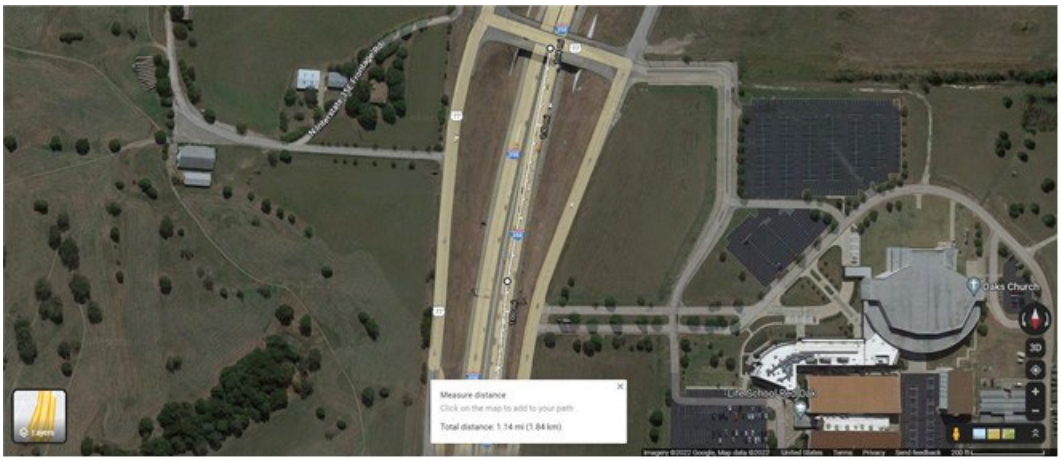

Original Photo: © 2022 Google® (see Acknowledgments page)

Figure 2-20. Photo. Google aerial view: Major access Point 1.14 mi.

2.6.3. Crash at State Highway 14 Bridge on I-45, Corsicana, Texas

This bridge is located at the following longitude and latitude: 31.9322707, -96.4245898.

A semi-trailer truck, with an approximate weight of 80,000 lb, collided into the southernmost bridge pier column of southernmost column of the west pier located on the shoulder of I-45 on September 8, 2002 (Buth et al. (2010). The piers support the State Highway 14 Bridge, which carries traffic over and onto I-45 in Corsicana, TX. The 30-inch diameter pier column failed due to the collision, and the bridge collapsed in response. The vehicle was reported travelling at a high rate of speed when the driver lost control of the vehicle and slid down the embankment and collided with the pier column. The pier column that failed was designed with eight #9 bars for the longitudinal direction and #2 spiral stirrups for transverse reinforcement.

Figure 2-21 shows the current condition after reconstruction of the southbound approach of State Highway 14 Bridge over I-45. At the time of the collision, this stretch of highway consisted of only southbound traffic flow. Figure 2-22 shows an estimated lane width of 13.61 ft using Google Maps measurement. Figure 2-23 shows the nearest major access point to southbound I-45 estimated to be 4,078.28 ft. In Figure 2-24 the radius of the horizontal curve was estimated at 1,522.30 ft. This estimation was completed by finding the center of a circle that overlaid the horizontal curve, then using Google Maps measurement tool to determine the distance. The roadway curves away from pier that was impacted during the collision. This factor affects the site-specific adjustment factor.

Original Photo: © 2022 Google® (see Acknowledgments page)

Figure 2-21. Photo. Google street view of State Highway 14 bridge over I-45.

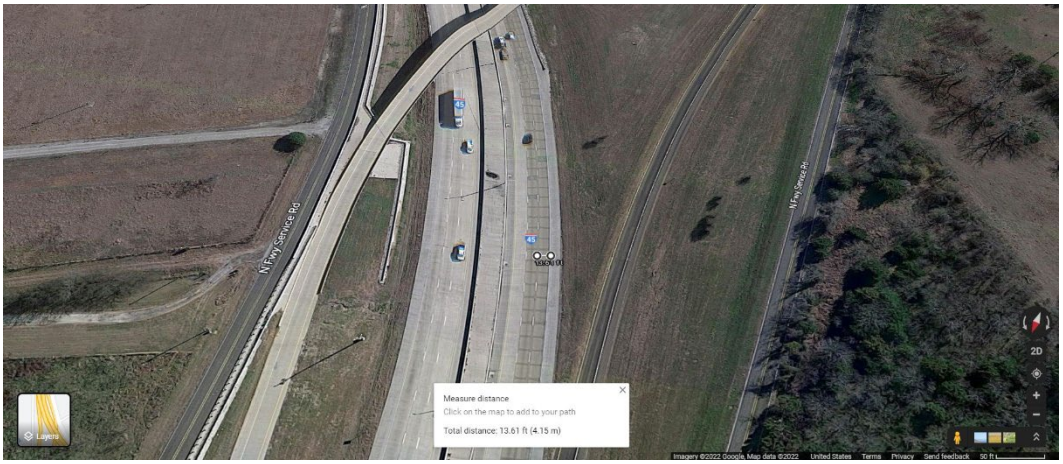

Original Photo: © 2022 Google® (see Acknowledgments page)

Figure 2-22. Photo. Google aerial view: Lane width 13.61 ft.

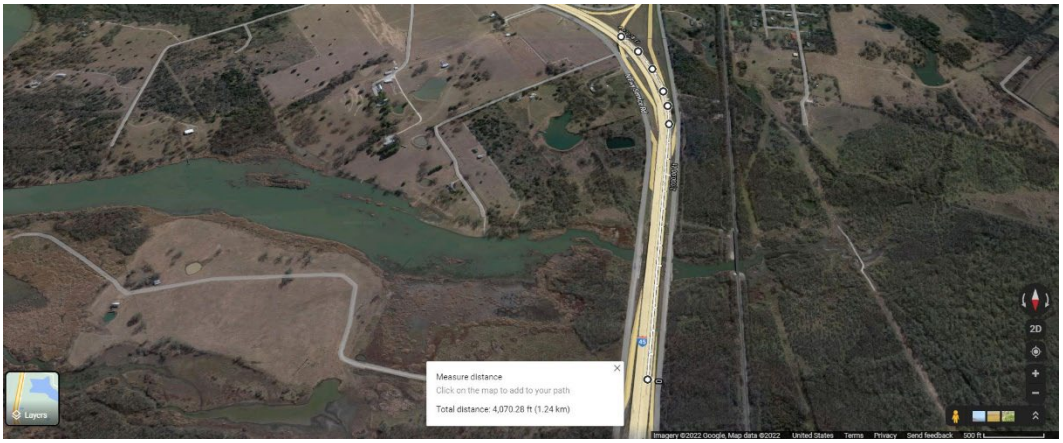

Original Photo: © 2022 Google® (see Acknowledgments page)

Figure 2-23. Photo. Google aerial view: Major Access Point 4,070.28 ft.

Original Photo: © 2022 Google® (see Acknowledgments page)

Figure 2-24. Photo. Aerial top view: Horizontal Curve Radius 1,522.30 ft.

2.6.4. Crash at Roane Road Bridge on I-45, Navarro County, Texas

This bridge is located at the following longitude and latitude: 32.1164446, -96.4452298

On May 30, 2007, an approximately 80,000 lb semi-trailer truck traveling approximately 60 mph collided with the northernmost pier of the center two-column bent on I-45 (Buth et al. 2010). The 30-inch pier column is one of the two center columns that supports the Roane Road Bridge that carries traffic over I-45. The impact caused cracking in the pier, but no failure to the bridge. The pier column was 30 inches in diameter, with eight #9 rebars longitudinally and #2 spiral stirrups for transverse reinforcement. Figure 2-25 shows the current condition of the southbound approach of Roane Road Bridge on I-45. Figure 2-26 shows a top view of I-45 and an estimated lane width of 14.16 ft measured with Google Maps. Figure 2-27 shows an enlarged view of the nearest Major Access Point. Using Google Maps measurement, the distance was estimated at 2.49 miles between the major access point and the impacted pier.

Original Photo: © 2022 Google® (see Acknowledgments page)

Figure 2-25. Photo. Google street view of Roane Road bridge over I-45.

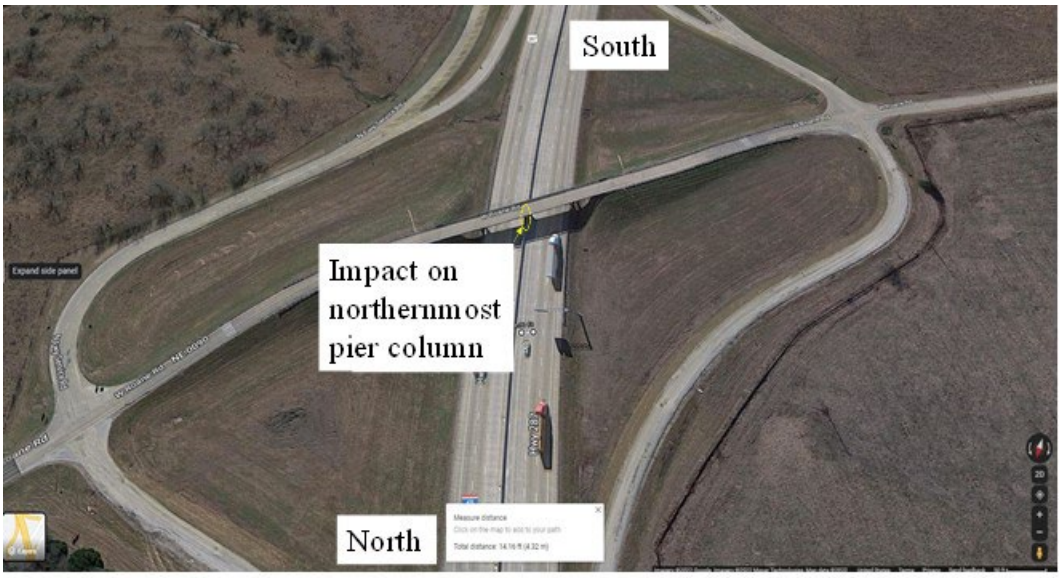

Original Photo: © 2022 Google® (see Acknowledgments page)

Figure 2-26. Photo. Aerial top view: Lane width 14.16 ft.

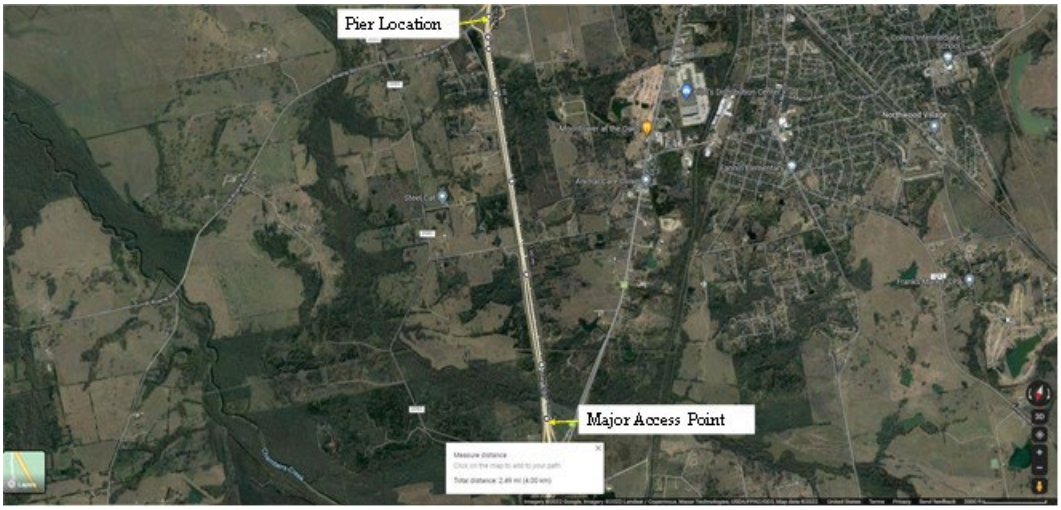

Original Photo: © 2022 Google® (see Acknowledgments page)

Figure 2-27. Photo. Aerial top view: Major access point 2.49 mi.

2.6.5. Crash at State Route 25B on I-80, Big Springs, Nebraska

The bridge is located at the following longitude and latitude: 41.0488571, -102.0711623

On May 23, 2003, a semi-trailer truck collided with the easternmost pier column of the center pier that supports the State Route 25B Bridge carrying traffic over I-80 in Big Springs, Nebraska. Reported by Buth et al. (2010) and Wehbe et al. (2017), the vehicle was exceeding 65 mph when the driver lost control and drove into the median and collided with the bridge pier. The collision caused the pier columns to fail and the bridge to collapse. The load being carried was not identified within reports, so the weight of the heavy truck can only be assumed based on typical values of tractor-trailer units. Figure 2-28 shows the most recent condition of I-80 based on

Google Maps. At the time of pier protection also consisted of steel guard rails. Figure 2-29 shows a top view of I-80. The lane width was estimated using the Google Maps measurement tool. The width is estimated at 10.85 ft.

Original Photo: © 2022 Google® (see Acknowledgments page)

Figure 2-28. Photo. Google street view of State Route 25B bridge over I-80.

Original Photo: © 2022 Google® (see Acknowledgments page)

Figure 2-29. Photo. Aerial top view: Lane width 10.85 ft.

2.6.6. Crash at N Stadium Blvd Bridge over I-70, Columbia, Missouri

The bridge is located at the following longitude and latitude: 38.9682082, -92.3713355

Late night on July 19, 2020, a semi-trailer truck collided with the westernmost pier column of the N Stadium Boulevard Bridge that carries traffic over I-70. The pier is located beyond the right shoulder of I-70. According to the incident report the vehicle impacted the guardrail first before colliding with the bridge pier. The load of vehicle is unknown, so the weight of the semi-trailer is

estimated at approximately 80,000 lb. The speed of the vehicle was traveling before the collision was also not disclosed, but it was assumed to exceed 60 mph. The design of the rectangular pier column impacted is not known, and the bridge was open to traffic soon after the cleanup without any significant damage to the bridge.

Figure 2-30 shows the street view of the current condition of the North Stadium Boulevard Bridge passing over I-70. Figure 2-31 shows a top view of I-70 and an estimated lane width, measured using Google Maps, of 13.76 ft. Figure 2-32 shows an estimated radius of the horizontal curve at 2,519.66 ft. The roadway curves toward the impacted pier.

Original Photo: © 2022 Google® (see Acknowledgments page)

Figure 2-30. Photo. Google street view of N Stadium Blvd bridge over I-70.

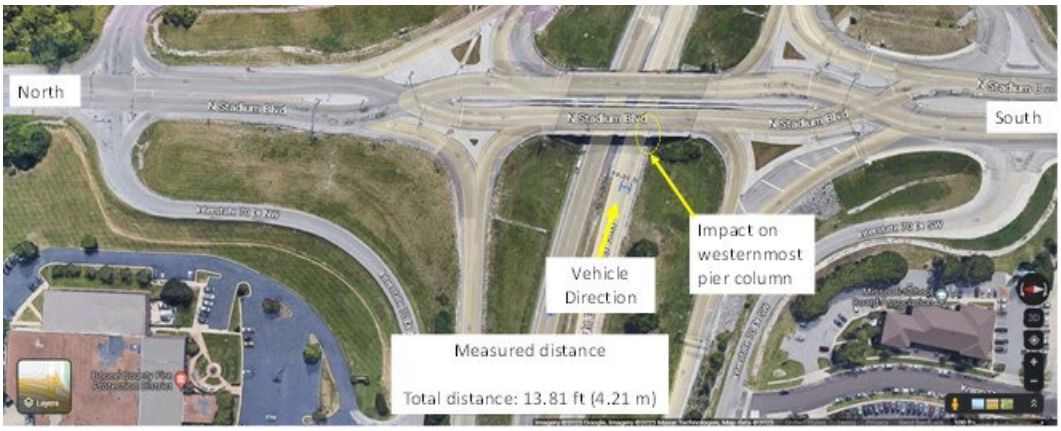

Original Photo: © 2022 Google® (see Acknowledgments page)

Figure 2-31. Photo. Aerial top view: Lane width 13.76 ft.

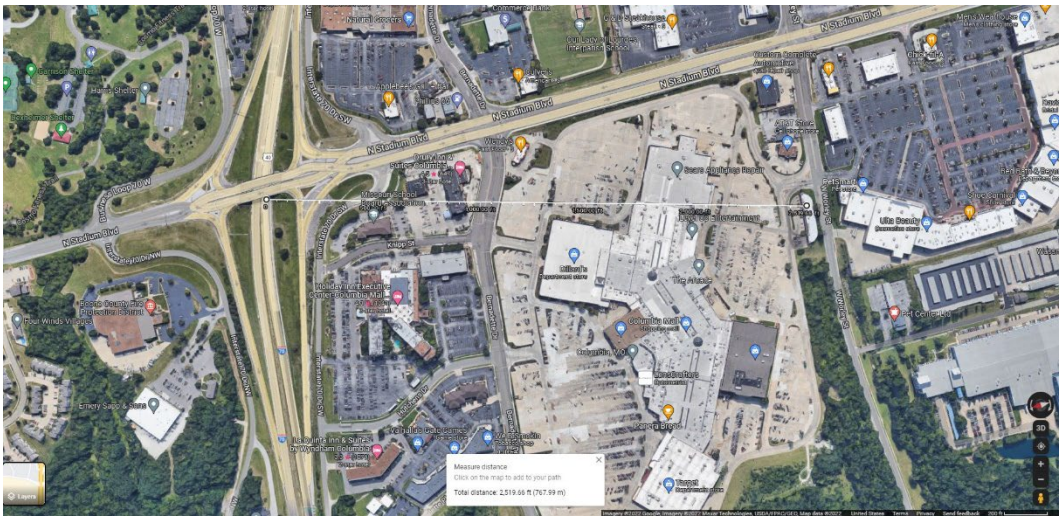

Original Photo: © 2022 Google® (see Acknowledgments page)

Figure 2-32. Photo. Aerial top view: Horizontal curve radius 2,519.66 ft.

2.6.7. Crash at 15th Street Bridge on I-80, Laramie, Wyoming

The bridge is located at the following longitude and latitude: 41.293728, -105.580139.

On May 21, 2017, a semi-trailer truck collided with the easternmost pier column of the 15th Street Bridge on I-80. The vehicle was traveling between 65 and 70 mph when it drove through the guardrail and struck the five-column bent located on the right shoulder of I-80. The collision caused the easternmost column to fail. The failure of the pier column did not cause the bridge to collapse. The design of the rectangular pier columns is unknown.

Figure 2-33 shows the west bound approach of the 15th Street Bridge. The 15th Street Bridge carries traffic over I-80. Figure 2-34 shows a top view of I-80. An estimated lane width, completed with Google Maps, can also be seen here. Figure 2-35 shows a zoomed-out view of I-80, detailing the nearest major access point located upstream from the impacted pier. The distance to the pier was estimated, using the Google Maps measurement tool, to be 2.53 miles.

Original Photo: © 2022 Google® (see Acknowledgments page)

Figure 2-33. Photo. Street view of 15th Street bridge over I-80.

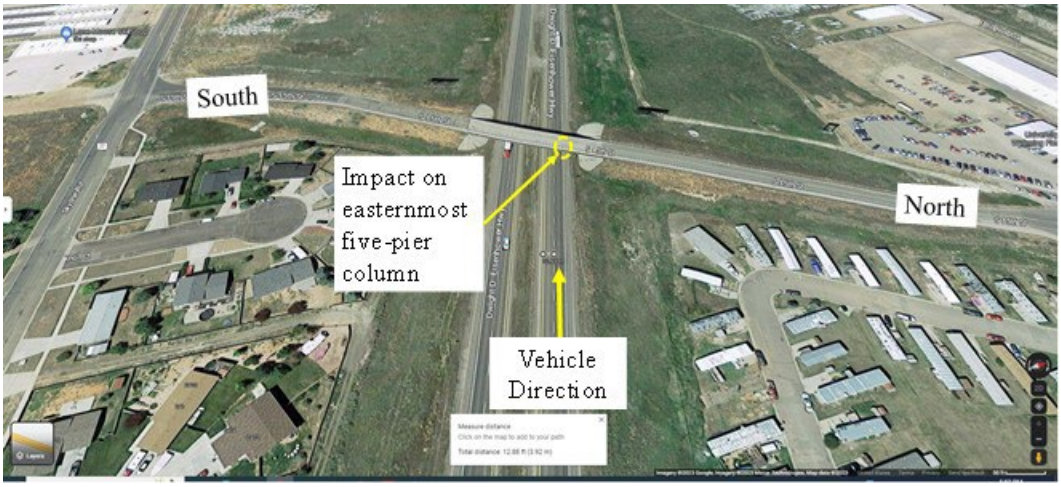

Original Photo: © 2022 Google® (see Acknowledgments page)

Figure 2-34. Photo. Aerial top view: Lane width 12.94 ft.

Original Photo: © 2022 Google® (see Acknowledgments page)

Figure 2-35. Photo. Aerial top view: Major access point 2.53 mi.

2.6.8. Crash at Mount. Juliet Road Bridge over I-40, Mount Juliet, Tennessee

The bridge is located at the following longitude and latitude: 36.1715483, -86.5126679

On June 23, 2021, a semi-truck travelling westbound collided with the easternmost pier column located just beyond the right shoulder of I-40. The pier impacted is one of the multi-pier bents that supports the Mount Juliet Road Bridge that carries traffic over and onto I-40. The vehicle first veered into the guardrail before straddling it, and ultimately collided with the bridge pier columns. The vehicle's speed before the collision is unknown, but it is assumed to be greater than 70 mph. The design of the pier is also not known; however, the multi-column bents consist of circular pier columns.

Figure 2-36 shows the most recent condition of the street view of Mount Juliet Road Bridge over I-40. Figure 2-37 shows the top view of I-40 with an estimated lane measurement of 11.58 feet. Figure 2-38 shows the nearest major access point to the pier that was impacted. The distance of 2.99 miles was estimated using Google Maps.

Original Photo: © 2022 Google® (see Acknowledgments page)

Figure 2-36. Photo. Street view of Mt. Juliet Road bridge over I-40.

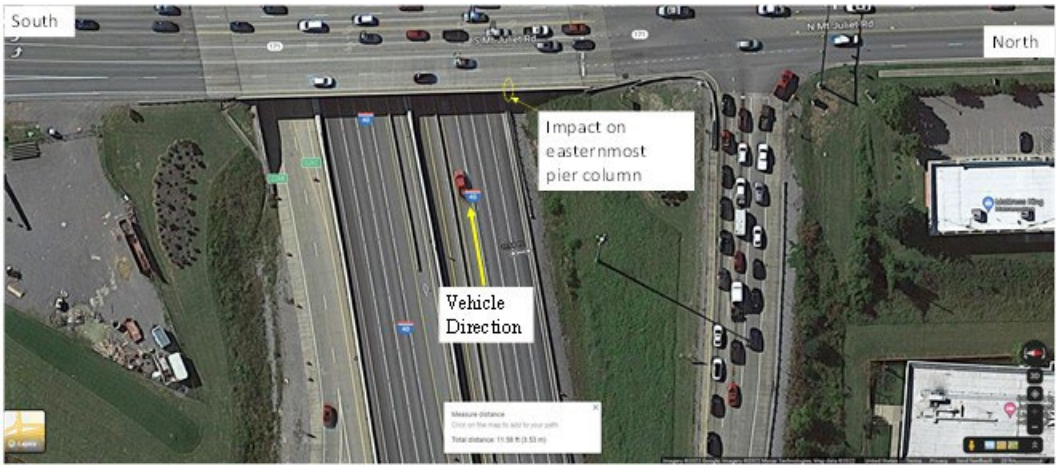

Original Photo: © 2022 Google® (see Acknowledgments page)

Figure 2-37. Photo. Aerial top view: Lane width 11.58 ft.

Original Photo: © 2022 Google® (see Acknowledgments page)

Figure 2-38. Photo. Aerial top view: Major access point 2.99 mi.

2.6.9. Crash at West Lake Road Bridge on I-20, Abilene, Texas

The bridge is located at the following longitude and latitude: 32.4902375, -99.7233226

On February 22, 2022, a semi-truck collided with the westernmost pier column of the 5-column bent located within the median of I-20. The impacted pier column helps support the West Lake Road Bridge, which carries traffic over I-20. The collision occurred when the truck veered from the left most lane into and over the guardrails and into the median. The truck then collided with the bridge pier and exploded on impact. The pier column did not fail due to the collision and the only repairs that were needed was the guardrail and a replacing of the bridge height clearance sign. The design information for the pier was not made available.

Figure 2-39 shows the current condition of W Lake Road Bridge passing over I-20. It is important to note the scorch marks that can still be seen from the collision. Figure 2-40 shows a top view of I-20. Here the direction of traffic can be seen, as well as an estimated lane width measured by Google Maps. Figure 2-41 shows the nearest major access point onto I-20 to the impacted pier.

Original Photo: © 2022 Google® (see Acknowledgments page)

Figure 2-39. Photo. Street view of West Lake Road Bridge on I-20.

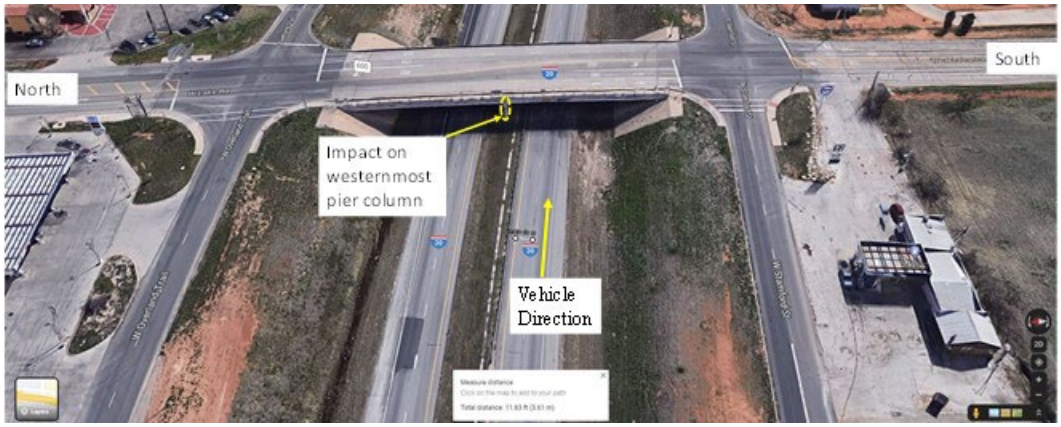

Original Photo: © 2022 Google® (see Acknowledgments page)

Figure 2-40. Photo. Aerial top view: Lane width 11.83 ft.

Original Photo: © 2022 Google® (see Acknowledgments page)

Figure 2-41. Photo. Aerial top view: Major access point at 2,892.17 ft.

2.6.10. Crash at County Road 704 Bridge on I-55, Matthews, Missouri

The bridge is located at the following longitude and latitude: 36.7224431, -89.5378163

On September 27, 2021, a semi-truck traveling northbound on I-55 collided with the southernmost center bridge pier of the County Road 704 Bridge. The bridge carries traffic over I-55. According to the incident report, the vehicle veered off the left side of I-55 and into the median. The semi-truck damaged 20 feet of guardrail before colliding with the southernmost column of the center pier. The pier column failed due to the collision and the adjacent pier column was damaged. The bridge did not collapse. The design details of the bridge are unknown. The vehicle was believed to exceed 60 mph.

Figure 2-42 shows the most recent condition of the street view of County Road 704 Bridge passing over I-55. Figure 2-43 shows a top view of I-55 along with the direction the vehicle was travelling before the collision as well as an estimated lane width of 12.72 feet.

Original Photo: © 2022 Google® (see Acknowledgments page)

Figure 2-42. Photo. Street view (County Road 704 Bridge over I-55).

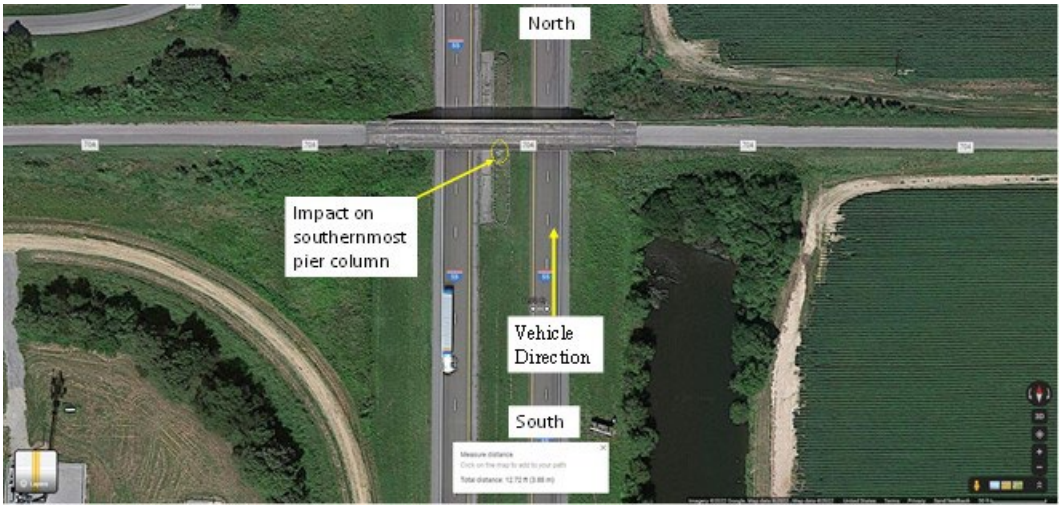

Original Photo: © 2022 Google® (see Acknowledgments page)
Figure 2-43. Photo. Aerial Top view: Lane width 12.72 ft.

CHAPTER 3 - DATA MINING

Data mining was conducted to estimate frequency and severity of traffic collisions, eccentricity of collisions, bridge members sizes and deterioration condition of bridges, as well as type, mass, and speed of the vehicle causing the collision. Given the on-site availability of these specified data types, 17 bridges were selected from the commonwealth of Virginia to form a test-bed study site. The test-bed study site will be further discussed in detail in Section 4.1. Data mining was extended to include data on collisions, bridges, and traffic detectors in Virginia that can be used in creating synthetic data to further augment the collected data. Data mining was conducted in research areas of traffic analyses and failure evaluation of bridges against vehicular collisions. Traffic related applications and technologies rely on extensive traffic detector and collision data analysis aimed at understanding trends associated with the safety of the surface road transportation systems.

Data mining of these bridge elements can aid in the development of the following stochastic variables and models:

- Probabilistic assessment of parametric loading functions and associated performance limit states for Extreme Event II type events such as vehicular collisions.

- Structural resistance fragility curves for bridge girders and bridge pier elements necessary to assess disproportionate collapse of bridges.

- Structural resistance fragility curves for the effects of collisions involving flammable fuel or cargo that results in a fire event with high consequences.

The FHWA National Bridge Inventory (NBI) contains detailed information on more than 600,000 highway bridges. Bridge elements for data query are often defined in the literature as NBI elements. This database contains bridge elements for every single bridge and can be queried based on a wide range of bridge elements that makes it possible to evaluate bridges and assess their structural conditions (NBI 2023).

This chapter outlines the results obtained from data mining of the NBI (2023) database using the LTBP InfoBridge^{TM} portal (FHWA- LTBP 2021). Data mining was used in developing a comprehensive assessment of bridges crossing over traffic lanes in Virginia and to formulate models for the resistance of bridge columns and girders against vehicular collisions. Likewise, frequency and severity of traffic collisions were performed by investigating the Virginia Department of Motor Vehicles (Virginia DMV, 2022), Virginia Department of Transportation (VDOT, 2022), U.S. Department of Transportation Bureau of Transportation Statistics (BTS, 2021), FHWA Highway Safety Information System (HSIS 2021) and National Highway Traffic Safety Administration (NHTSA, 2021). A numerical analysis conducted while utilizing these databases allowed determining the distributions of trucks by weight, the average daily weight of trucks passing a given roadway segment and the different roadway crashes proportions by vehicle type. These results were then translated into multiple measures including large heavy truck involvement rate in fatal crashes and average daily trucks carrying flammable fuels.

3.1. IDENTIFICATION OF STRUCTURAL CHARACTERISTICS

Data collected and analyzed in this section is relevant in identifying the many structural characteristics that can have a direct impact on the resistance of bridges to vehicular collisions. Data mining was further used in developing stochastic models that can represent bridge deterioration, bridge type, site location and its associated ADTT within Virginia.

3.1.1. LTBP InfoBridge™ Data Mining for the Commonwealth of Virginia

The FHWA LTBP InfoBridge™ facilitates data mining of the NBI (2023) database via a web portal to access, visualize, and analyze bridge performance data. In this web portal users collect information to analyze and evaluate bridges in the United States. Other information such as bridge type and specifications, operational conditions, bridge data including geometric data and functional description, and inspection data are also available through LTBP InfoBridge™ (FHWA- LTBP 2021).

3.1.1.1. Bridges Susceptible to Heavy Truck Collisions

A query of LTBP InfoBridge™ (FHWA- LTBP 2021) for Virginia was used for collecting performance-related data and information for all bridges. A query of the 2020 LTBP InfoBridge™ shows the total number of bridges in Virginia is 13,963. Since this research focuses only on bridge pier columns and/or girders susceptible to traffic collisions, all culverts and bridges not crossing over traffic lanes were excluded from the dataset. In the dataset this was accomplished when the NBI Item 43B *Main Span Design* is set to *Culvert* and the NBI Item 28B number of *Lanes Under the Structure* is zero.

Bridges that are susceptible to either overhead and/or pier collisions should cross over at least one traffic lane. This narrow dataset of bridges with traffic lanes under the structure and excluding culverts is 2,689 bridges. Only these 2,689 bridges were included in this dataset, because this report deals with heavy truck collisions with bridge pier columns and girders. This dataset includes single and multiple span bridges. Figure 3-1 depicts the geographical location of 353 single-span bridges, and Figure 3-2 depicts the geographical location of 2,336 multiple-span bridges in Virginia. In this work single span bridges were only considered for overhead collisions and multiple-span bridges were considered in evaluating pier and overhead vehicular collisions. Single and multiple span bridges were queried from the NBI Item 45, which specifies the *Number of Spans in Main Unit*.

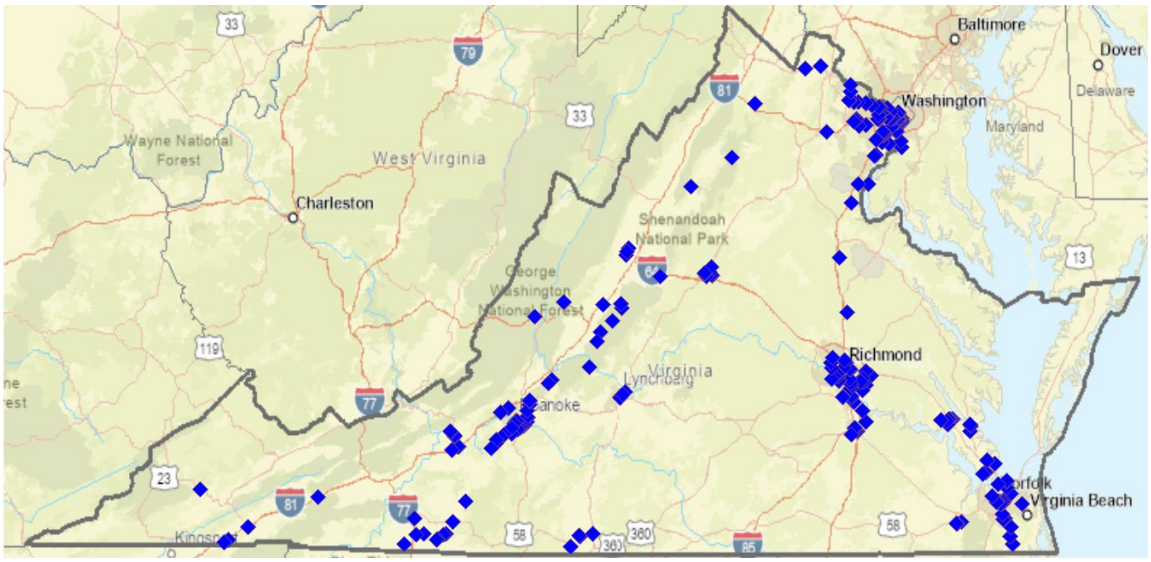

Note: Data overlay on Original Map: © 2022 TomTom (see Acknowledgments page).

Figure 3-1. Graph. Map of 353 single-span bridges over roadways in Virginia.

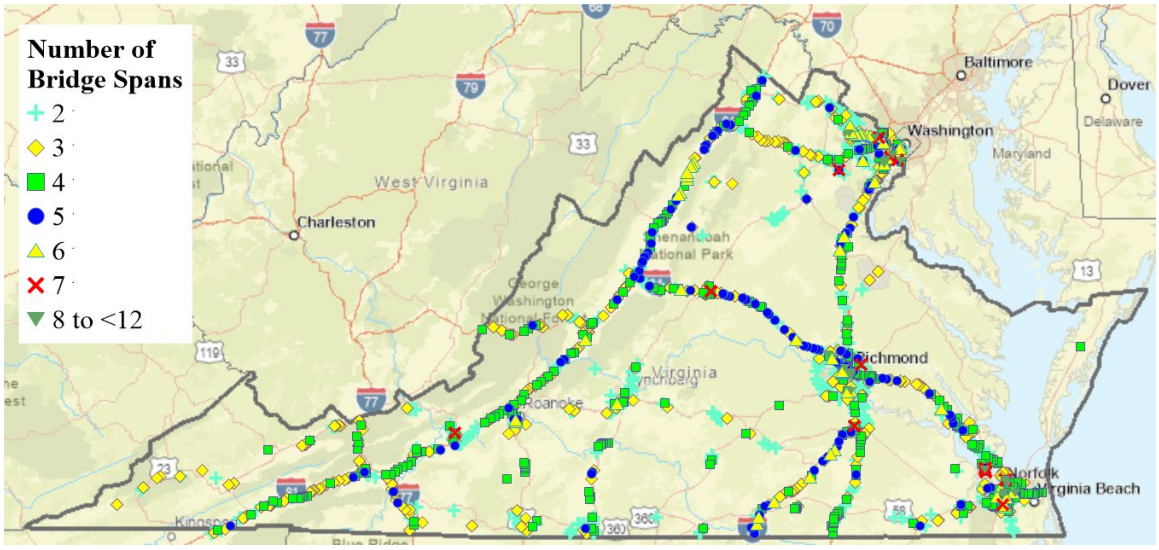

Note: Data overlay on Original Map: © 2022 TomTom (see Acknowledgments page).

Figure 3-2. Graph. Map of 2,336 multiple-span bridges over roadways in Virginia.

3.1.1.2. Distribution of Bridges based on Average Daily Truck Traffic (ADTT)

AASHTO LRFD BDS, 8th Edition[1], Article C3.6.5.1 specifies exemptions based on site conditions for pier protection as a function of the annual frequency of heavy truck collisions, AF_{HBP}. As discussed in Section 2.1.1.1 of this report, AF_{HBP} is directly related to ADTT. In this work the ADTT was queried using the NBI Item 109 (*Average Daily Truck Traffic*). Figure 3-3 depicts the geographical distribution of ADTT. In this figure, the maximum registered ADTT is 16,096.

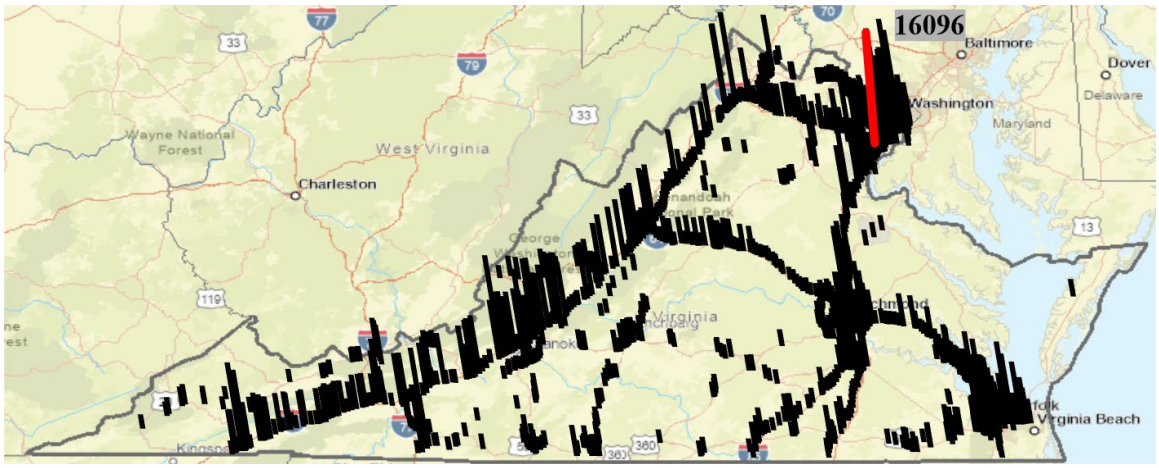

Note: Data overlay on Original Map: © 2022 TomTom (see Acknowledgments section).

Figure 3-3. Graph. Map of bridges according to ADTT.

3.1.1.3. Distribution of Materials Used in the Main Spans

Materials used in the construction of the main span are critical in evaluating the resiliency of bridges against vehicular collision. Results from querying NBI Item 43A (*Main Span Material*) are presented in Figure 3-4 and Figure 3-5. Figure 3-4 shows a pie chart depicting the distribution of materials used in main spans. This figure shows that simply supported steel, reinforced concrete, and prestressed concrete girders constitute nearly 85 percent of the main span types used in Virginia. Continuous steel, concrete, and prestressed concrete girders constitute nearly 14 percent of the main span types. Figure 3-5 suggests that near urban regions the main form of material used in the main span are continuous steel girders. Along highway interchanges and away from urban regions the main form of material used in the main span is prestressed concrete girders.

Definition of *Others* in Figure 3-4 relates to the following materials used in the main span:

- Aluminum, Wrought Iron, or Cast Iron
- Other Material Main Span
- Wood or Timber
- Masonry

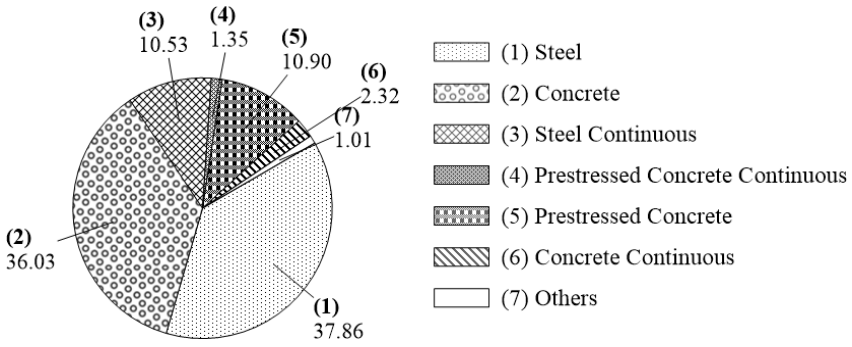

A. All 13,963 Virginia bridges and culverts.

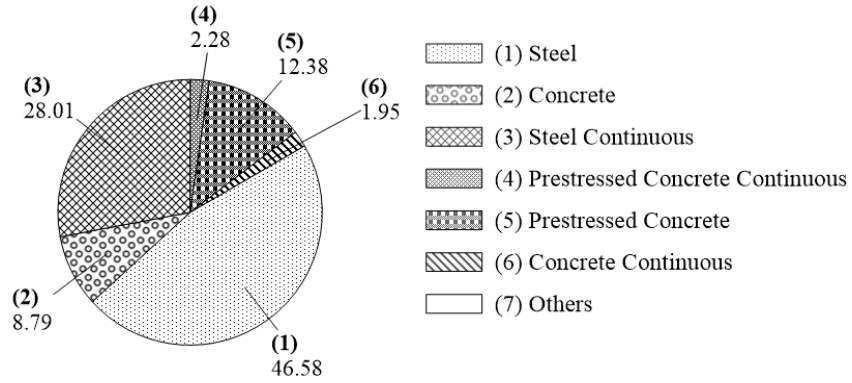

B. All 2,696 Virginia bridges crossing over traffic lanes.

Figure 3-4. Charts. Distribution of materials used in main spans.

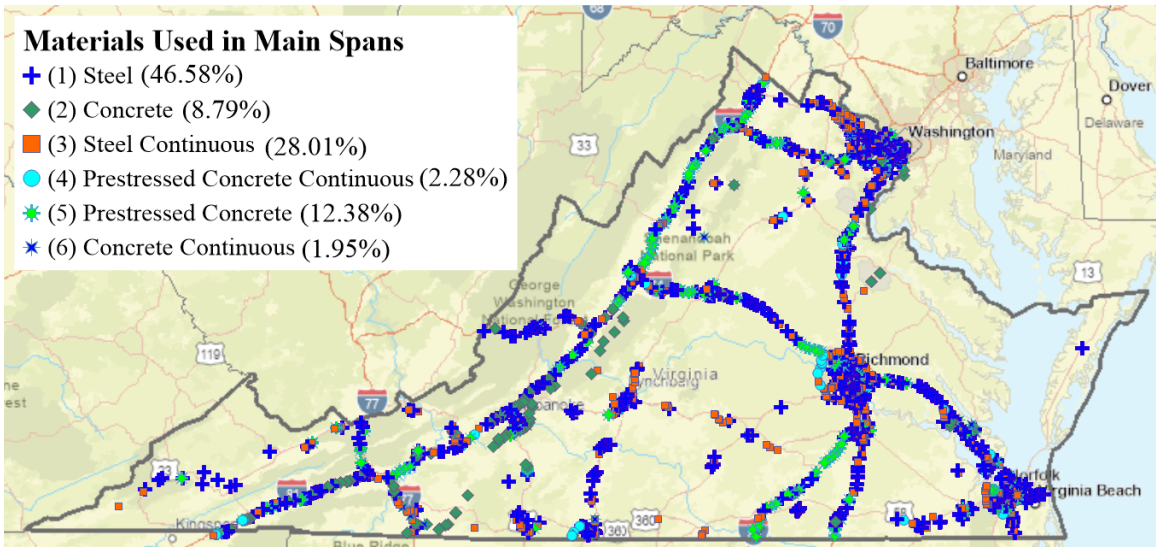

Note: Data overlay on Original Map: © 2022 TomTom (see Acknowledgments section).

Figure 3-5. Graph. Map of bridges according to materials used in main spans.

3.1.1.4. Bridge Deck Condition Rating

In this section, bridge deck condition ratings were extracted from NBI Item 58 (*Deck Condition Rating*). Pie charts and geographical distributions of bridge deck conditions are depicted in Figure 3-6 and Figure 3-7, respectively. Figure 3-6A and Figure 3-7 show bridges deck condition

rated as *Good*, *Satisfactory*, and *Fair* are 44.01, 38.19, and 11.44 percent, respectively, of decks for bridges with traffic crossing over traffic lanes in Virginia. Figure 3-7 depicts that near urban regions the main rank is *Good*, and away from these regions there are a significant number of bridge decks rated as *Fair*.

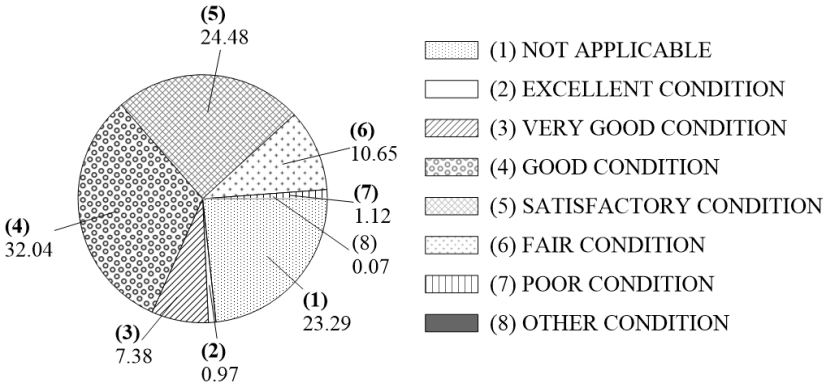

A. All 13,963 Virginia bridges and culverts.

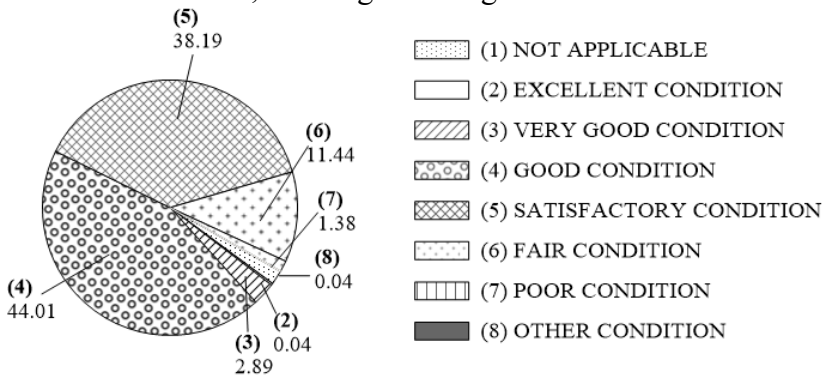

B. All 2,696 Virginia bridges crossing over traffic lanes.

Figure 3-6. Charts. Distribution of deck condition ratings.

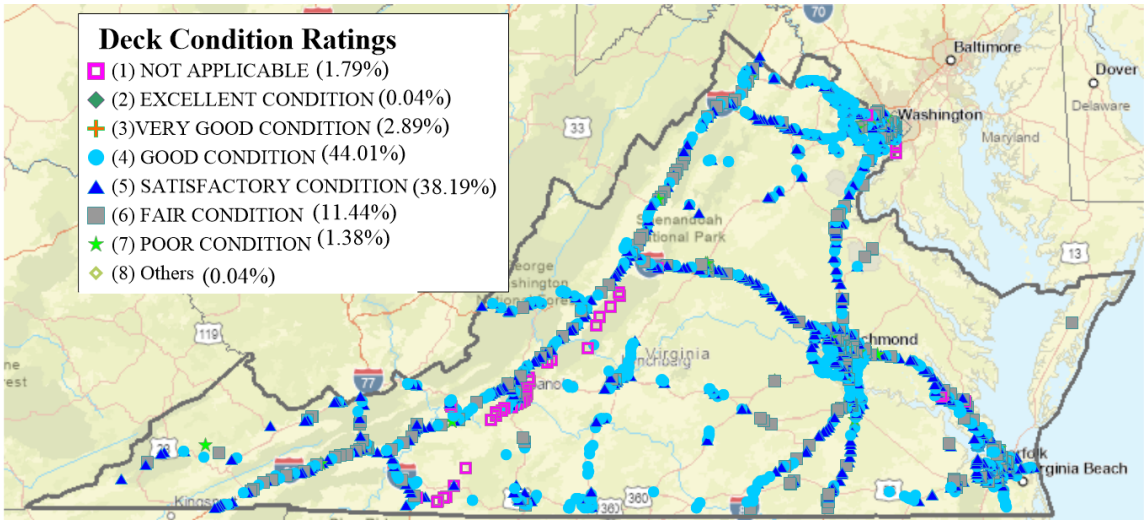

Note: Data overlay on Original Map: © 2022 TomTom (see Acknowledgments section).

Figure 3-7. Graph. Map of bridges according to deck condition ratings.

3.1.1.5. Bridge Superstructure Condition Ratings

Bridge superstructure condition is from NBI Item 59 (*Superstructure Condition Rating*). Pie charts and geographical distributions of superstructure conditions are depicted in Figure 3-8 and Figure 3-9, respectively. These figures show that bridge superstructure condition was rated as *Good*, *Satisfactory*, and *Fair* in nearly 35.69, 37.00, and 18.80 percent, respectively, of superstructures for bridges crossing over traffic lanes in Virginia. Figure 3-9 depicts that near urban regions the most common rating is Good, and away from these regions there are a significant number of bridge superstructures rated as Fair.

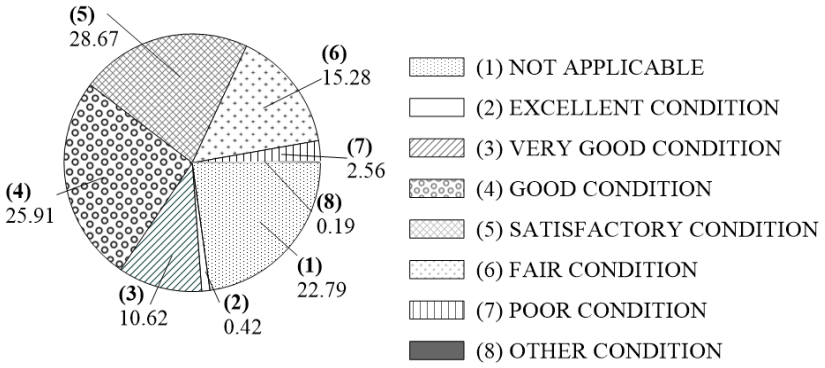

A. All 13,963 Virginia bridges and culverts.

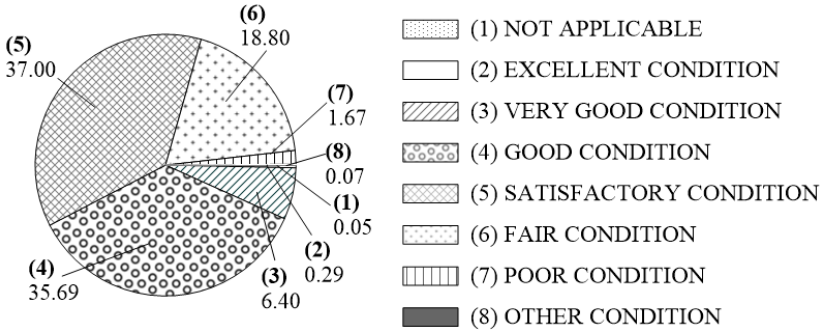

B. All 2,696 Virginia bridges crossing over traffic lanes.

Figure 3-8. Charts. Distribution of superstructure condition ratings.

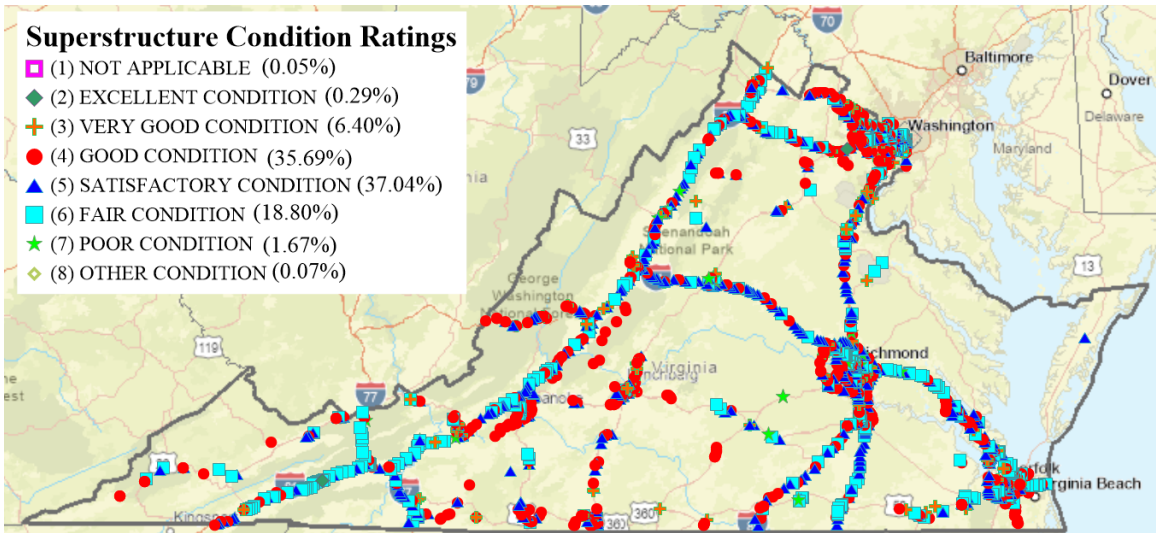

Note: Data overlay on Original Map: © 2022 TomTom (see Acknowledgments section).

Figure 3-9. Graph. Map of bridges according to superstructure condition ratings.

3.1.1.6. Bridge Substructure Condition Ratings

Bridge Substructure condition was extracted from NBI Item 60 (*Substructure Condition Rating*). Pie charts and geographical distributions of superstructure conditions are depicted in Figure 3-10 and Figure 3-11, respectively. These figures show that bridge substructure condition has been rated as *Good*, *Satisfactory*, and *Fair* in nearly 34.20, 40.18, and 22.00 percent of substructure for bridges crossing over traffic lanes in Virginia.

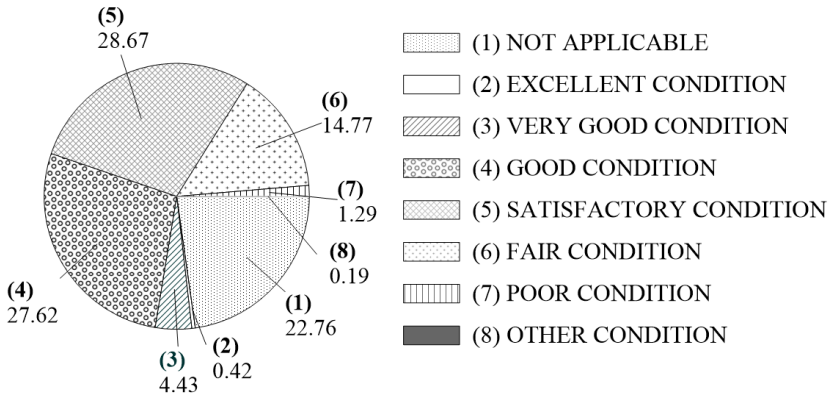

A. All 13,963 Virginia bridges and culverts.

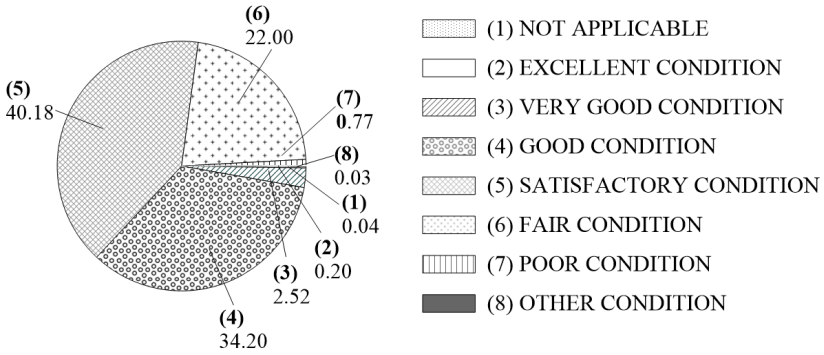

B. All 2,696 Virginia bridges crossing over traffic lanes.

Figure 3-10. Charts. Distribution of substructure condition ratings.

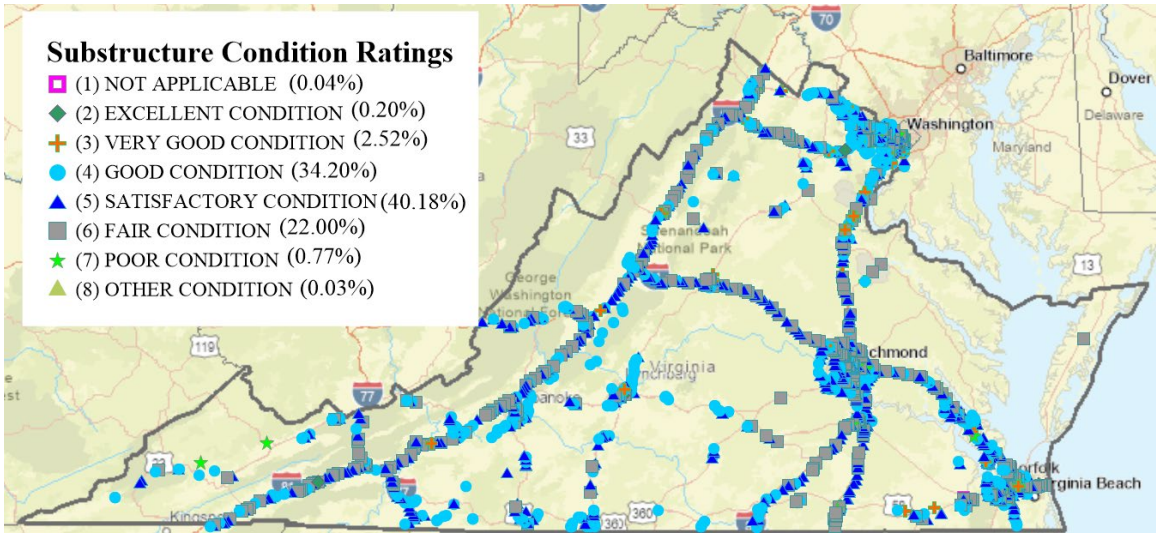

Note: Data overlay on Original Map: © 2022 TomTom (see Acknowledgments section).

Figure 3-11. Graph. Map of bridges according to substructure condition ratings.

3.1.1.7. Bridge Overall Condition Ratings

Bridge overall condition ratings were extracted from the LTBP InfoBridge™ portal (FHWA-LTBP 2021) bridge element *CAT10 Bridge Condition*. Pie charts and geographical distributions of bridge overall condition ratings are depicted in Figure 3-12 and Figure 3-13, respectively. These figures show that bridge overall condition ratings, which were rated as *Good*, *Fair*, or *Poor* is, respectively, 25.57, 71.62, and 2.81 percent for bridges crossing over traffic lanes in Virginia. Figure 3-17 depicts that near urban regions the main rank is *Good*, and away from these regions many bridges rated as *Fair*.

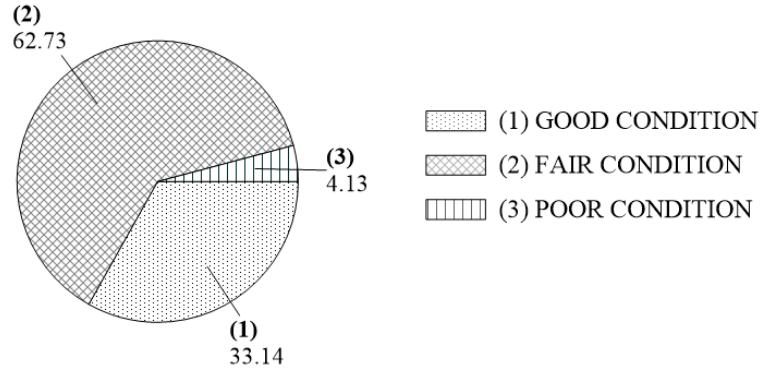

A. All 13,963 Virginia bridges and culverts.

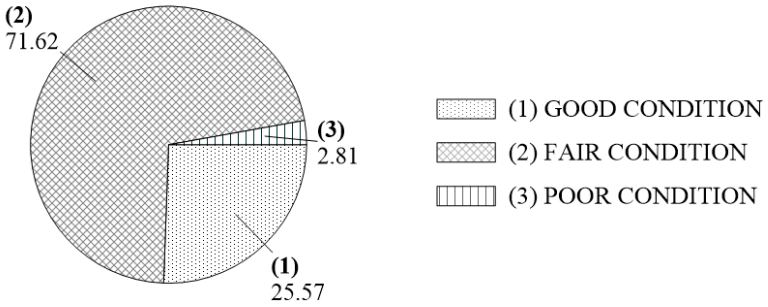

B. All 2,696 Virginia bridges crossing over traffic lanes.

Figure 3-12. Charts. Distribution of bridge overall condition ratings.

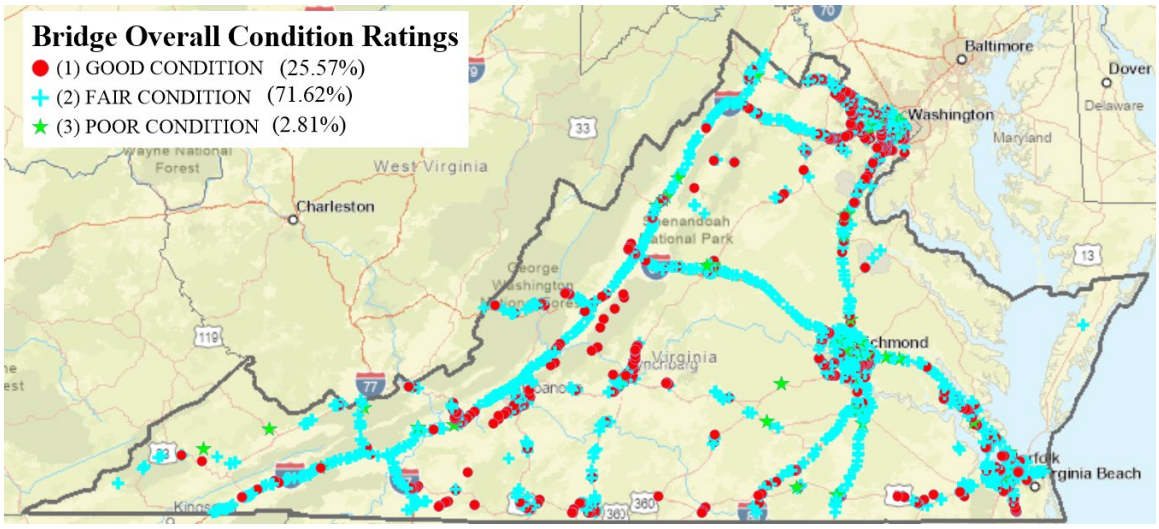

Note: Data overlay on Original Map: © 2022 TomTom (see Acknowledgments section).

Figure 3-13. Graph. Map of bridges according to overall condition ratings.

3.1.1.8. Bridge Number of Spans

The number of spans in the main unit were extracted from NBI Item 45 (*Number of Spans in Main Unit*). Figure 3-14 depicts the geographical distributions of bridges number of spans. As indicated in the figure most bridges have 2, 3, or 4 spans. The research team has developed an API that was also used to assess the position of each of the bridge piers in relation to the degree of curvature of the traveling lanes roadway under the bridge.

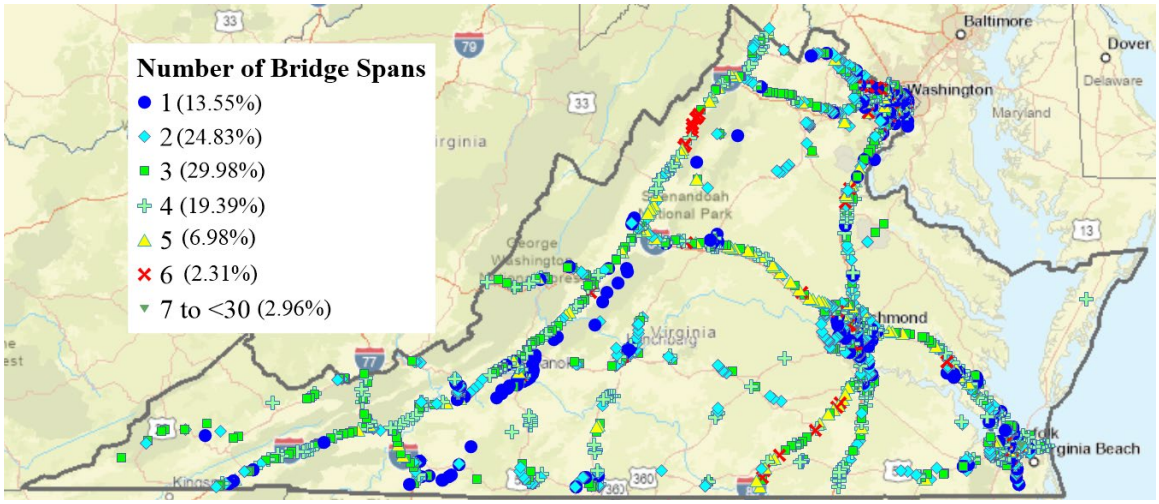

Note: Data overlay on Original Map: © 2022 TomTom (see Acknowledgments section).

Figure 3-14. Graph. Map of bridges according to number of spans.

3.1.1.9. Number of Lanes under the Bridge

The number of lanes under the structure were extracted from NBI Item 28B (*Lanes Under the Structure*). Figure 3-15 and Figure 3-14 depict the geographical distributions of number of lanes under the structure. As shown, the number of lanes passing under the bridge is mostly 2, 4 or 6.

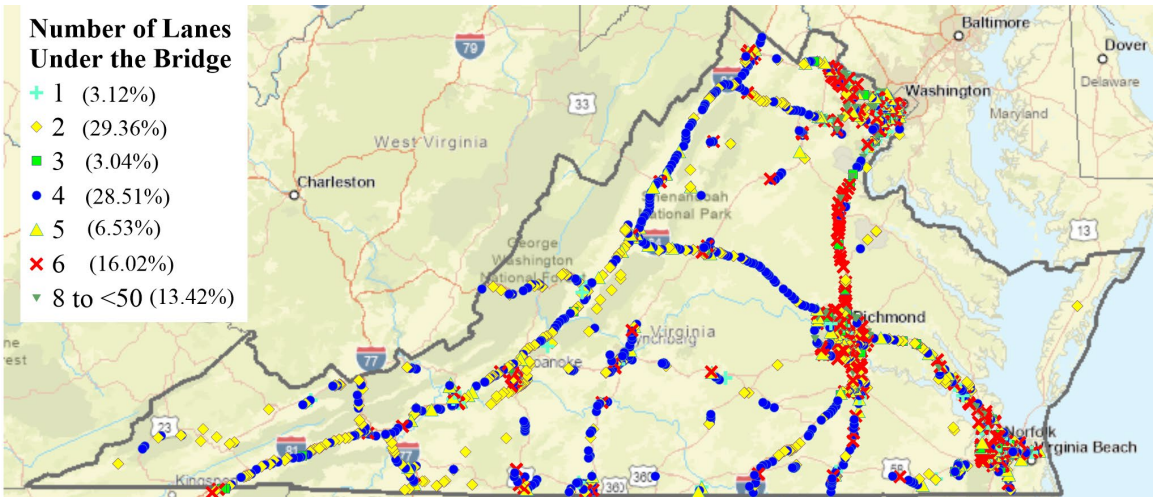

Note: Data overlay on Original Map: © 2022 TomTom (see Acknowledgments page).

Figure 3-15. Graph. Map of bridges according to number of crossing lanes.

3.1.2. Project Specific Application Programming Interface (API) for Data Mining

Other bridge attributes used in assessing the severity of vehicular collisions on bridge piers are: type of pier protection, type of pier construction, number of pier elements per bent, and a measure of the angle of vehicular collision with bridge piers. Since these bridge elements cannot be queried from the LTBP InfoBridge™ portal (FHWA- LTBP 2021), a project specific application programming interface (API) program was developed for ease of data mining each of these five bridge elements. In this API the bridge is queried using Google Maps. As shown in Figure 3-16, the bridge location on Google Maps is assessed in terms of the bridge latitude and longitude, which are linked to the values queried from the LTBP InfoBridge™ portal (FHWA-LTBP 2021).

In Figure 3-17A and Figure 3-17B, the user progressively approaches the facility under the structure and queries the type of pier protection, pier construction, number of piers per bent, and the qualitative measure of the vehicular angle of collision with bridge piers. The process is completed for each data entry by recording and saving the record on the API.

Original Photo: © 2022 Google® (see Acknowledgments page)

Figure 3-16. Photo. API aerial views with Google Maps.

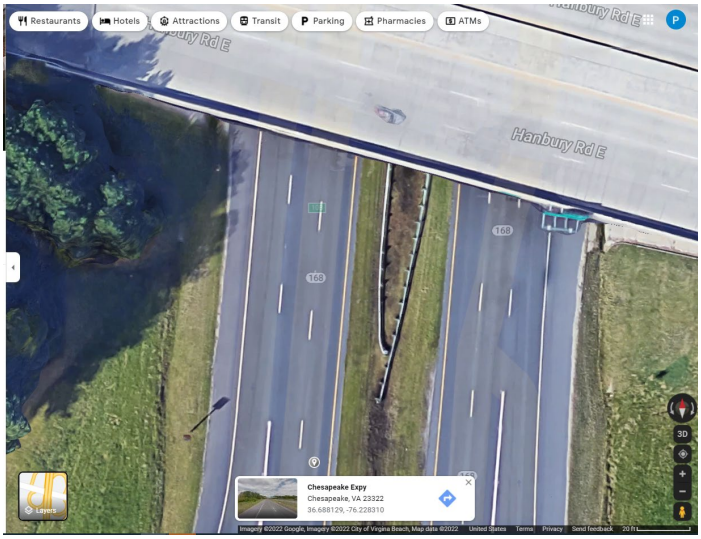

Original Photo: © 2022 Google® (see Acknowledgments page)

A. Facility under structure.

Original Photo: © 2022 Google® (see Acknowledgments page)

B. Street view image.

Figure 3-17. Photo. Example of an API close-up view with Google Maps.

3.1.2.1. Bridge Pier Protection

Bridge pier protection systems in Virginia can be categorized as steel barriers, concrete barriers, and combined concrete and steel barriers. Figure 3-18 shows a bridge with no pier protection where the pier is close to the roadway. Figure 3-19 shows a condition of no pier protection where the pier is far from the roadway. Figure 3-20 depicts the geographical distribution of bridges with pier protection system categories noted above. Figure 3-20 shows that nearly 80 percent of bridges over roadways have pier protection systems. The remaining 20 percent do not have pier protection systems.

Piers with no protection are more susceptible to significant damage from vehicular collisions. Figure 3-21 shows the geographical distribution of bridges with no pier protection. This figure shows a significant number of bridges with no pier protection are in regions near Washington, Richmond, Roanoke, and Norfolk with significant ADT and ADTT.

Original Photo: © 2022 Google® (see Acknowledgments page)

Figure 3-18. Photo. Example of no pier/abutment protection and a HRC < 30.0 ft.

Original Photo: © 2022 Google® (see Acknowledgments page)

Figure 3-19. Photo. Example of no pier/abutment protection and a HRC > 30.0 ft.

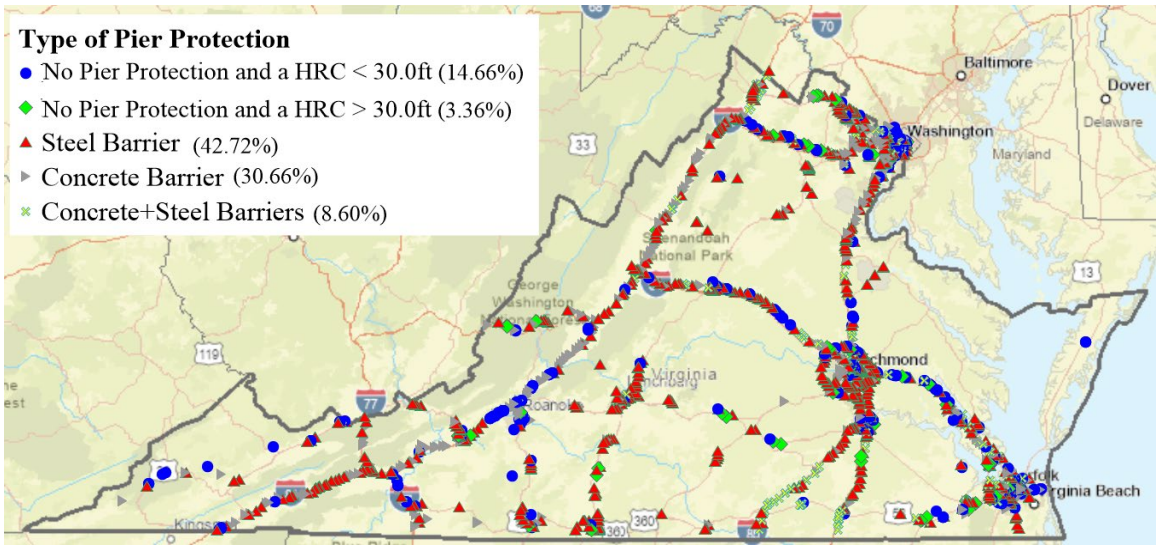

Note: Data overlay on Original Map: © 2022 TomTom (see Acknowledgments page).

Figure 3-20. Graph. Map of bridges according to pier protection.

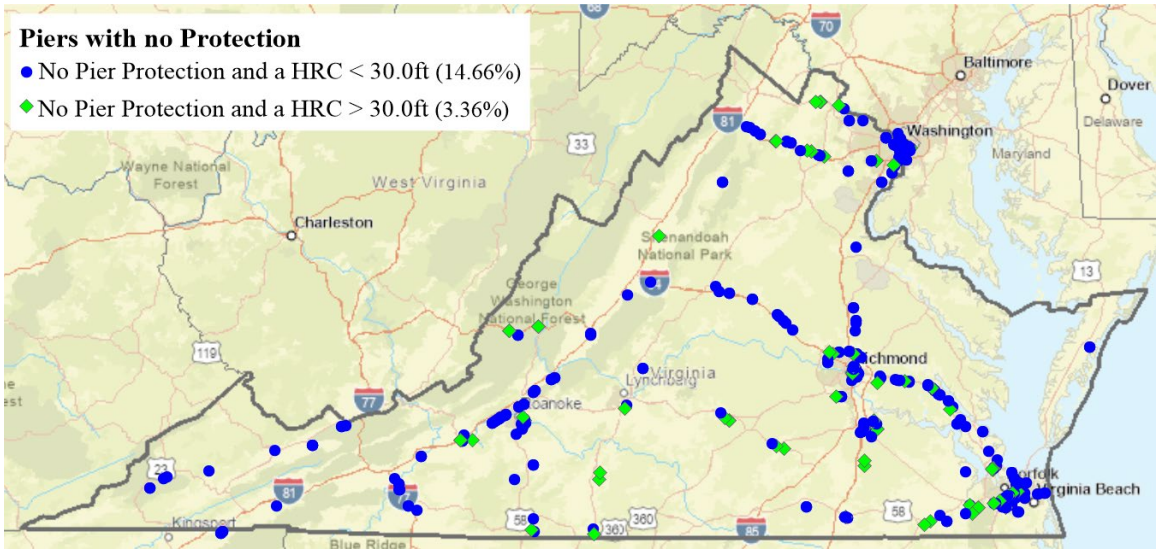

Note: Data overlay on Original Map: © 2022 TomTom (see Acknowledgments page).

Figure 3-21. Graph. Map of bridges with no pier protection.

3.1.2.2. Bridge Pier Construction

This study includes the main forms of pier construction in Virginia, which are: circular reinforced concrete (RC) bridge pier columns, rectangular RC bridge pier columns, RC bridge pier walls and bridge pier steel portal frames. Figure 3-26 depicts the geographical distribution for these types of pier construction. This figure shows that bridge pier RC circular columns constitute nearly 73.23 percent of all bridge pier columns and are widely dispersed throughout Virginia. Next, rectangular RC bridge pier columns are nearly 18.68 percent of the Virginia bridge inventory, followed by RC bridge pier walls at 7.8 percent, and steel shapes constitute 0.29 percent or 6 bridges.

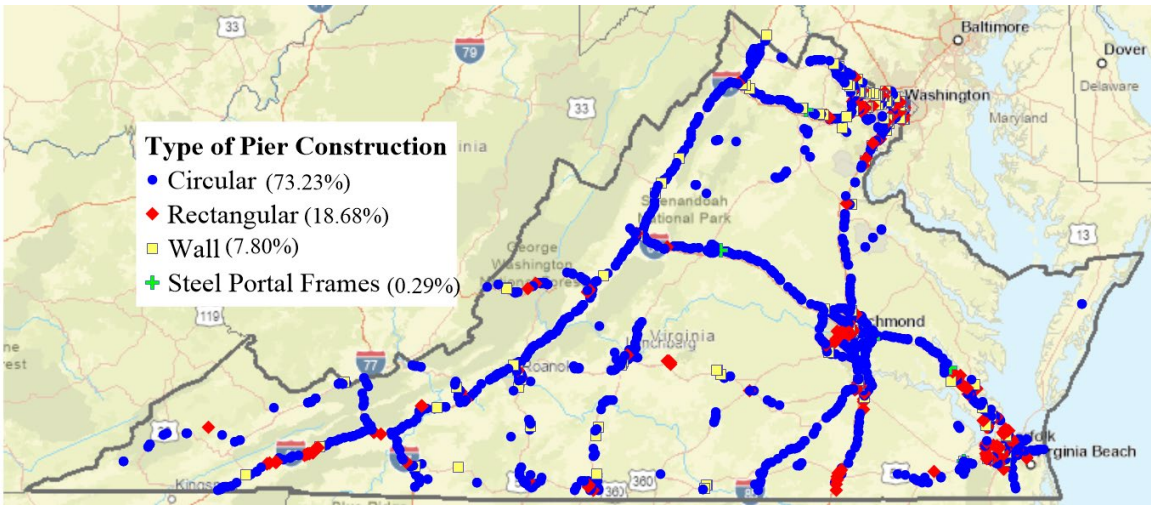

Note: Data overlay on Original Map: © 2022 TomTom (see Acknowledgments page)

Figure 3-22. Graph. Map of bridges based on type of bridge pier construction.

3.1.2.3. Number of Bridge Elements per Pier

The number of bridge elements per pier is critical in assessing the vulnerabilities of bridges against vehicular collisions. Bents with higher number of columns increase the resistance for the superstructure against disproportionate collapse. The literature review discussed how to evaluate disproportionate collapse by removing any column in the pier system including the combined full dead load with a load factor of 1.1 and a live load in the permanent travel lanes with a load factor of 1. Figure 3-27 depicts the geographical distribution of bridge elements per pier. As shown in the figure, the largest percentage of these bridges, 38.01 percent, have 3 bridge elements per pier.

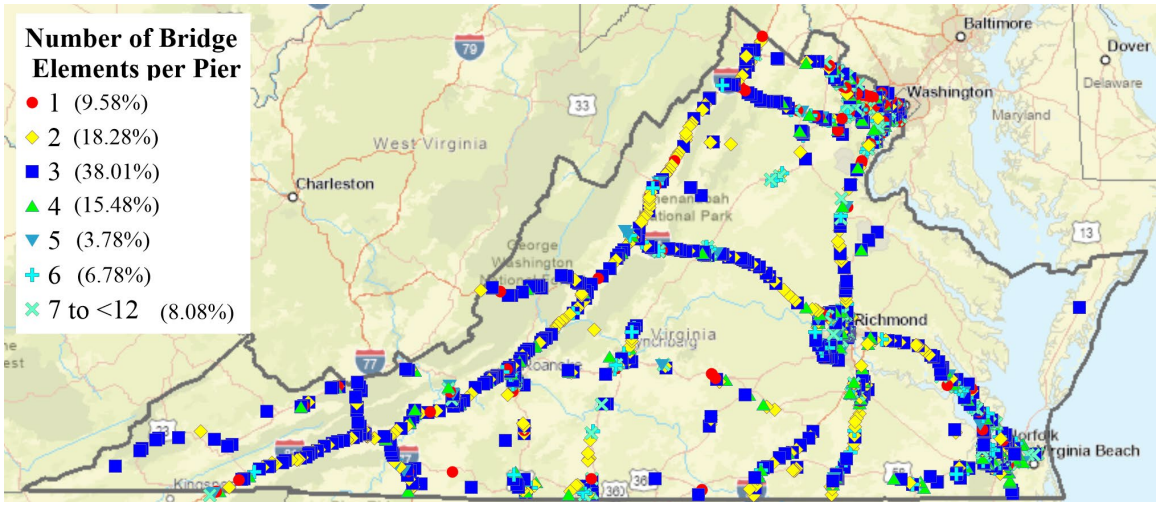

Note: Data overlay on Original Map: © 2022 TomTom (see Acknowledgments page)

Figure 3-23. Graph. Map of bridges based on number of bridge elements per pier.

3.1.2.4. Horizontal Curve Radius (HCR)

AASHTO LRFD BDS, 9th Edition3 Table C3.6.5.1-1 shows the site-specific adjustment factor, N_i (AASHTO 2020) in terms of the horizontal curve radius of the roadway under the bridge. Based on this table, horizontal curve radius (HCR) was categorized as *Low* (less than 10,000 feet), *Moderate* (between 432 and 10,000 feet), and *Sharp* (less than 432 feet), as shown Figure 3-24, Figure 3-25, and Figure 3-26 respectively. Figure 3-27 depicts the geographical distribution of each of these categories.

Original Photo: © 2022 Google® (see Acknowledgments page)

Figure 3-24. Photo. Example of *Low* curvature of driving lane below structure.

Original Photo: © 2022 Google® (see Acknowledgments page)

Figure 3-25. Photo. Example of *Moderate* curvature of driving lane below structure.

Original Photo: © 2022 Google® (see Acknowledgments page)

Figure 3-26. Photo. Example of *Sharp* curvature of driving lane below structure.

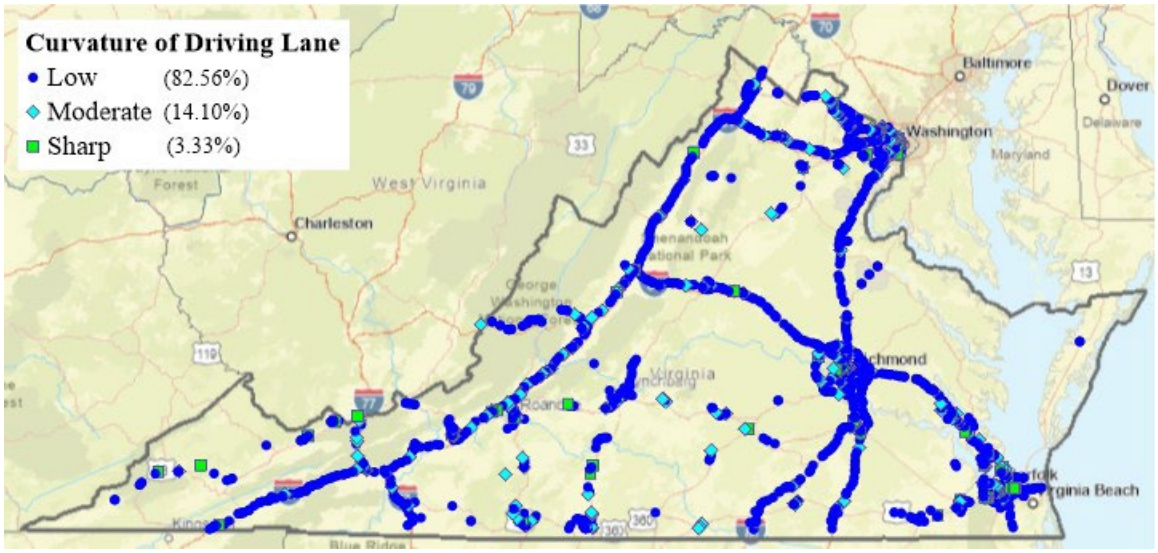

Note: Data overlay on Original Map: © 2022 TomTom (see Acknowledgments page).

Figure 3-27. Graph. Map of bridges based on curvature of driving lanes below structure.

3.2. FREQUENCY AND SEVERITY OF TRAFFIC COLLISIONS

This section discusses how the information of traffic states at present and past time steps predict a specific type of collision at the next time step. This is accomplished analyzing a specified data set between 2011 and 2016 and in the bounded location of Virginia. Collision data and traffic detector data are linked to bridge data information.

3.2.1. Virginia Department of Transportation Detector Data

Traffic detector data from 2011 to 2016 in Virginia was queried from over 700 detector stations maintained by the Virginia Department of Transportation (VDOT). The geographical distribution of the active detector stations is depicted in Figure 3-28. Depending on the types of detectors deployed at the stations, these detectors continuously register the number of vehicles passing and

assign them in incremental speed bins for every 5- or 15-minute interval. The data was used to determine the annual average daily traffic (AADT), as shown in Figure 3-29. This figure shows that there is a continuous increase in traffic since 2014.

The AADT was averaged over the stations in each jurisdiction (i.e., county). The roadways in and between the three major metropolitan areas, the Northern Virginia Area, the Richmond Metropolitan Area, and the Virginia Beach-Norfolk-Newport News Metropolitan Area are exposed to more traffic in general. These areas, the eastern freeway and urban roadway links, are more congested.

To further understand the relation between collision frequency and AADT, collisions within a half-mile range from the detector stations were extracted and discussed in Section 4.2 of this report. This spatial correlation between the detector data and the collision data is relevant to this study because the AADT obtained at the detector station locations can only evaluate the traffic operations associated with their corresponding local roadway segments.

Note: Data overlay on Original Map: © 2022 TomTom (see Acknowledgments page).

Figure 3-28. Graph. Geographical distribution of traffic detector stations in Virginia.

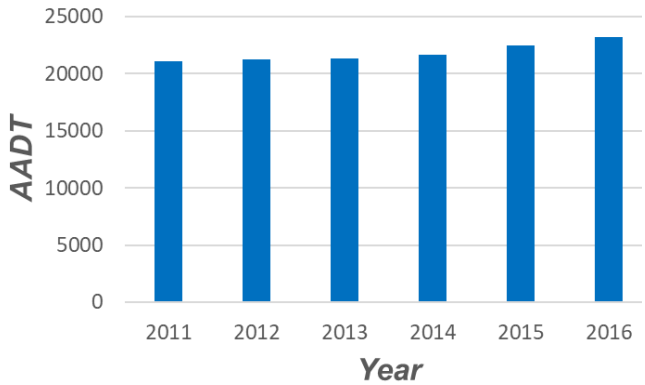

Figure 3-29. Chart. 2011-2016 traffic detector data based AADT in Virginia.

3.2.2. Virginia Department of Motor Vehicles Collision Data

3.2.2.1. Geographical Distribution of Collision Data

Figure 3-30 shows the geographical distribution of vehicular collisions within a one-mile distance to a bridge crossing over traffic lanes in either direction of travel from traffic detector data in Virginia from 2011-2016, provided by the Virginia Department of Motor Vehicles (Virginia DMV). Figure 3-31 shows the collision data subdivided and grouped in categories of increasing levels of traffic collisions. Collisions were recorded and maintained by gathering data from police reports and transportation agencies responsible for maintaining the associated roadway sections. The information includes the time of the collision, the location of each reported collision, and the collision severity. Binary information (i.e., Yes or No) whether heavy vehicles and pedestrians were involved is reported. This information was associated with the speed distributions extracted from the detector data and matched by geographical coordinates and time of occurrence for the selected 17 bridges. This is outlined in Section 4.1 of this report.

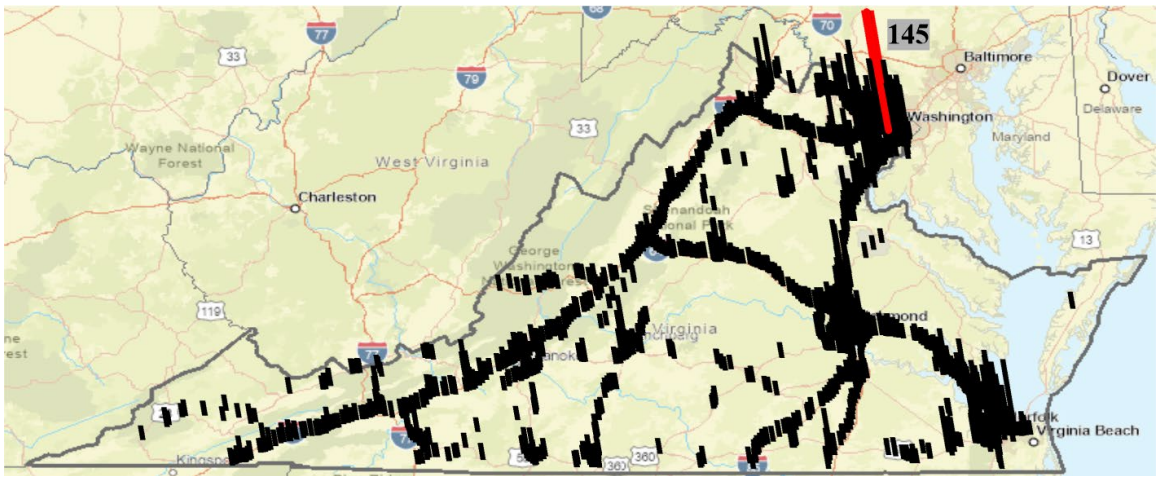

Note: Data overlay on Original Map: © 2022 TomTom (see Acknowledgments page)

Figure 3-30. Graph. Map of vehicular collisions within one mile of piers.

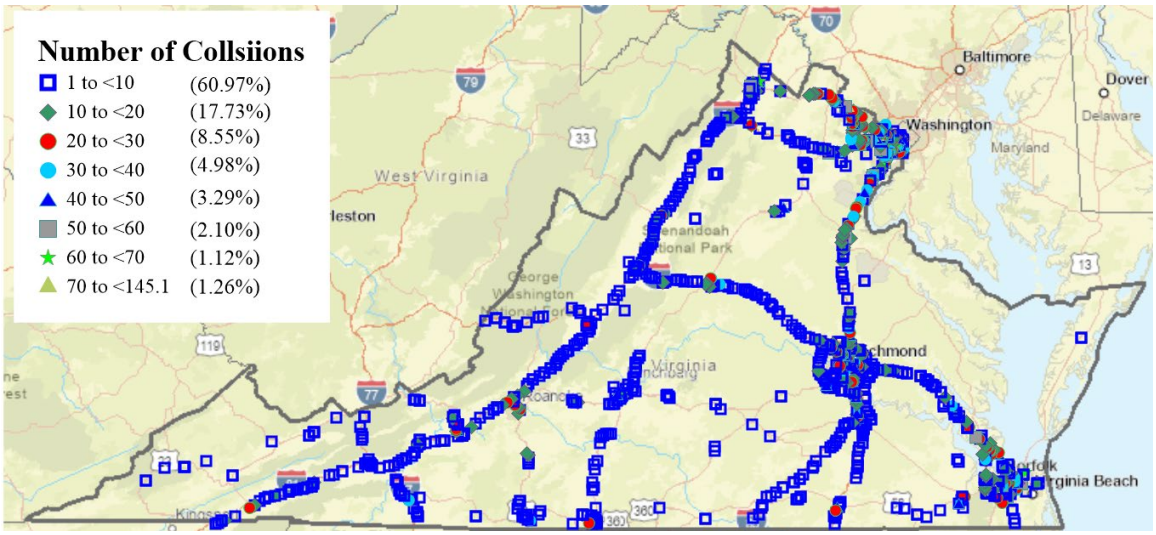

Note: Data overlay on Original Map: © 2022 TomTom (see Acknowledgments page)

Figure 3-31. Graph. Geographical distribution of all traffic collisions in Virginia.

3.2.2.2. Collisions Distribution According to Severity Levels K through O

The 2011-2016 collision data were provided by the Virginia Department of Motor Vehicles (Virginia DMV) with descriptive information including collision occurrence time, location of collision site, and the corresponding severity level. The KABCO Injury Classification Scale adopted in Virginia (FHWA 2022) categorizes collision severities as follows:

- K: Dead
- A: Serious Injury
- B: Minor/Possible Injury
- C: No Apparent Injury
- O: No Injury (driver only)

Figure 3-32 presents the percentages of collisions with different severity levels. Collisions in severity level of O are the most prevailing ones, followed by collisions in severity levels of B, C, A, and K. Figure 3-33, Figure 3-34, and Figure 3-35 present the spatial distributions in Virginia for all documented collisions that were previously presented in Figure 3-30. Figure 3-33 shows major collisions (severity levels K and A). Figure 3-34 shows minor collisions (severity levels B and C). Figure 3-35 shows the collisions with property damage only (severity level O).

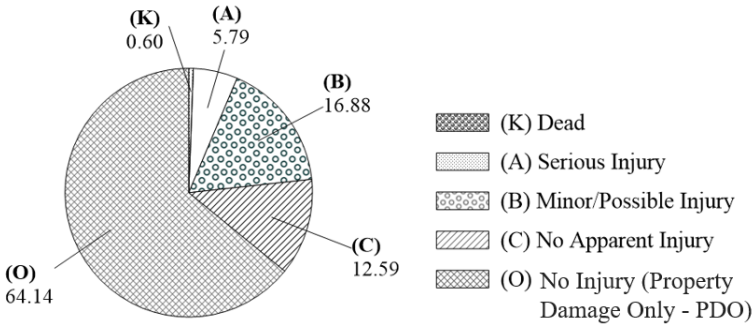

Note: Data is for the period from 2011-2016.

Figure 3-32. Charts. Percentage of collisions with severity levels K through O.

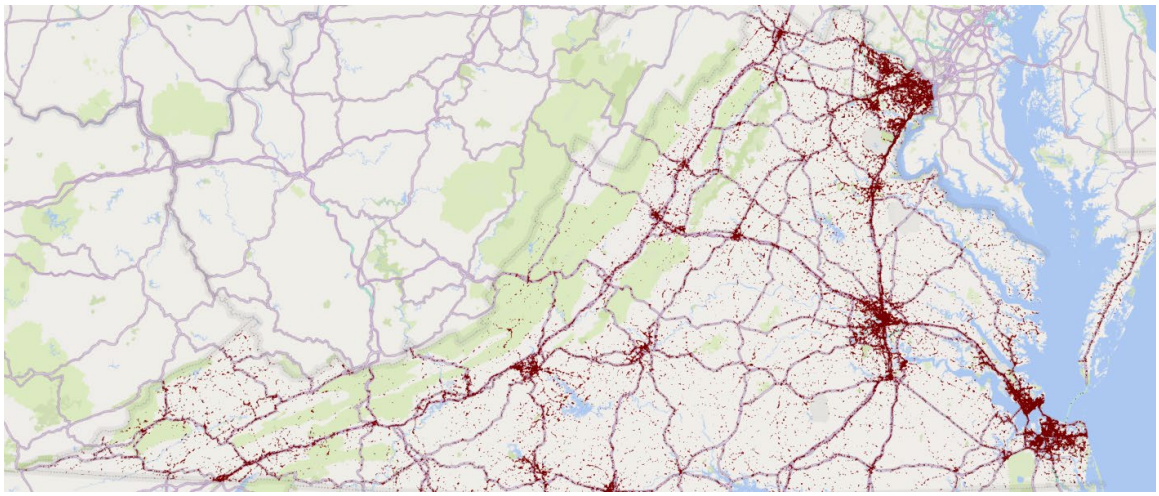

Note: Original Map: © 2022 TomTom (see Acknowledgments page)

Figure 3-33. Graph. Spatial distribution of documented collisions: Severity levels K and A.

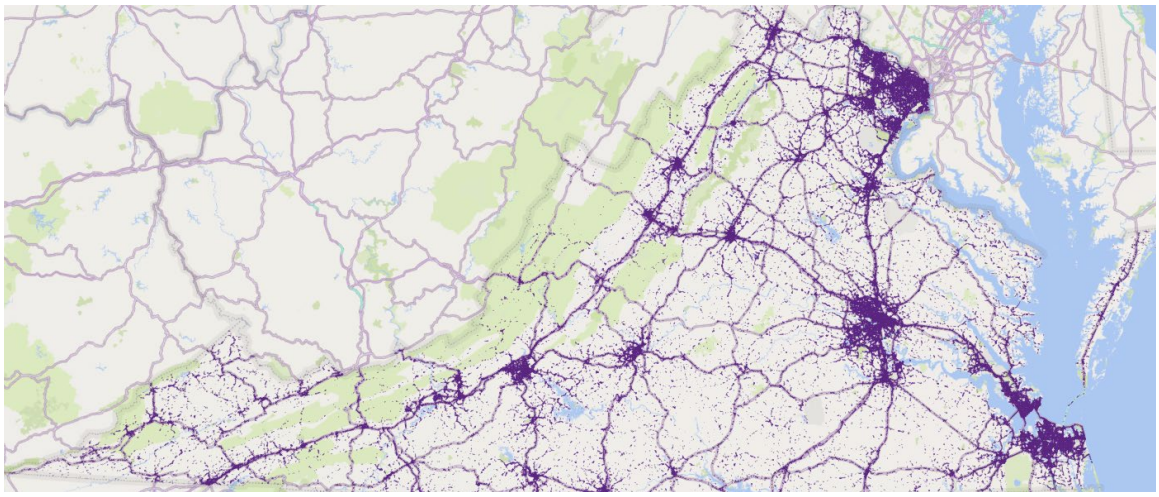

Note: Original Map: © 2022 TomTom (see Acknowledgments page)

Figure 3-34. Graph. Spatial distribution of documented collisions: Severity levels B and C.

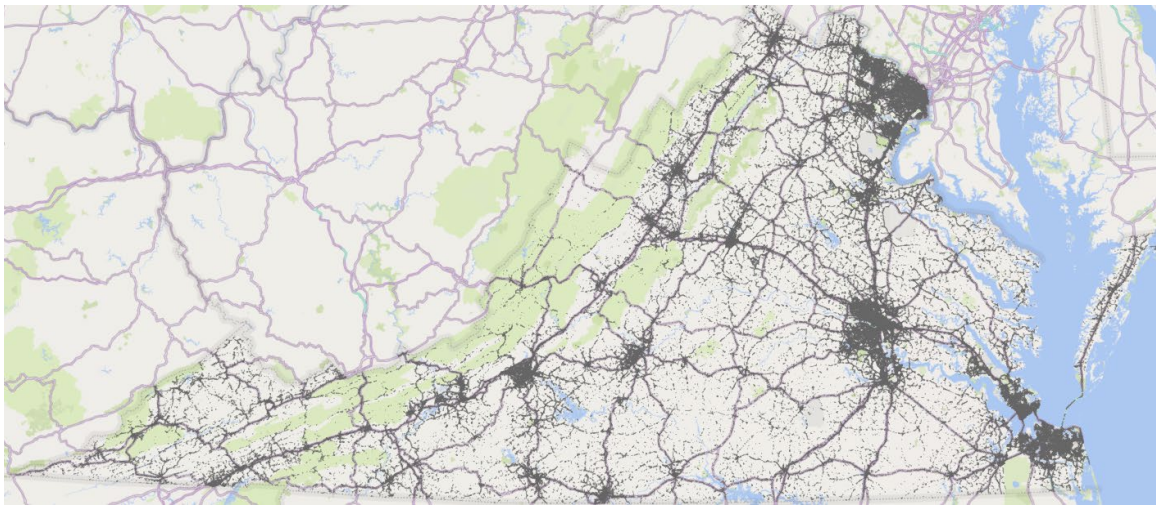

Note: Original Map: © 2022 TomTom (see Acknowledgments page)

Figure 3-35. Graph. Spatial distribution of documented collisions: Severity level O.

CHAPTER 4 - HEAVY TRUCK COLLISIONS STOCHASTIC MODELS

This chapter outlines a possible stochastic methodology for quantifying the probability of bridge failure against heavy truck collisions. This methodology outlines the stochastic nature of the following variables:

- Individual weight and speed of heavy trucks circulating in traffic flows.
- Frequency of heavy truck collisions at a given bridge location and its direct impact on bridge safety.
- Parametric impulse loading functions associated with the intensity of the collisions between heavy trucks and bridge piers/girders.
- Strain rate effects on material properties from the resulting impact loads.

4.1. COMMONWEALTH OF VIRGINIA TEST BED STUDY SITES

In this research project, 17 bridges were selected to form a test bed study site to investigate the analytical and econometrics approaches developed in this research program. These 17 bridges were selected based on its vulnerability to traffic collisions and structural failure. Stochastic models for traffic density were developed from traffic detector data from the Commonwealth of Virginia. There are over 700 active traffic detector stations distributed on the Virginia roadway network. These traffic detector stations were previously depicted in Figure 3-28. Maintained by the Virginia Department of Transportation (VDOT), these stations continuously register traffic flow and place them in different speed intervals (or bins). In this work traffic data from the 2011-2016 statewide traffic detector data was used in developing the heavy truck collision stochastic models. For each station, the numbers of vehicles in a series of incremental speed bins were archived every 5 or 15 minutes (depending on the types of detector stations). The data was provided in a tabular form where rows correspond to different observation periods and columns correspond to different speed bins.

For side-fire radar detector stations, there are 15 specified speed bins with the following range sequence: [0, 15), [15, 25), [25, 30), [30, 35), [35, 40), [40, 45), [45, 50), [50, 55), [55, 60), [60, 65), [65, 70), [70, 75), [75, 80), [80, 85), and [85, 225)—in miles per hour (MPH). For inductive loop detector stations, there are 21 specified speed bins with the following range sequence: [0, 5), [5, 10), [10, 15), [15, 20), [20, 25), [25, 30), [30, 35), [35, 40), [40, 45), [45, 50), [50, 55), [55, 60), [60, 65), [65, 70), [70, 75), [75, 80), [80, 85), [85, 90), [90, 95), [95, 100), and [100, 147) in MPH. In the above range sequences the number in next to the parenthesis means that the number is to be excluded.

Based on the spatial pairing between bridges in Virginia and traffic detector stations, 17 study sites reported in Figure 4-1 were chosen to form a test bed study site. The selection sites featured the following characteristics:

- A bridge intersecting a roadway segment with the bridge pier elements exposed to traffic under the bridge structure.

- The roadway segment monitored by a detector station with vehicle classification and the detector station is in proximity to (i.e., within the 0.1 mile range from) the intersecting point of the bridge and the roadway segment, and the bridge piers not protected by high concrete barriers (i.e., concrete barriers with a height greater than 24 inches).

These two features reflect the following representative distributions:

- Speed of vehicles (or trucks in particular) traversing under the bridges.

- Volume of trucks traversing under the bridges.

The 17 study sites are illustrated in the next section. The sites are presented in terms of route, GPS, and traffic detector location. Each bridge site is further depicted by a photo extracted from Google Maps.

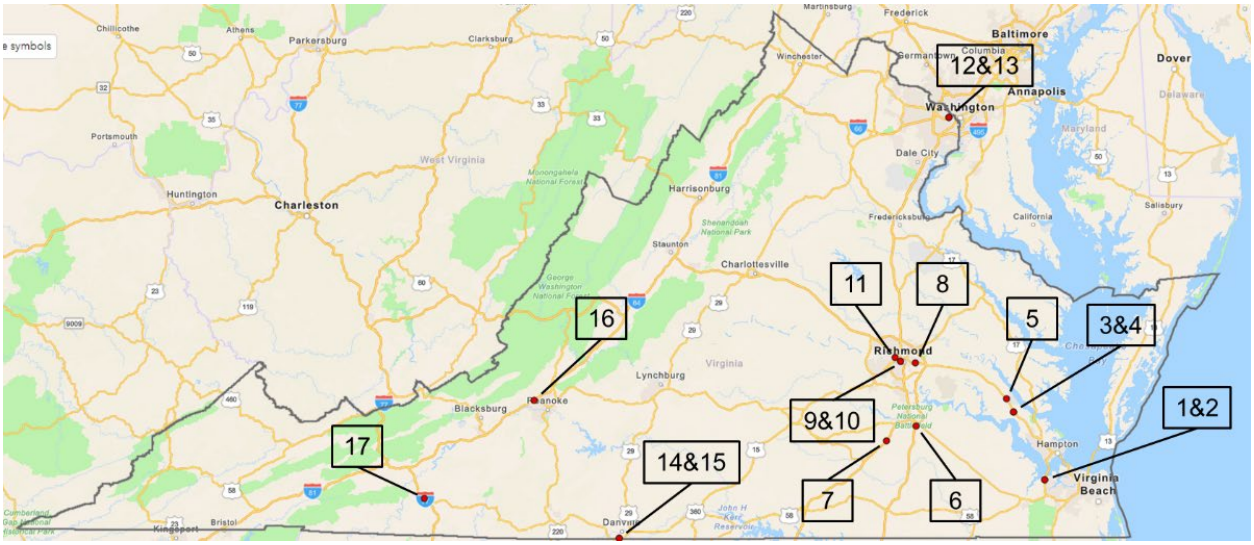

Data overlay on Original Map: Google Earth Toolbox ® MATLAB (see Acknowledgments page).

Figure 4-1. Graph. Geographical distribution of bridges at the 17 study sites.

4.1.1. Test Bed Study Site Bridge No. 1

- Route: I-664E, NBI Structure Number: 23086
- Two individual bridges in parallel:
  - Bridge 1 and 2 GPS Coordinates: (36.87627, -76.43364) (36.87642, -76.43362)
- Detector GPS Coordinates: (36.87584, -76.43356)

Original Photo: © 2022 Google® (see Acknowledgments page)

Figure 4-2. Photo. Test Bed Study Site Bridge No. 1 on I-664E.

4.1.2. Test Bed Study Site Bridge No. 2

- Route: I-664W, NBI Structure Number: 23087
- Two individual bridges in parallel:
  - Bridge 1 and 2 GPS Coordinates: (36.87627, -76.43364) (36.87642, -76.43362)
- Detector GPS Coordinates: (36.87601, -76.43306)

Original Photo: © 2022 Google® (see Acknowledgments section)

Figure 4-3. Photo. Test Bed Study Site Bridge No. 2 on route I-664W.

4.1.3. Test Bed Study Site Bridge No. 3

- Route: VA-199E, NBI Structure Number: 19881
- Bridge GPS Coordinates: (37.25515, -76.653)
- Detector GPS Coordinates: (37.25507, -76.6534)

Original Photo: © 2022 Google® (see Acknowledgments page)

Figure 4-4. Photo. Test Bed Study Site Bridge No. 3 on route VA-199E.

4.1.4. Test Bed Study Site Bridge No. 4

- Route: VA-199W, NBI Structure Number: 19881
- Bridge GPS Coordinates: (37.25515, -76.653)
- Detector GPS Coordinates: (37.25507, -76.6534)

Original Photo: © 2022 Google® (see Acknowledgments section)

Figure 4-5. Photo. Test Bed Study Site Bridge No. 4 on route VA-199W.

4.1.5. Test Bed Study Site Bridge No. 5

- Route: I-64W, NBI Structure Number: 19871
- Bridge GPS Coordinates: (37.32907, -76.7055)
- Detector GPS Coordinates: (37.33022, -76.70577)

Original Photo: © 2022 Google® (see Acknowledgments page)

Figure 4-6. Photo. Test Bed Study Site Bridge No. 5 on route I-64W.

4.1.6. Test Bed Study Site Bridge No. 6

- Route: I-295W, NBI Structure Number: 23419
- Bridge GPS Coordinates: (37.17803, -77.34015)
- Detector GPS Coordinates: (37.17694, -77.33948)

Original Photo: © 2022 Google® (see Acknowledgments section)

Figure 4-7. Photo. Test Bed Study Site Bridge No. 6 on route I-295W.

4.1.7. Test Bed Study Site Bridge No. 7

- Route: I-85N, NBI Structure Number: 6013
- Bridge GPS Coordinates: (37.09486, -77.55076)
- Detector GPS Coordinates: (37.09365, -77.55055)

Original Photo: © 2022 Google® (see Acknowledgments page)

Figure 4-8. Photo. Test Bed Study Site Bridge No. 7 on Route I-85N.

4.1.8. Test Bed Study Site Bridge No. 8

- Route: I-64E, NBI Structure Number: 9628
- Bridge GPS Coordinates: (37.53103, -77.34466)
- Detector GPS Coordinates: (37.53088, -77.34335)

Original Photo: © 2022 Google® (see Acknowledgments section)

Figure 4-9. Photo. Test Bed Study Site Bridge No. 8 on route I-64E.

4.1.9. Test Bed Study Site Bridge No. 9

- Route: VA-195S, NBI Structure Number: 21335
- Bridge GPS Coordinates: (37.54262, -77.45285)
- Detector GPS Coordinates: (37.54271, -77.45383)

Original Photo: © 2022 Google® (see Acknowledgments page)

Figure 4-10. Photo. Test Bed Study Site Bridge No. 9 on route VA-195S.

4.1.10. Test Bed Study Site Bridge No. 10

- Route: VA-195N, NBI Structure Number: 21335
- Bridge GPS Coordinates: (37.54262, -77.45285)
- Detector GPS Coordinates: (37.54315, -77.45388)

Original Photo: © 2022 Google® (see Acknowledgments page)

Figure 4-11. Photo. Test Bed Study Site Bridge No. 10 on route VA-195N.

4.1.11. Test Bed Study Site Bridge No. 11

- Route: I-195S, NBI Structure Number: 21310
- Bridge GPS Coordinates: (37.56037, -77.48891)
- Detector GPS Coordinates: (37.55927, -77.48938)

Original Photo: © 2022 Google® (see Acknowledgments page)

Figure 4-12. Photo. Test Bed Study Site Bridge No. 11 on route I-195S.

4.1.12. Test Bed Study Site Bridge No. 12

- Route: I-66E, NBI Structure Number: 47
- Bridge GPS Coordinates: (38.88923, -77.10831)
- Detector GPS Coordinates: (38.88974, -77.10675)

Original Photo: © 2022 Google® (see Acknowledgments page)

Figure 4-13. Photo. Test Bed Study Site Bridge No. 12 on route I-66E.

4.1.13. Test Bed Study Site Bridge No. 13

- Route: I-66W, NBI Structure Number: 47
- Bridge GPS Coordinates: (38.88923, -77.10831)
- Detector GPS Coordinates: (38.89008, -77.10712)

Original Photo: © 2022 Google® (see Acknowledgments page)

Figure 4-14. Photo. Test Bed Study Site Bridge No. 13 on route I-66W.

4.1.14. Test Bed Study Site Bridge No. 14

- Route: US-29N, NBI Structure Number: 13816
- Bridge GPS Coordinates: (36.54612, -79.43221)
- Detector GPS Coordinates: (36.5468, -79.43102)

Original Photo: © 2022 Google® (see Acknowledgments page)

Figure 4-15. Photo. Test Bed Study Site Bridge No. 14 on route US-29N.

4.1.15. Test Bed Study Site Bridge No. 15

- Route: US-29S, NBI Structure Number: 13816
- Bridge GPS Coordinates: (36.54612, -79.43221)
- Detector GPS Coordinates: (36.5468, -79.43102)

Original Photo: © 2022 Google® (see Acknowledgments page)

Figure 4-16. Photo. Test Bed Study Site Bridge No. 15 on route US-29S.

4.1.16. Test Bed Study Site Bridge No. 16

- Route: I-81N, NBI Structure Number: 14968
- Bridge GPS Coordinates: (37.32423, -80.03333)
- Detector GPS Coordinates: (37.32338, -80.03429)

Original Photo: © 2022 Google® (see Acknowledgments page)

Figure 4-17. Photo. Test Bed Study Site Bridge No. 16 on route I-81N.

4.1.17. Test Bed Study Site Bridge No. 17

- Route: I-77N, NBI Structure Number: 4717
- Bridge GPS Coordinates: (36.76926, -80.80453)
- Detector GPS Coordinates: (36.76912, -80.80359)

Original Photo: © 2022 Google® (see Acknowledgments page)

Figure 4-18. Photo. Test Bed Study Site Bridge No. 17 on route I-77N.

4.2. HEAVY TRUCK TRAFFIC COLLISIONS

As previously stated in Section 2.1.1 of this report, AASHTO LRFD BDS, 8th Edition[1] (AASHTO 2017) requires that abutments and piers located within a distance of 30.0 ft to the edge of roadway are investigated for collision, unless the Owner determines that site conditions indicate otherwise. The next section outlines bridge collision stochastic models using a compilation of speed distributions and truck weights. The speed distributions and truck weights information are also used to develop parametric impulse loading functions.

4.2.1. Speed Distribution

Vehicle speeds observed at a specific location during a sufficiently long observation period (e.g., one hour) may follow the Extreme Value Type I distribution (i.e., Gumbel distribution) as illustrated in Figure 4-19.

As shown in Figure 4-19, the observed distribution of vehicle speeds is asymmetric and more left-tailed given the posted speed limit. The left-tailed (or maximum-type) Gumbel distribution may capture such asymmetry. Furthermore, the corresponding location and scale parameters of Gumbel distribution can be used to represent the central tendency and the variance level of the speed values. Figure 4-20 presents the respective distributions of the location and scale parameters of the Gumbel distributed hourly vehicle speed distributions observed at a specific location during the six-year period from 2011 to 2016. The respective distributions of the location and scale parameters may also follow the Gumbel distribution. The distribution of

location parameter is of the maximum type which indicates the central tendency of speed distribution is more restricted from reaching higher values. Furthermore, the distribution of scale parameter is of the minimum type which indicates the variance level of speed distribution is more restricted from reaching lower values.

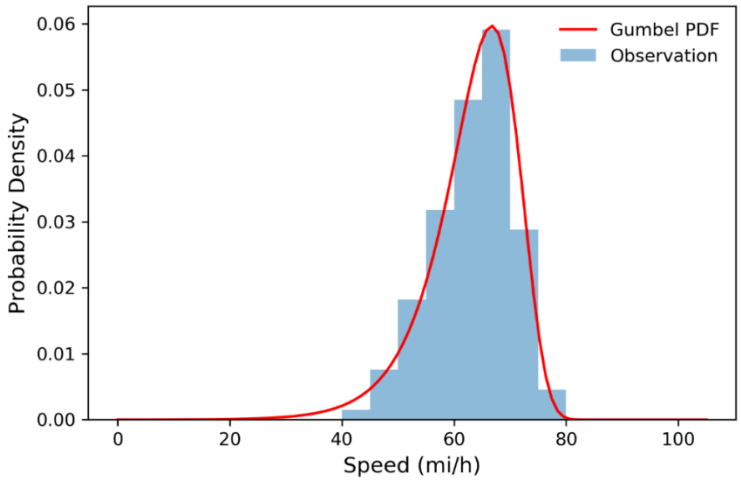

Note: This graph was developed using data query for Site No 15 (see Table 4-1).
This table indicates that for this site the posted speed limit is 65 mph.

Figure 4-19. Graph. Sample hourly vehicle speed distribution.

For Gumbel distribution, the location parameter μ is also the mode of the distribution, which represents the peak of the probability density function, or the point with the greatest probability density. The scale parameter β is a measure of dispersion parameter of the Gumbel distribution. This follows the convention of notation for a statistical distribution with two parameters or normal distribution.

Spearman's correlation test was performed at each of the 17 study sites and the resulting Spearman's correlation coefficient r is presented in Table 4-1. The adopted values of the location and scale parameters of the representative speed distribution at each study site are provided in Table 4-1.

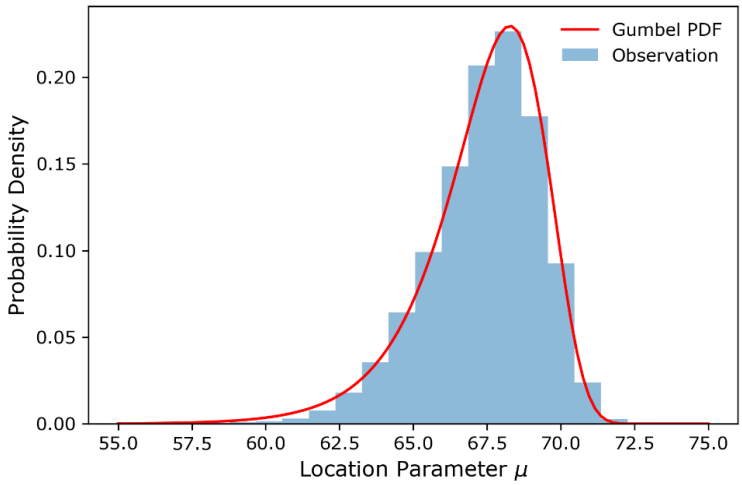

A. Location parameter probability distribution.

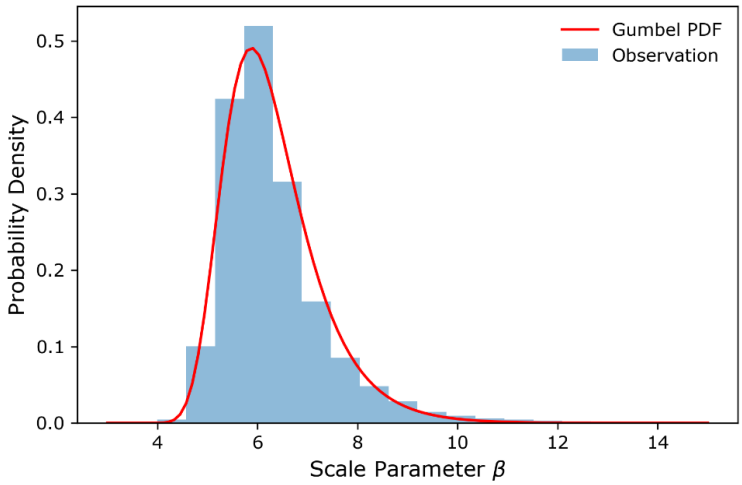

B. Scale parameter probability distribution.

Note: This graph was developed using data query for Site No 15 (see Table 4-1). This table indicates that for this site the posted speed limit is 65 mph.

Figure 4-20. Chart. Gumbel distributions for different hourly vehicle speed distributions.

Table 4-1. Speed distribution information for the 17 study sites.

No.	Posted Speed Limit (mph)	Adopted Speed Distribution Location Parameter μ	Adopted Speed Distribution Scale Parameter β	Spearman's r between μ and β
1	60	70.4	6.13	0.050
2	60	70.0	6.04	0.058
3	55	61.4	5.65	0.329
4	55	62.7	5.06	0.119
5	70	74.1	5.22	-0.168
6	70	74.2	5.36	0.007
7	70	75.7	5.92	-0.224
8	65	72.2	5.89	0.180
9	55	59.5	5.70	0.099
10	55	60.0	5.42	-0.078
11	55	63.7	5.42	-0.017
12	55	63.7	6.04	0.020
13	55	63.3	6.38	-0.375
14	65	69.1	5.39	0.064
15	65	68.2	5.89	-0.354
16	60	66.4	5.60	0.069
17	65	71.4	5.69	0.129

4.2.2. Weight Distribution

The traffic detector stations with vehicle classification categorize the passing through vehicles into the following 15 categories:

- Motorcycles
- Passenger Cars
- Two Axle 4 Tire Single Unit Vehicles
- Buses
- Two Axle 6 Tire Single Unit Trucks
- Three Axle Single Unit Trucks
- Four or More Axle Single Unit Trucks
- Four Axle or Fewer Single Trailers

- Five Axle Single Trailers
- Six or More Axle Single Trailers
- Five Axle or Fewer Multi-Trailers
- Six Axle Multi-Trailers
- Seven or More Axle Multi-Trailers
- Other
- Unclassified

The above classification is mainly based on the number of axles rather than the gross weight of vehicles. The New York City (NYC) Weigh-in-Motion (WIM) OpenData (NYC WIM, 2024) provides a rigorous source of data regarding axle weights and gross vehicle weights registered from sensors installed on all six lanes of the Brooklyn-Queens Expressway at Pearl Street, Brooklyn. These types of sensors have not yet been installed in Virginia. Data extracted from the city of New York WIM OpenData from 2019 to 2024 (NYC WIM, 2024) and presented in Table 4-2 were utilized in supplementing the weight distribution of trucks/trailers at the chosen test bed study sites. As shown in Table 4-2, this research focuses on trucks and trailers in the Two Axle 6 Tire Single Unit Trucks category and the outlined categories of trucks/trailers with three or more axles (i.e., medium-duty and heavy-duty vehicles). Market share statistics were obtained from Table 4-2 and are presented in Table 4-3 as percent of totals per the listed categories. Subsequently, Table 4-3 in combination with the annual average truck traffic volumes at the study sites presented in Table 4-4 were used in developing an assumed truck weight distribution in percent at the 17 study sites. This assumed weight distribution is presented in Table 4-5. Annual average truck traffic volume was queried from over 700 detector stations maintained by the Virginia Department of Transportation (VDOT) from 2011 to 2016.

Table 4-2. Truck weight distribution from City of New York WIM OpenData from 10/11/2019 to 01/31/2024

Truck Type	less than 14,000 lb	14,001 to 16,000 lb	16,001 to 19,500 lb	19,501 to 26,000 lb	26,001 to 33,000 lb	33,001 to 50,000 lb	50,001 to 58,000 lb	58,001 to 66,000 lb	66,001 to 74,000 lb	more than 74,001 lb
Two Axle 6 Tire Single Unit Trucks	783,915	190,166	438,301	1,229,583	525,511	79,402	2,024	706	318	6,287
Three Axle Single Unit Trucks	38,895	21,822	55,399	150,998	198,046	587,143	117,694	33,600	8,349	7,055
Four or More Axle Single Unit Trucks	1,536	1,403	3,813	10,007	14,495	35,220	20,982	27,909	24,936	20,843
Four Axle or Fewer Single Trailers	36,241	9,710	15,611	40,746	71,339	302,571	115,660	39,045	8,881	4,167
Five Axle Single Trailers	4,031	4,443	12,320	43,165	109,347	543,704	336,110	292,245	293,879	624,576
Six or More Axle Single Trailers	247	234	702	2,308	4,177	18,290	11,520	11,825	9,324	81,534
Five Axle or Fewer Multi-Trailers	257	248	642	1,890	2,293	11,106	9,814	13,646	18,859	22,709
Six Axle Multi-Trailers	265	256	695	1,620	1,931	4,834	4,438	5,838	5,461	2,061
Seven or More Axle Multi-Trailers	487	282	594	1,156	1,300	3,146	1,561	1,561	1,370	4,903

Data Source from New York City WIM OpenData (2024).

Table 4-3. Calculated truck weight distribution from City of New York WIM OpenData from 10/11/2019 to 01/31/2024

Truck Type	less than 14,000 lb	14,001 to 16,000 lb	16,001 to 19,500 lb	19,501 to 26,000 lb	26,001 to 33,000 lb	33,001 to 50,000 lb	50,001 to 58,000 lb	58,001 to 66,000 lb	66,001 to 74,000 lb	more than 74,001 lb
Two Axle 6 Tire Single Unit Trucks	24.07%	5.84%	13.46%	37.76%	16.14%	2.44%	0.06%	0.02%	0.01%	0.19%
Three Axle Single Unit Trucks	3.19%	1.79%	4.54%	12.39%	16.25%	48.17%	9.65%	2.76%	0.68%	0.58%
Four or More Axle Single Unit Trucks	0.95%	0.87%	2.37%	6.21%	9.00%	21.86%	13.02%	17.32%	15.47%	12.93%
Four Axle or Fewer Single Trailers	5.63%	1.51%	2.42%	6.33%	11.08%	46.99%	17.96%	6.06%	1.38%	0.65%
Five Axle Single Trailers	0.18%	0.20%	0.54%	1.91%	4.83%	24.02%	14.85%	12.91%	12.98%	27.59%
Six or More Axle Single Trailers	0.18%	0.17%	0.50%	1.65%	2.98%	13.05%	8.22%	8.44%	6.65%	58.17%
Five Axle or Fewer Multi-Trailers	0.32%	0.30%	0.79%	2.32%	2.81%	13.63%	12.05%	16.75%	23.15%	27.88%
Six Axle Multi-Trailers	0.97%	0.93%	2.54%	5.91%	7.05%	17.64%	16.20%	21.31%	19.93%	7.52%
Seven or More Axle Multi-Trailers	2.98%	1.72%	3.63%	7.07%	7.95%	19.23%	9.54%	9.54%	8.37%	29.97%

Table 4-4. Annual average truck/trailer traffic volumes at the study sites.

Site No.	Two Axle 6 Tire Single Unit Trucks	Three Axle Single Unit Trucks	Four or More Axle Single Unit Trucks	Four Axle or Fewer Single Trailers	Five Axle Single Trailers	Five Axle or Fewer Multi-Trailers	Six or More Axle Single Trailers	Six Axle Multi-Trailers	Seven or More Axle Multi-Trailers	Total
1	56,813	48,957	5,498	30,695	233,984	3,354	5,143	1,242	34	385,720
2	54,615	51,048	5,603	31,468	259,559	5,105	5,283	2,245	21	414,947
3	19,273	10,013	5,797	4,707	16,074	12	699	142	1	56,718
4	16,439	14,561	1,663	4,705	56,301	23	387	8	0	94,087
5	45,274	40,769	5,164	27,650	382,899	6,447	6,113	3,353	28	517,697
6	17,608	11,259	1,202	9,785	356,375	2,242	6,285	2,130	23	406,909
7	19,341	19,542	1,186	18,875	349,704	23,942	7,460	10,807	448	451,305
8	45,541	22,232	6,706	17,316	110,891	849	2,302	1,224	4	207,065
9	16,380	12,349	3,433	4,633	18,497	217	1,194	105	2	56,810
10	20,851	13,865	3,792	4,495	18,154	184	377	68	2	61,788
11	46,714	18,794	4,332	15,389	61,526	5,927	2,529	742	2	155,955
12	36,427	8,112	197	1,578	1,238	2	67	2	0	47,623
13	28,912	7,510	201	1,616	1,645	4	65	1	0	39,954
14	16,329	21,095	8,843	15,213	227,760	8,406	4,405	1,428	9	303,488
15	15,867	25,435	3,545	16,839	223,764	7,935	5,458	1,776	96	300,715
16	58,403	52,992	6,593	45,871	1,165,882	63,518	8,892	27,185	454	1,429,790
17	35,219	37,922	655	32,368	983,683	56,093	6,549	23,275	232	1,175,996

Data Source: Virginia Department of Transportation traffic detector data from 2011 to 2016.

Table 4-5. Assumed truck weight distribution in percent at the 17 study sites.

Site No	less than 14,000 lb	14,001 to 16,000 lb	16,001 to 19,500 lb	19,501 to 26,000 lb	26,001 to 33,000 lb	33,001 to 50,000 lb	50,001 to 58,000 lb	58,001 to 66,000 lb	66,001 to 74,000 lb	more than 74,001 lb
1	4.53%	1.35%	3.14%	8.94%	8.47%	25.44%	12.12%	9.24%	8.65%	18.12%
2	4.12%	1.25%	2.92%	8.33%	8.22%	25.56%	12.36%	9.54%	9.00%	18.70%
3	9.36%	2.57%	5.99%	16.75%	11.61%	22.48%	8.90%	6.59%	5.64%	10.10%
4	5.11%	1.51%	3.55%	10.09%	8.95%	25.05%	11.56%	8.81%	8.25%	17.14%
5	2.81%	0.90%	2.12%	6.17%	7.06%	24.94%	13.19%	10.71%	10.38%	21.72%
6	1.43%	0.52%	1.28%	3.89%	5.77%	24.04%	14.02%	11.92%	11.80%	25.33%
7	1.59%	0.59%	1.42%	4.21%	6.00%	24.20%	13.88%	11.97%	12.01%	24.12%
8	6.24%	1.74%	4.04%	11.45%	9.18%	23.51%	11.16%	8.57%	7.93%	16.16%
9	8.22%	2.32%	5.41%	15.15%	11.29%	24.51%	9.45%	6.63%	5.69%	11.34%
10	9.36%	2.60%	6.05%	16.95%	11.90%	23.59%	8.76%	6.05%	5.15%	9.59%
11	8.27%	2.23%	5.15%	14.50%	10.23%	22.07%	9.84%	7.39%	6.86%	13.47%
12	19.15%	4.83%	11.18%	31.28%	15.65%	12.36%	2.74%	1.11%	0.58%	1.12%
13	18.26%	4.64%	10.73%	30.02%	15.43%	13.84%	3.28%	1.41%	0.82%	1.57%
14	1.98%	0.70%	1.68%	4.94%	6.59%	25.15%	13.63%	11.38%	11.14%	22.82%
15	2.02%	0.72%	1.71%	5.01%	6.72%	25.67%	13.59%	11.11%	10.83%	22.62%
16	1.47%	0.55%	1.34%	4.02%	5.88%	24.11%	14.00%	12.11%	12.18%	24.36%
17	1.16%	0.47%	1.16%	3.54%	5.65%	24.10%	14.18%	12.33%	12.47%	24.94%

4.2.3. Truck-Related Collision Involvement Rate, Φ_T

Given collisions, especially those involving trucks, are low-frequency events, all traffic detector stations with vehicle classification in Virginia are leveraged to estimate an overall truck-related collision involvement rate, Φ_T. The rate Φ_T represents the number of truck-related collisions per million truck miles traveled as follows:

$$\Phi_T = \frac{\sum \widehat{N}_i}{\sum \widehat{V}_i \cdot L_i} \times 1{,}000{,}000 = \frac{756}{991{,}359{,}898} \times 1{,}000{,}000 = 0.7626 \qquad \textbf{(4-1)}$$

Where $\widehat{N}_i$ denotes the number of truck-related collisions occurring on Link i, $\widehat{V}_i$ denotes the volume of trucks traversing Link i, and L_i denotes the length of Link i in miles. Link i here is defined as the roadway stretch on which the ith traffic detector station with vehicle classification is deployed, bounded by the nearest upstream and downstream off-ramps (i.e., exits) from the detector station. Traffic volumes are assumed to remain constant along the links as detected by the corresponding detectors on the links.

In total, 402 links were examined, accounting for 1103 miles of roadways of the Virginia network. 756 truck-related collisions were identified on these links over roughly one billion truck miles traveled during the six-year period from 2011 to 2016 (given the available data on vehicle classification). Figure 4-21 illustrates the distribution of the 756 truck-related collisions on the 402 links being examined. Figure 4-22 illustrates a specific link on I-64W in Richmond City with detector deployment and truck-related collisions during the test period.

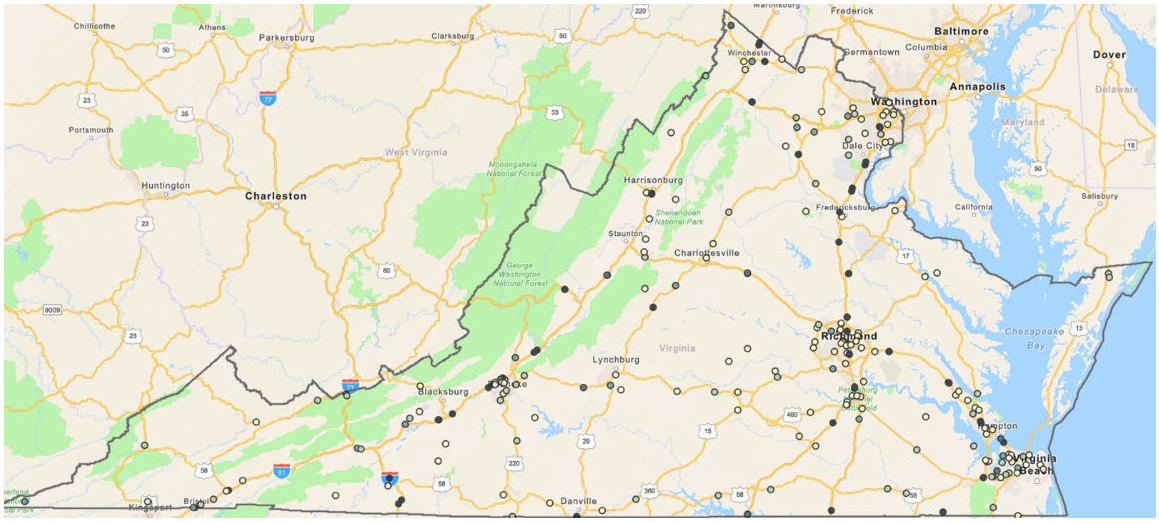

Data overlay on Original Map: © 2022 TomTom (see Acknowledgments page).

Figure 4-21. Graph. Distribution of truck-related collisions on the links examined.

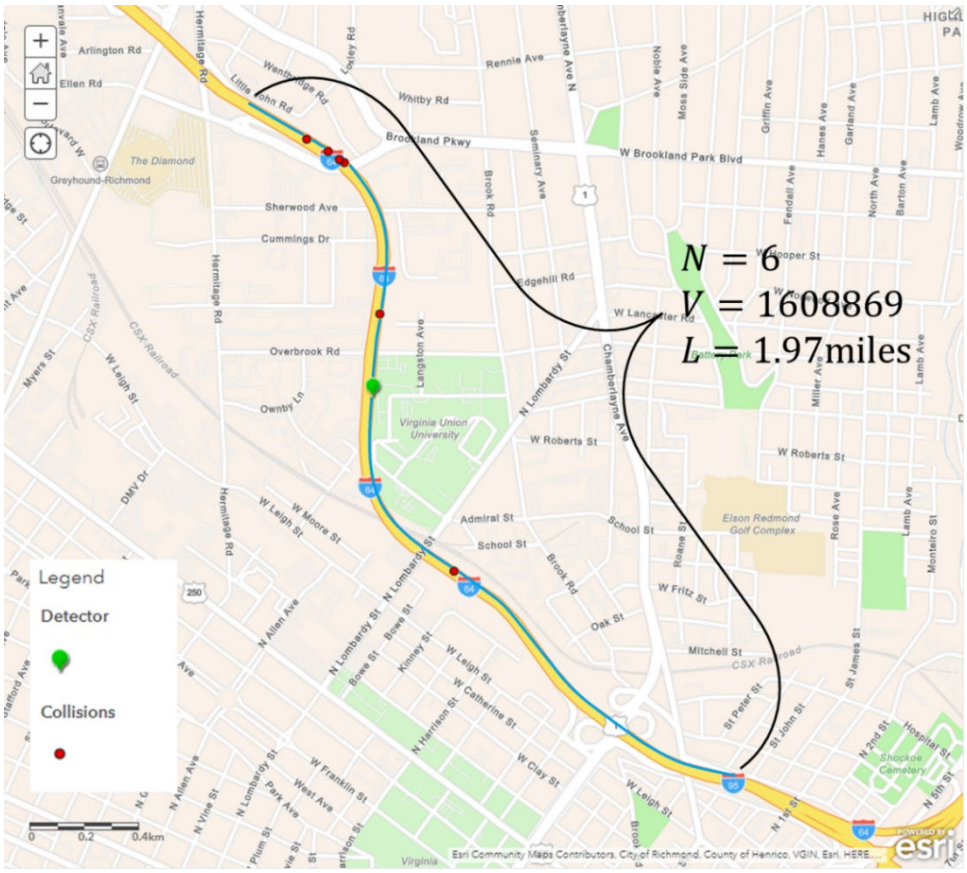

Original Photo: © 2022 Google® (see Acknowledgments page)

Figure 4-22. Graph. Link on I-64W with detector and truck-related collisions.

4.2.4. Test Bed Study Sites: Expected Annual Number of Truck Related Collision

In this work the expected annual number of truck-related collisions that would occur under the bridge is obtained by multiplying the involvement rate, ΦT, multiplied by the width of a specific bridge, W_b, and the estimated annual truck volume traversing under the bridge. The expected annual number of truck-related collisions, λ, impacting bridge piers corresponding to one direction of travel can be estimated by the following equation:

$$\lambda = \left(\frac{\hat{V}}{1{,}000{,}000}\right)\left(\frac{W_b}{5280}\right)\Phi_T \qquad (4\text{-}2)$$

In Equation (4-2), $\hat{V}$ denotes the annual truck volume travelling under the bridge in one direction of travel and W_b denotes the width of bridge in feet. Table 4-6 presents the expected number of truck-related collisions for the study sites.

Equation (4-2) indicates the number of truck-related collisions that may occur under bridges; however, it does not directly provide a measure of collisions to bridge piers. Therefore, it helps to refine the collision frequency Φ_T to evaluate the extent to which the bridges are exposed to truck-related collisions. This is achieved by multiplying Φ_T by a conditional probability of the

likelihood of under-bridge truck-related collisions colliding into bridge piers. This conditional probability may be estimated by a Monte Carlo simulation that considers various endogenous (e.g., the weight and speed of trucks involved in collisions) and exogenous factors (e.g., the type of protection for bridge piers and the roadway geometric under bridges).

Table 4-6. Expected annual number of truck-related collisions for the study sites.

Bridge No.	Annual Truck Volume $\widehat{V}$	Bridge Width W_b (unit: feet)	Expected Annual Number of Truck-Related Collisions, λ
1	385,720	68.8	0.003833
2	414,947	68.8	0.004123
3	56,718	25.9	0.000212
4	94,087	25.9	0.000352
5	517,697	29.9	0.002236
6	406,909	38.4	0.002257
7	451,305	26.6	0.001734
8	207,065	27.9	0.000834
9	56,810	29.9	0.000245
10	61,788	29.9	0.000267
11	155,955	51.8	0.001167
12	47,623	58.1	0.000400
13	39,954	58.1	0.000335
14	303,488	34.4	0.001508
15	300,715	34.4	0.001494
16	1,429,790	67.9	0.014022
17	1,175,996	25.9	0.004399

4.2.5. Probability of Bridge Failure

Assuming truck collisions under bridges occur independently of time with a constant rate, λ, it can be inferred the occurrence of truck-related collisions follows a Poisson distribution. This is supported by the exponentially distributed interarrival time of truck-related collisions as illustrated by Figure 4-23, Figure 4-24 and Figure 4-25. Such distribution holds when the area of focus is narrowed down from state level (see Figure 4-23) to county/city level (see Figure 4-24), then to link level (see Figure 4-25). Although distributions on county/city level and on link level present more nondeterministic shapes if compared to the distribution on state level, an Anderson-Darling test fails to reject the null hypothesis assuming these observations are from exponential distribution at the 5 percent significant level. As such, truck-related collisions at a specific bridge location likely form a Poisson distribution.

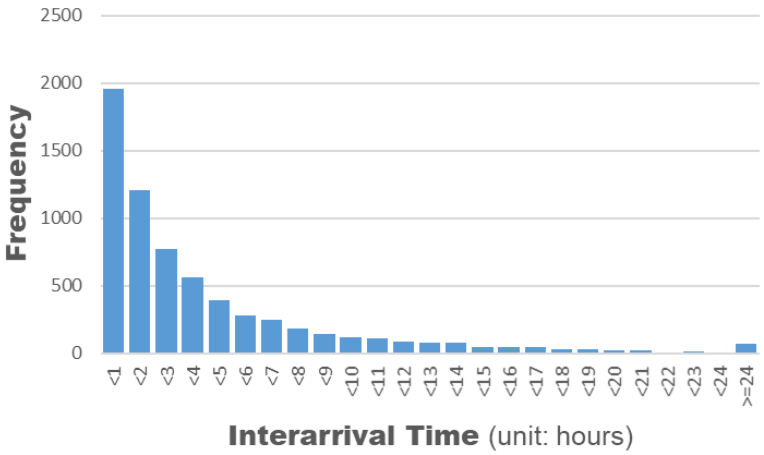

Note: Data pertain to the entire state of Virginia.

Figure 4-23. Chart. State level interarrival time of truck-related collision.

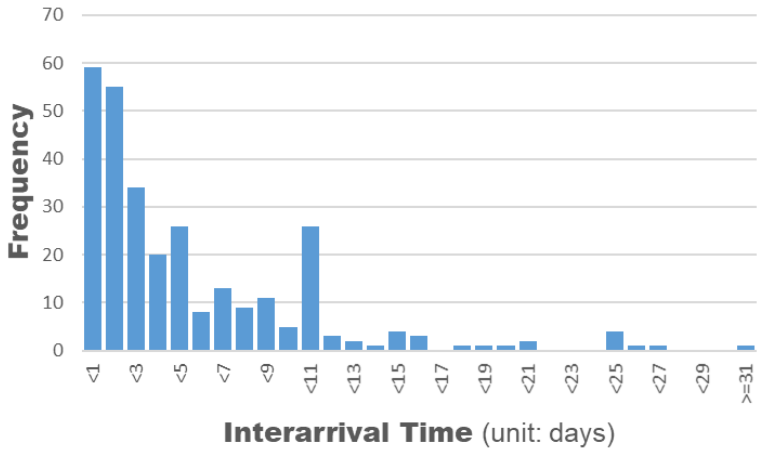

Note: Data pertain only to Richmond, Virginia.

Figure 4-24. Chart. City level interarrival time of truck-related collision.

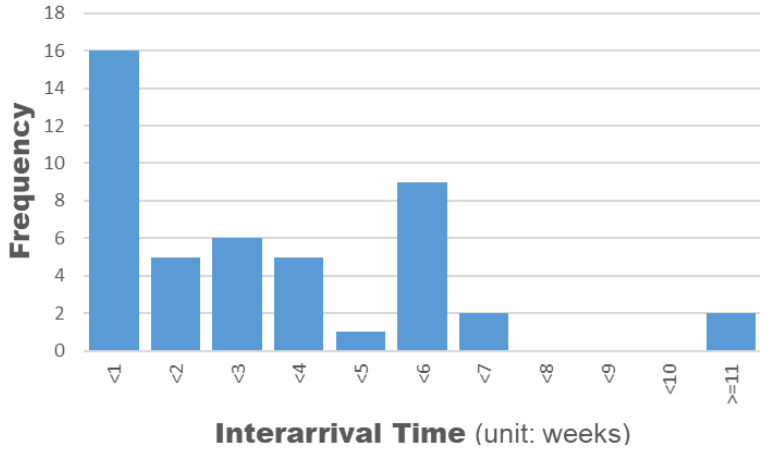

Note: Data pertain only to a Specific Link on I-95S in Prince William County.

Figure 4-25. Chart. Link level interarrival time of truck-related collision.

Assuming truck-related collisions at a specific bridge location form a Poisson distribution, the probability of observing k truck-related collisions given the expectation of λ at this location is as follows:

$$Pr(X = k) = \frac{\lambda^k e^{-\lambda}}{k!} \tag{4-3}$$

Where X denotes the number of truck-related collisions; λ denotes the corresponding expectation, i.e., $\lambda = \mathrm{E}(X)$. Let $Pr(Q|C)$ denote the probability of bridge failure due to a specific truck-related collision given the weight and speed distribution of trucks and the width of bridge piers. The probability of bridge failure for a specific bridge in a year with unidirectional roadway under the bridge can be formulated as follows:

$$\mathrm{Pr}_{bf} = 1 - \sum_{k}^{\mathbb{Z}\geq 0} \left(\frac{\lambda^k e^{-\lambda}}{k!} \cdot (1 - \mathrm{Pr}(Q|C))^k \right) \tag{4-4}$$

The probability of bridge failure for a specific bridge in a year with bidirectional roadway under the bridge can be formulated as follows:

$$\mathrm{Pr}_{bf} = 1 - \sum_{k_1}^{\mathbb{Z}\geq 0} \sum_{k_2}^{\mathbb{Z}\geq 0} \left\{ \left(\frac{\lambda^{k_1} e^{-\lambda_1}}{k_1!} \right) . \left(\frac{\lambda^{k_2} e^{-\lambda_2}}{k_2!} \right) . [1 - \mathrm{Pr}_1(Q|C)]^{k_1} \cdot [1 - \mathrm{Pr}_2(Q|C)]^{k_2} \right\} \tag{4-5}$$

Similarly, the probability of bridge failure for a specific bridge in T years with unidirectional roadway under the bridge can be formulated as follows:

$$\mathrm{Pr}_{bf} = 1 - \sum_{k}^{\mathbb{Z}\geq 0} \left\{ \frac{(\lambda T)^k e^{-\lambda T}}{k!} \cdot [1 - \mathrm{Pr}(Q|C)]^k \right\} \tag{4-6}$$

The probability of bridge failure for a specific bridge in T years with bidirectional roadway under the bridge can be formulated as follows:

$$\mathrm{Pr}_{bf} = 1 - \sum_{k_1}^{\mathbb{Z}\geq 0} \sum_{k_2}^{\mathbb{Z}\geq 0} \left(\left[\frac{(\lambda_1 T)^{k_1} e^{-\lambda_1 T}}{k_1!} \right] \cdot \left[\frac{(\lambda_2 T)^{k_2} e^{-\lambda_2 T}}{k_2!} \right] \cdot [1 - \mathrm{Pr}_1(Q|C)]^{k_1} \cdot [1 - \mathrm{Pr}_2(Q|C)]^{k_2} \right) \tag{4-7}$$

Given bridge failures induced by collisions are low frequency events and these events may not occur for a specific bridge during the testing period, Equations (4-6) and (4-7) estimate the probability of such events (other than their expected frequency). The probability Pr_{bf} can be estimated for an extended period of time (e.g., the service life of a bridge) and used as a metric for evaluating vulnerability of a location-specific bridge to pier collisions.

4.3. STOCHASTIC PARAMETRIC IMPULSE LOADING FUNCTION

4.3.1. Dynamic Impact Forces

The parametric impulse loading functions previously depicted in Figure 2-13 and calculated using Equations (2-4) to (2-14), as outlined in Agrawal et al. (2018), were subsequently used in calculating the equivalent static force (ESF) of an equivalent single degree of freedom system. The ESF was obtained using the equations of motion as expressed in Equation (4-8), the system impulse response $x_{p,i}(t)$ in Equation (4-9), and the impulse response functions $h(t-\tau)$ characterized in Equation (4-10).

$$\ddot{x}_i(t) + 2\xi_{eff}\omega_{eff}\dot{x}_i(t) + \omega_{eff}^2 x_i(t) = \frac{F_i(t)}{m} \qquad T_{i-1} \le t \le T_i \tag{4-8}$$

$$x_{p,i}(t) = \frac{1}{m}\int_{t_i}^{t_{i+1}} f_i(\tau)h(t-\tau)d\tau \tag{4-9}$$

$$h(t-\tau) = \frac{1}{w_d} e^{-\xi w_{ff}(t-\tau)} \sin[w_d(t-\tau)] \tag{4-10}$$

In these equations the variables are as follows:

- Subscripts *i* and *i−1* indicate the pulse region in each of the time limits *t*. These time limits are represented at each time interval T_i and T_{i-1}, and are calculated using Equations (2-9) to (2-14) .

- $\ddot{x}_i(t)$, $\dot{x}_i(t)$, and $x_i(t)$ are the acceleration, velocity, and displacement of the oscillator, respectively.

- ξ_{eff}, ω_{eff}, and ω_d are the equivalent viscous damping ratio, undamped natural frequency, and damped natural frequency, respectively, which are used in characterizing the performance damage limit state of bridge pier column. In this research, the equivalent static force was evaluated at ξ_{eff} of 5 percent, 10 percent, and 20 percent. These values represent damping ratios stipulated in the literature to characterize three performance damage limit states for reinforced concrete columns. These performance damage limit states are: “essentially elastic”, “minor damage”, and “major damage”, respectively (Hose et al. 2000).

- In Equation (4-8), $F_i(t)$ represents each of the force branches in Figure 2-13, and $f_i(\tau)$ in Equation (4-9), defines the linear loading function at each of the time limits as expressed in Equation (4-11) (Lu and Silva 2006; Silva et al. 2009).

$$f_i(\tau) = F_{i-1} + \left(\frac{F_i - F_{i-1}}{t_i - t_{i-1}}\right)(\tau - t_{i-1}) \tag{4-11}$$

Calculating the ESF starts with solving the sequence of Equations (4-8) to (4-10). A detailed methodology on solving these equations is proposed in the work by Silva et al. (Lu and Silva 2006; Silva et al. 2009). Finally, once the system impulse response $x_{p,i}(t)$ is evaluated the maximum equivalent static force, ESF is calculated using the following expression:

$$ESF = |x_p|_{max} K_{eff} \quad \textbf{(4-12)}$$

In this expression K_{eff} is the equivalent system stiffness evaluated at each of the three performance damage limit states for reinforced concrete columns and $|x_p|_{max}$ is the peak displacement of the single degree of freedom oscillator. This methodology followed similar steps proposed by Silva et al. (2009) in estimating the equivalent static force of reinforced concrete members under impulse loads.

The research team has conducted a total of 4,394 simulations for truck weights ranging between 20 to 48 tons, pier width ranges of 24 to 48 inches, and truck velocities in the range of 30 to 80 mph. Sample results for a pier width of 36 inches and truck weights of 20 and 48 tons are presented in Figure 4-26. These variations of truck weight and velocity exceeds in many instances the maximum limits stipulated by the NHTSA (2021). However, these values were selected herein for completeness and to have a wider range of variabilities.

Histograms for all 4,394 simulations were performed by grouping results in terms of the achieved maximum shear force demand values and performance levels. Figure 4-27 shows the histograms developed for the data in "bins" of equal width, Results show that in most of the cases the maximum required shear force resistance necessary to maintain the system response at or below the desired performance level exceeds the AASHTO proposed equivalent static force of 600 kips. Results presented in Figure 4-27 lead to mean values of 917, 829, and 732 kips, respectively, for the *Essentially Elastic*, *Minor Damage*, and *Major Damage* performance levels. Furthermore, for the *Essentially Elastic*, *Minor Damage*, and *Major Damage* performance levels, respectively, there is a probability of 93, 68 and 56 percent that the equivalent static force will exceed the stipulated design value of 600 kips. This project considered only deterministic values for truck speed and weight and structural properties. Future research will include stochastic models in assessing these three variables.

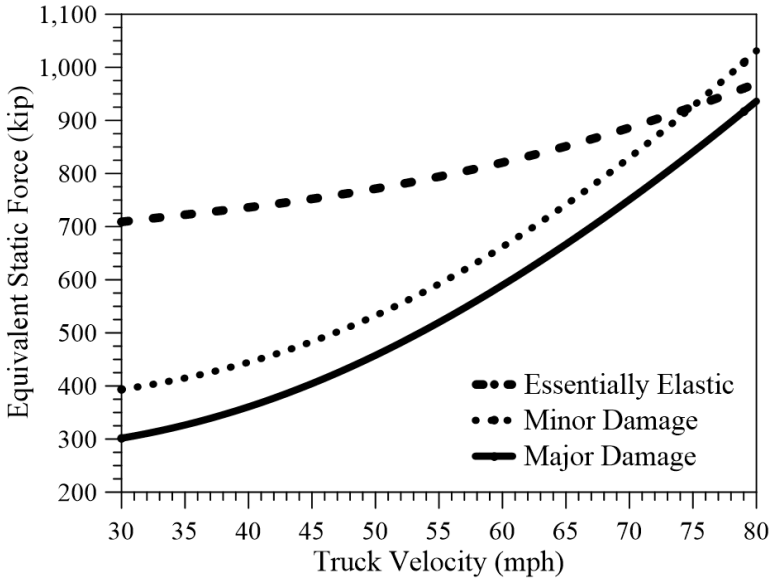

A. Results as a function of impact velocity for a truck weight of 20 tons.

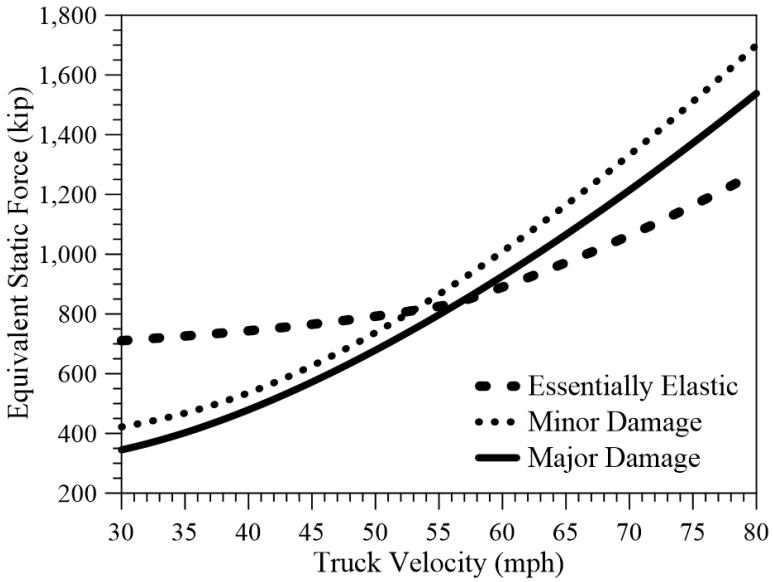

B. Results as a function of impact velocity for a truck weight of 48 tons.

Figure 4-26. Graph. Equivalent static force on a pier width of 36 inches.

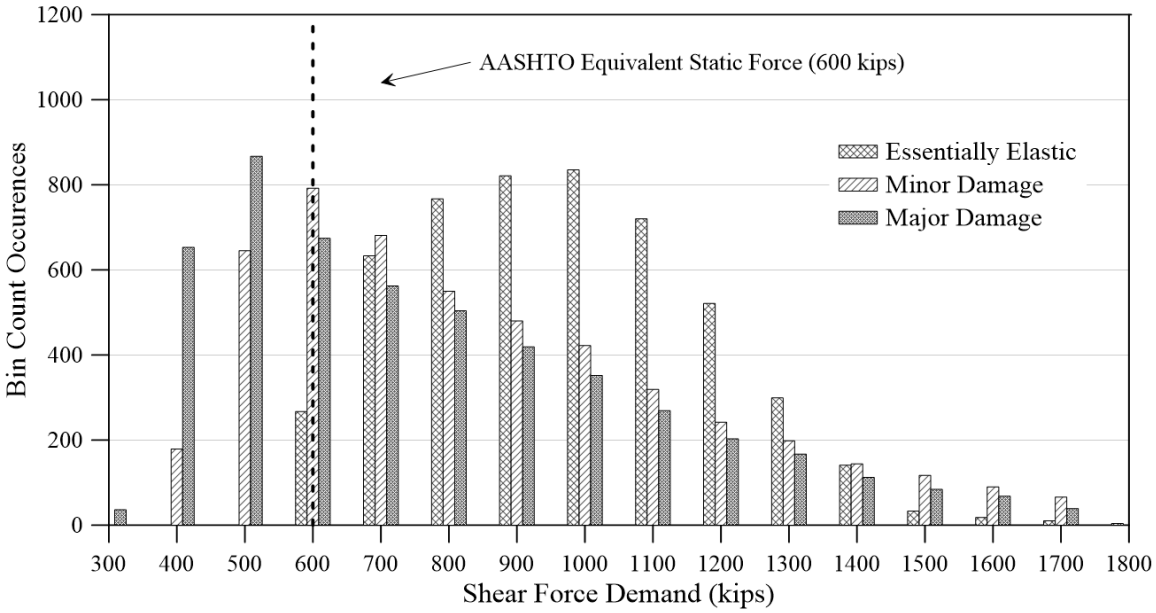

Figure 4-27. Graph. Histogram for shear force demands.

4.3.2. Evaluation of Peak Dynamic Forces Published in the Literature

As outlined in Section 2.5.1 of this report, Agrawal et al. (2018) proposed a general shape for predicting the parametric impulse loading functions for frontal collisions on bridge piers. The parametric impulse loading functions are evaluated using the truck velocity and weight, and width of the bridge pier. Table 4-7 summarizes a reference list of experimental and numerical research projects that were conducted to evaluate the peak dynamic forces resulting from traffic collisions. Agrawal et al. (2018) proposed impulse loading function that have considered two types of large trucks that are likely to collide with bridge pier. These two types are the single-unit (SU) truck and the tractor semitrailer (TS). As in Agrawal et al. (2018), the work presented in this report presents a possible methodology for probabilistic assessment of bridge safety against collisions considering the SU and TS truck types.

This table lists the corresponding reference, velocity ranges, truck weight, pier width and number of simulations used in assessing the PDF. In total, 470 data points were used from this reference list to assess the variability of the parametric impulse loading functions for frontal collision developed by Agrawal et al. (2018). Uncertainty in the speed distribution was previously addressed in Section 4.2.1 of this report. As previously discussed, Table 4-1 presents the uncertainty in the speed distribution for the 17 study sites. Likewise, Table 4-5 presents the uncertainty in the weight distribution for the 17 test bed study sites.

Table 4-7. List of references used in evaluating force ratio probability distribution.

Reference List	Velocity Range (mph)	Truck Weight Range (kip)	Pier Element Width Range (inch)	Number of Simulations
Gomez (2014)	34.18 – 74.56	17.78	23.62 – 47.24	27
AuYeung and Alipour (2016)	34.18 – 74.56	79.10	23.62 – 47.24	28
Chen et. al. (2016)	62.13 – 74.56	22.05 – 26.46	19.68 – 78.74	24
Chen et. al. (2020)	49.70 – 74.56	39.57 – 59.35	59.06	30
Abdelkarim & ElGawady (2017)	19.88 – 69.59	4.40 – 66.13	59.05 – 82.67	33
Do et. al. (2019)	37.28 – 74.56	19.84 – 30.85	31.49 – 82.67	30
Li et al. (2020)	24.85 – 74.56	6.61 – 66.13	39.37 – 55.11	108
Wu et al. (2020)	37.28 –74.56	25.22	35.43 –70.87	10
Li et al. (2021)	24.85 – 62.13	22.05 – 66.13	39.37	35
Zhao et al. (2021)	37.28 – 62.13	22.05 – 83.78	39.37 – 59.06	42
Zhou et al. (2021)	74.56	17.64 – 26.46	47.24 – 59.06	39
Heng et. al. (2021)	49.71 – 74.56	47.21 – 78.68	51.18	10
Heng et. al. (2022)	37.28 – 62.13	6.74 – 11.24	39.37 – 59.06	54

Uncertainties in the bridge pier element width are based on a normal distribution using the design values as the mean value and a coefficient of variation of 2.00 percent. Truck velocity and weight, and width of the bridge pier are treated as random variables. These random variables are sampled several times to represent the underlying probabilistic characteristics to develop truck parametric impulse loading functions for predicting the annual frequency of bridge collapse.

Equations (4-13), (4-14) and (4-15) are of the same format as those proposed by Agrawal et al. (2018). However, in this work correction factors are introduced to predict uncertainties in the parametric impulse loading function for $\overline{F_1}$, $\overline{F_3}$, and $\overline{F_5}$. These uncertainties use the following three correction factors: $\overline{\gamma_{F1,KE}}$, $\overline{\gamma_{F3,KE}}$ and $\overline{\gamma_{F5,KE}}$. The parametric impulse loading functions which were previously depicted in Figure 2-13 were slightly modified in terms of these three correction factors.

$$\overline{F_1} = \overline{\gamma_{F1,KE}}\left[109\,\overline{V}^{\,0.52}\left(\frac{\overline{b}}{36}\right)^{0.33}\right](kips) \quad \textbf{(4-13)}$$

$$\overline{F_3} = \overline{\gamma_{F3,KE}}\left[30\,\overline{V}^{\,0.95}\right]\,(kips) \quad \textbf{(4-14)}$$

$$\overline{F_5} = \overline{\gamma_{F5,KE}}\left[0.05\,\overline{V}^{1.77}\overline{W}^{0.61}\left(\frac{\overline{b}}{36}\right)^{1.14}\right](kips) \quad \textbf{(4-15)}$$

Uncertainties in mean forces $\overline{F_1}$, $\overline{F_3}$, and $\overline{F_5}$ were evaluated using the 470 data points from the list of references in Table 4-7. The peak dynamic forces reported in this list of references are plotted

in Figure 4-28. Using as input the numerical values presented in Table 4-7, peak dynamic forces (Peak-DF) were calculated in terms of the parametric impulse functions, previously depicted in Figure 2-13, and are plotted in Figure 4-29. In these figures the reported Peak-DF forces and the calculated Peak-DF on the Y-axis, were plotted against the impact kinetic energy, *KE*, on the X-axis, per width of bridge pier width in ft, b, according to the relation:

$$\frac{KE}{b} = \frac{1}{2}\frac{W\,V^2}{b} \qquad \textbf{(4-16)}$$

Where *W* is the total truck weight in kips and *V* is the truck speed in mph at first impact. To differentiate peak dynamic forces from the probability density function (PDF), the peak dynamic forces are identified as reported Peak-DF when referring to the values presented in the literature or calculated Peak-DF when referring to the values computed using the functions presented in Equations (4-13), (4-14) and (4-15). Using the data presented in Figure 4-28 and Figure 4-29, the ratio of reported versus calculated Peak-DF was obtained and results are presented in Figure 4-30. This figure shows there is wide scatter in the data.

Data plotted in Figure 4-31 for Force $\overline{F_1}$ ratio, depicts the probability density function at a Force $\overline{F_1}$ ratio of near 1.00 was 0.036. Since this value rapidly decreases, it suggests the equations proposed by Agrawal et al. (2018) seem to predict reasonably well the mean Peak-DF for force $\overline{F_1}$. However, for the mean force $\overline{F_3}$ and $\overline{F_5}$ ratios, depicted in Figure 4-32 and Figure 4-33, respectively, the probability density function is much lower with values, respectively, of 0.027 and 0.024. This indicates that for forces $\overline{F_3}$ and $\overline{F_5}$ the equations proposed by Agrawal et al. (2018) have a higher error in predicting the impulse loading function. In the next section, stochasticity in the impulse loading function for force $\overline{F_1}$, $\overline{F_3}$, and $\overline{F_5}$ are determined based on the 5 bin ranges outlined in Figure 4-30.

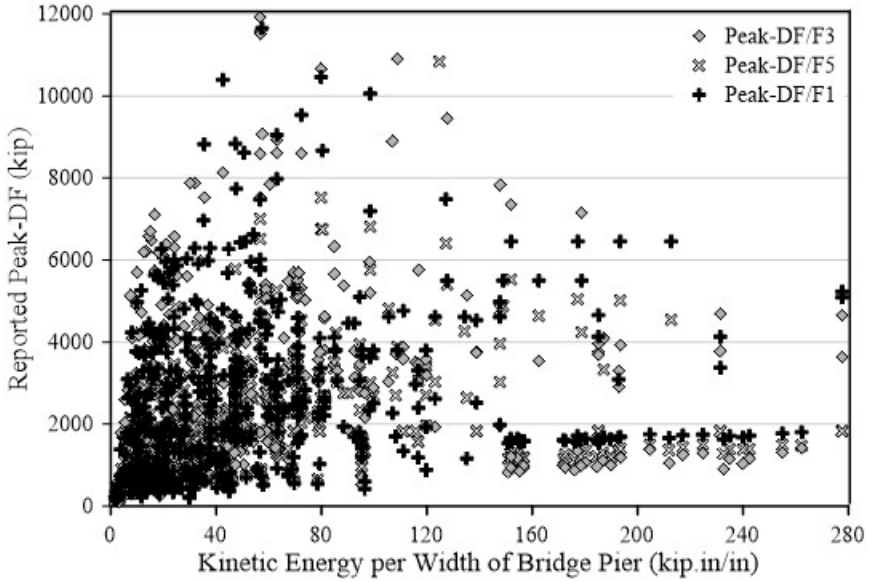

Figure 4-28. Graph. Reported Peak-DF from references presented in Table 4-7.

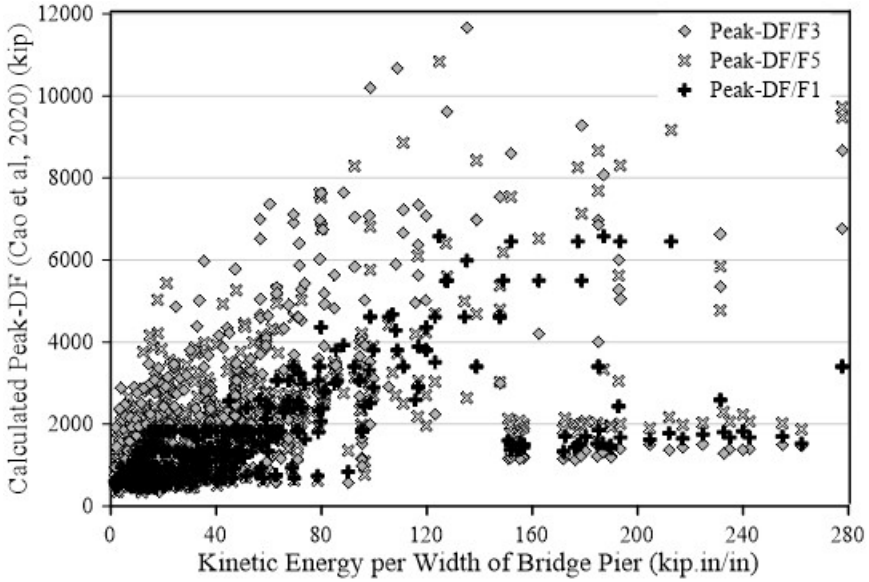

Figure 4-29. Graph. Calculated Peak-DF using as input the values presented in Table 4-7.

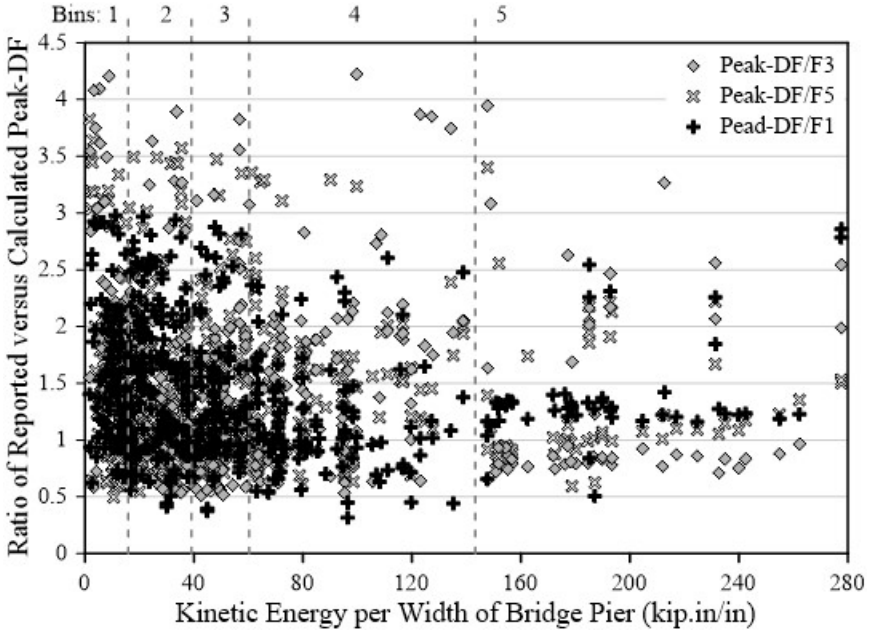

Figure 4-30. Graph. Ratio of reported versus calculated Peak-DF.

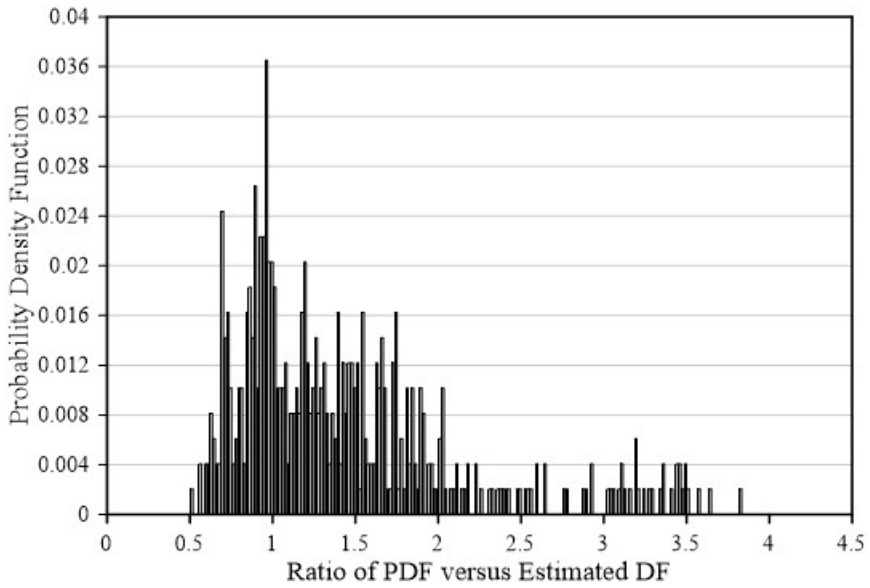

Figure 4-31. Chart. PDF for Force $\overline{F_1}$: Reported versus calculated Peak-DF.

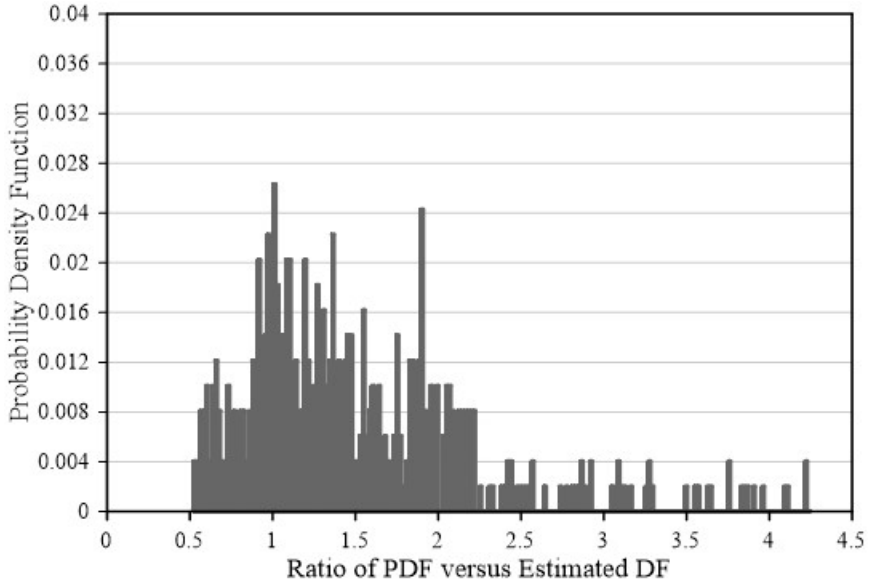

Figure 4-32. Chart. PDF for Force $\overline{F_3}$: Reported versus calculated Peak-DF.

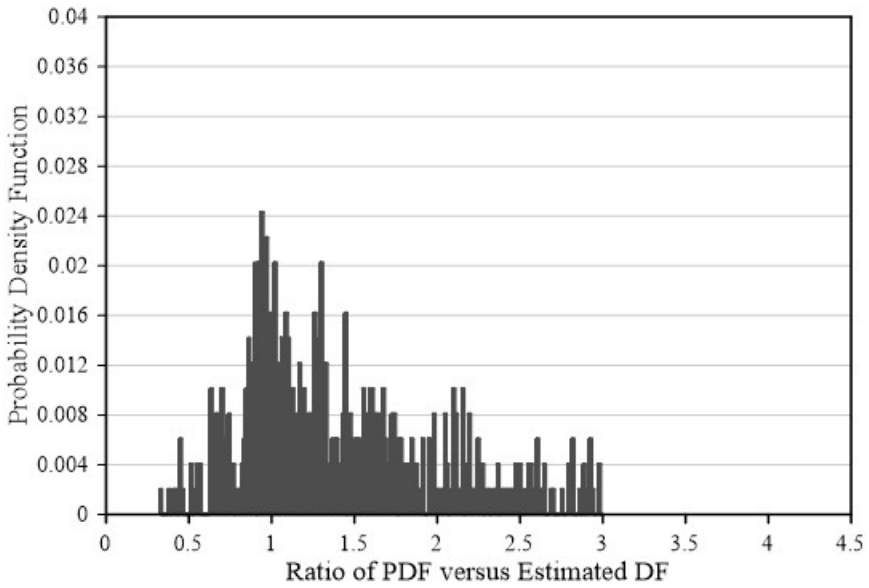

Figure 4-33. Chart. PDF for Force $\overline{F_5}$: Reported versus Calculated Peak-DF.

4.3.3. Percentage Confidence Interval for Force Ratios

For each of the force pulses, the data was subdivided in five bins as a function of the kinetic energy per width of bridge pier and information is presented in Table 4-8. The data sampling size for each of the bins is reported in the second column of Table 4-8. Using the bin values depicted in Figure 4-30 and the upper and lower bounds shown in Table 4-8, probability distribution function (PDF) for each of these bin values and forces $\overline{F_1}$, $\overline{F_3}$, and $\overline{F_5}$ were calculated and results are presented in Figure 4-34. Plots in this figure show the PDF for each of the respective bins and force values are skewed distributed. Furthermore, ratio values for forces $\overline{F_1}$, $\overline{F_3}$, and $\overline{F_5}$ cannot be approximated by a single distribution function and vary based on the distribution of data.

A curve fit test was performed to obtain the best fit theoretical distribution for each of the PDF show in Figure 4-31, Figure 4-32, and Figure 4-33. Best curve fits were evaluated using the following theoretical PDF: normal, lognormal, Weibull, Poisson, kernel, logistic, and gamma. The best fit data distribution or the "p" hypothesis test values are presented in parenthesis for each of the best curve fit PDFs. The best "p" hypothesis test values for the bin values are reported in Table 4-8. The corresponding cumulative distribution function for the collected data and the best fit data are reported in Figure 4-35 for force $\overline{F_1}$, Figure 4-36 for force $\overline{F_3}$, and Figure 4-37 for force $\overline{F_5}$. These figures show a reasonable correlation between the data and the best fit distribution function.

Table 4-8. Bin values with best fit data distribution.

Bin No	Data Points	Lower Bound	Upper Bound	Best Fit PDF Force $\overline{F_1}$	Best Fit PDF Force $\overline{F_3}$	Best Fit PDF Force $\overline{F_5}$
1	100	> 0.0	≤ 15.86	Kernel (0.66)	Lognormal (0.21)	Lognormal (0.88)
2	100	> 15.86	≤ 39.06	Kernel (0.63)	Lognormal (0.93)	Kernel (0.27)
3	100	> 39.06	≤ 60.26	Kernel (0.45)	Kernel (0.95)	Lognormal (0.89)
4	90	> 60.26	≤ 143.2	Kernel (0.80)	Kernel (0.58)	Lognormal (0.69)
5	80	> 143.2	≤ 280.0	Lognormal (0.85)	Kernel (0.60)	Kernel (0.51)

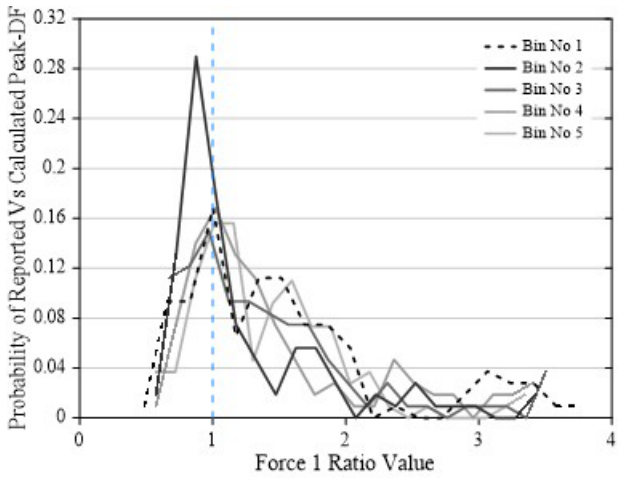

A. Ratio for segment force $\overline{F_1}$.

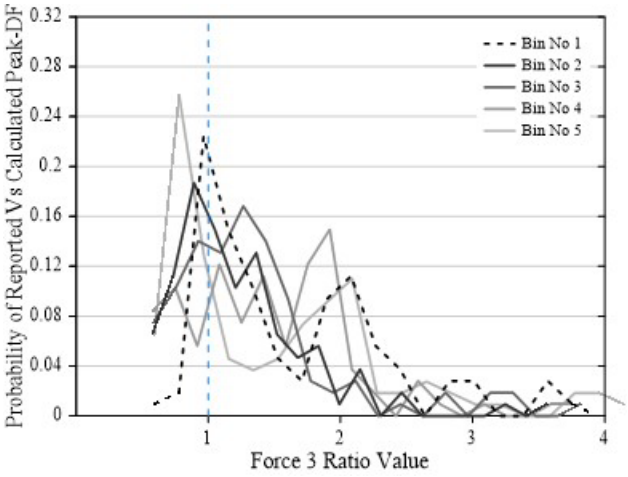

B. Ratio for segment force $\overline{F_3}$.

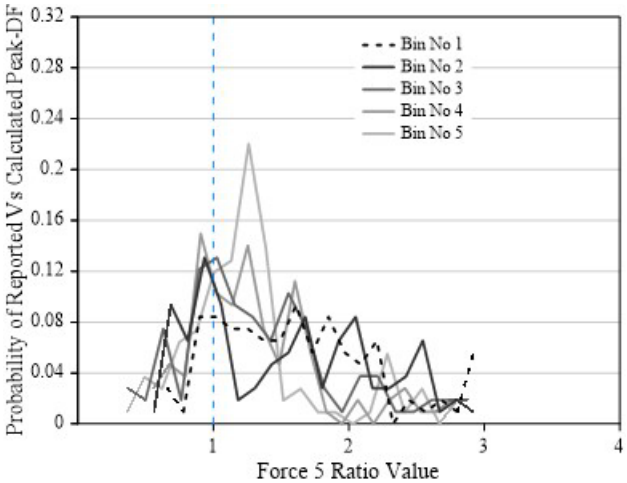

C. Ratio for segment force $\overline{F_5}$.

Figure 4-34. Graph. Probability distribution functions.

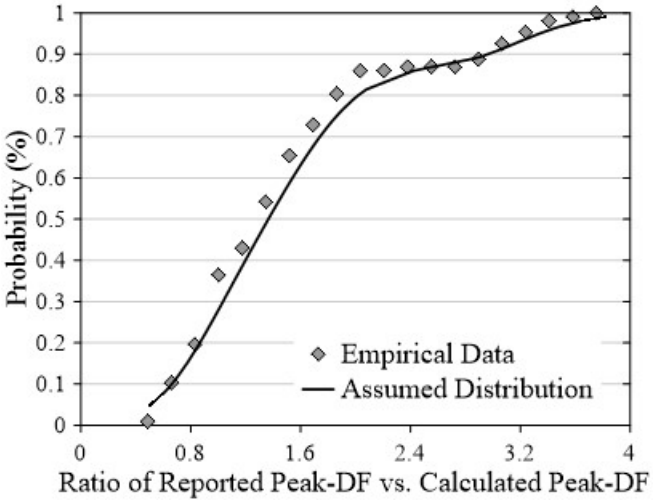

A. Bin No 1 and force $\overline{F_1}$.

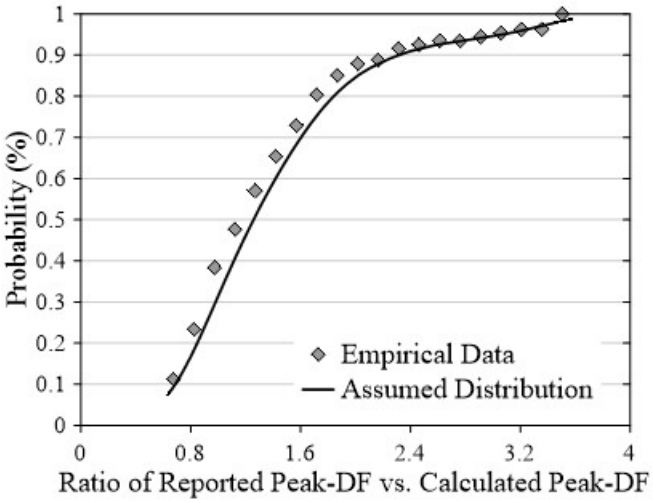

B. Bin No 3 and force $\overline{F_1}$.

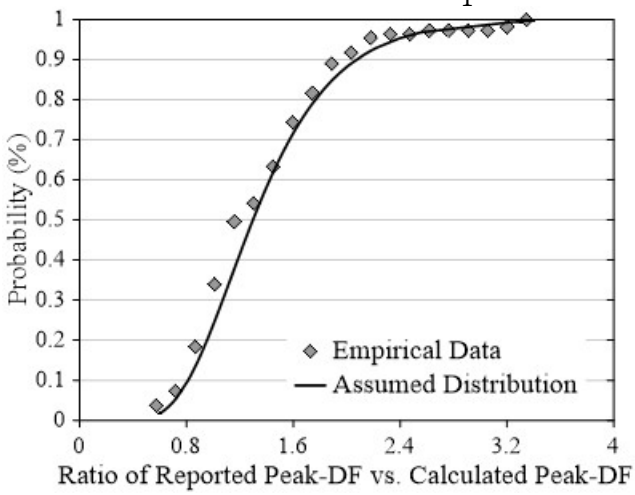

C. Bin No 5 and force $\overline{F_1}$.

Figure 4-35. Graph. Force F1 cumulative distribution function.

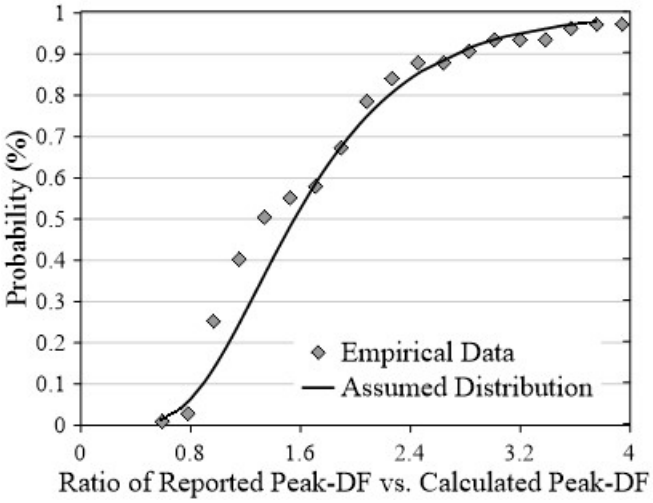

A. Bin No 1 and force $\overline{F_3}$.

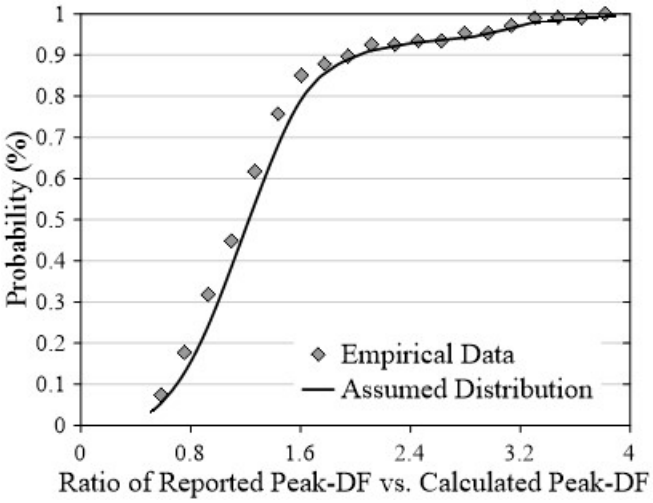

B. Bin No 3 and force $\overline{F_3}$.

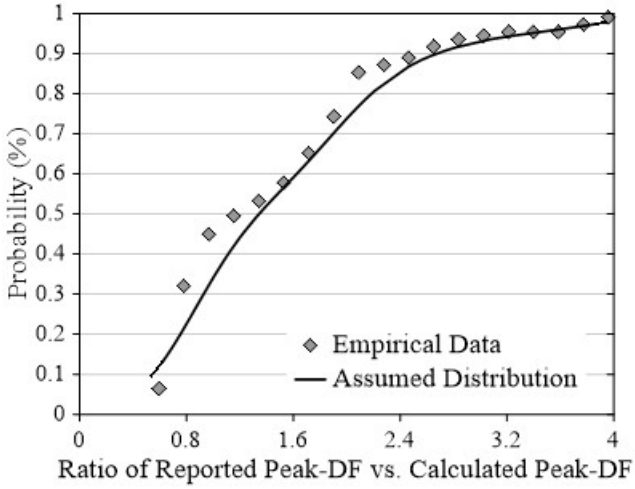

C. Bin No 5 and force $\overline{F_3}$.

Figure 4-36. Graph. Force F3 cumulative distribution function.

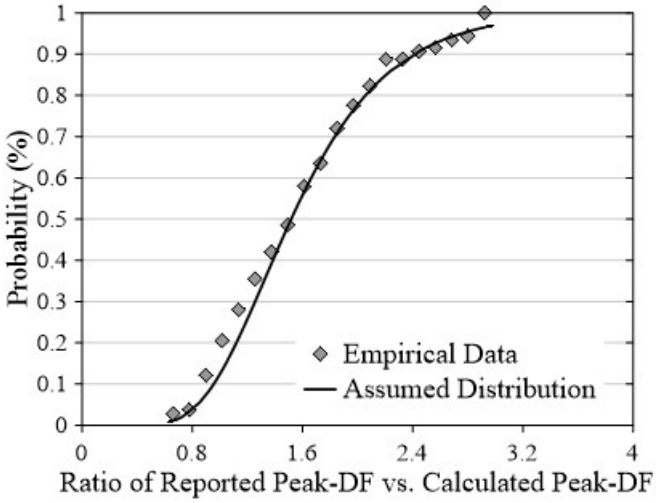

A. Bin No 1 and force $\overline{F_5}$.

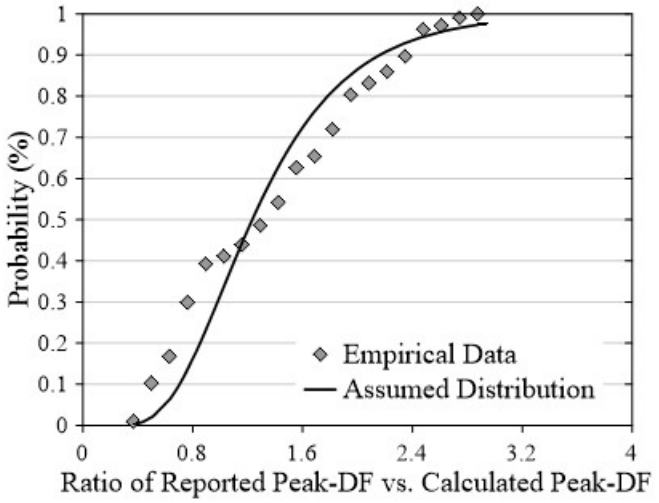

B. Bin No 3 and force $\overline{F_5}$.

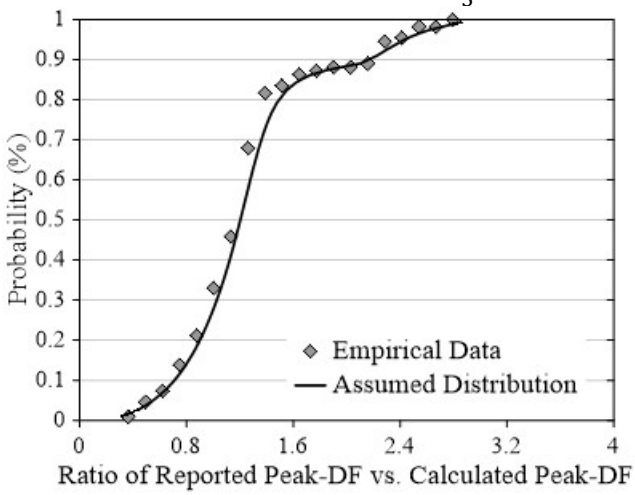

C. Bin No 5 and force $\overline{F_5}$.

Figure 4-37. Graph. Force F5 cumulative distribution function.

Estimating the peak dynamic force or the shape of the parametric impulse loading function is rather complex and involves stochastic models. The following parameters were assumed in developing the stochastic models for the impulse force:

- The vehicular velocity, $\overline{V}$, is a random variable with the Gumbel parameters outlined in Table 4-1.
- The vehicular weight, $\overline{W}$, follows the assumed weight distributions outlined in Table 4-5.
- The bridge pier width, $\overline{b}$, is a normal random variable with an assumed coefficient of variation of 2 percent.

Finally, using the best curve fit for PDF outlined in Table 4-8, upper- and lower-95 percent confidence intervals, and mean values were obtained. These results are plotted against the force ratio values presented in Figure 4-38 for force $\overline{F_1}$, Figure 4-39 for force $\overline{F_3}$, and Figure 4-40 for force $\overline{F_5}$. Next the random variables $\overline{\gamma_{F1,KE}}$, $\overline{\gamma_{F3,KE}}$, and $\overline{\gamma_{F5,KE}}$ upper- and lower-95 percent confidence intervals, and a linear regression analysis was conducted to obtain these values as a function of the kinetic energy per bridge pier width, *KE*. Linear regression analysis values for each of these random variables $\overline{\gamma_{F1,KE}}$, $\overline{\gamma_{F3,KE}}$, and $\overline{\gamma_{F5,KE}}$ are presented in terms of these relations:

- Upper- and lower-95 percent confidence intervals, and mean values are plotted in Figure 4-38. For force $\overline{F_1}$ ratio these are obtained using the following three equations:

$$\overline{\gamma_{1,KE}} = -0.0034964\,\overline{KE_b} + 3.1624793 \quad \textbf{(4-17)}$$

$$\overline{\gamma_{1,KE}} = 0.0003786\,\overline{KE_b} + 1.2113327 \quad \textbf{(4-18)}$$

$$\overline{\gamma_{1,KE}} = 0.0007480\,\overline{KE_b} + 0.5597238 \quad \textbf{(4-19)}$$

- Upper- and lower-95 percent confidence intervals, and mean values are plotted in Figure 4-39. For force $\overline{F_3}$ ratio these are obtained using the following three equations:

$$\overline{\gamma_{3,KE}} = 0.0031717\,\overline{KE_b} + 2.6116279 \quad \textbf{(4-20)}$$

$$\overline{\gamma_{3,KE}} = 0.00000408\,\overline{KE_b} + 1.3413177 \quad \textbf{(4-21)}$$

$$\overline{\gamma_{3,KE}} - 0.0014084\,\overline{KE_b} + 0.6714663 \quad \textbf{(4-22)}$$

- Upper- and lower-95 percent confidence intervals, and mean values are plotted in Figure 4-40. For force $\overline{F_5}$ ratio these are obtained using the following three equations:

$$\overline{\gamma_{5,KE}} = -0.0013861\,\overline{KE_b} + 2.6428531 \quad \textbf{(4-23)}$$

$$\overline{\gamma_{5,KE}} - 0.0012540\,\overline{KE_b} + 1.4281022 \quad \textbf{(4-24)}$$

$$\overline{\gamma_{5,KE}} = -0.0005047\,\overline{KE_b} + 0.6602125 \quad \textbf{(4-25)}$$

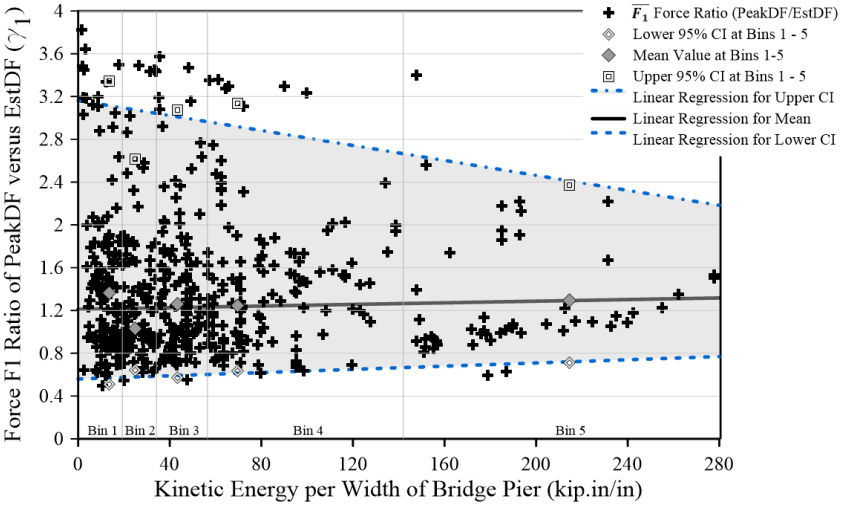

Figure 4-38. Graph. Upper- and lower-95 percent confidence interval for force $\overline{F_1}$ ratio.

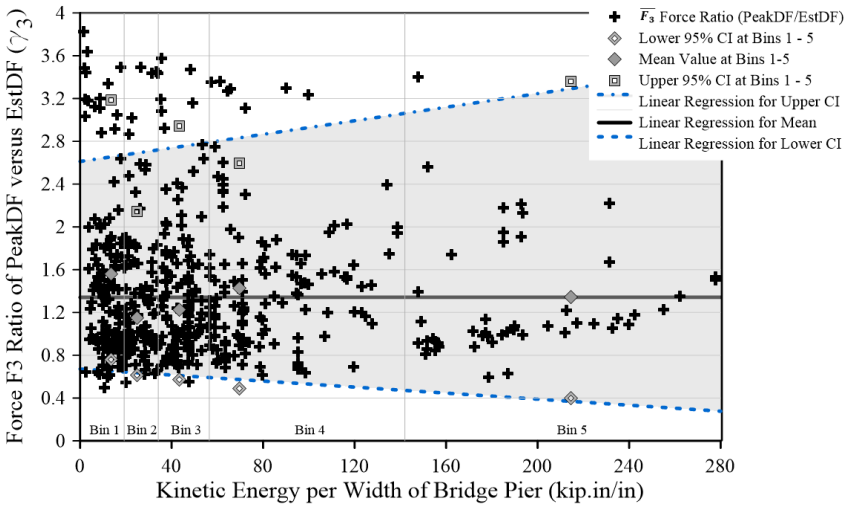

Figure 4-39. Graph. Upper- and lower-95 percent confidence interval for force $\overline{F_3}$ ratio.

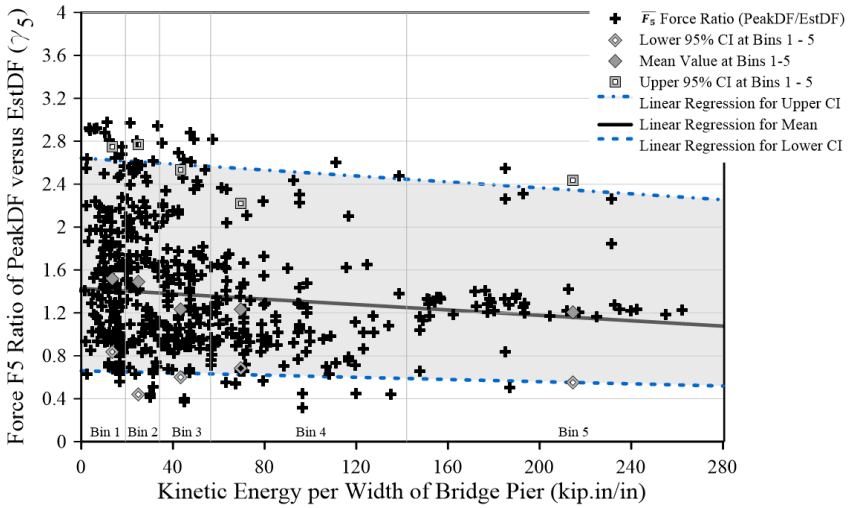

Figure 4-40. Graph. Upper- and lower-95 percent confidence interval for force $\overline{F_5}$ ratio.

4.4. STRAIN RATE EFFECTS ON MATERIAL PROPERTIES

This section describes the methods used to estimate the effects of heavy truck collisions on materials proprieties of concrete and reinforcing steel. Strain rate effects on reinforcing steel and concrete were evaluated for impact loads resulting from vehicular collisions. The CEB-FIP90 (1993) model was used to evaluate concrete properties for different strain rates (Malvar and Ross 1998). Strain rate effects of reinforcing steel were evaluated by Malvar (1998) and used in this study. Strain rate effects on concrete ($\dot{\varepsilon_c}$) and reinforcing steel ($\dot{\varepsilon_s}$) were based on average strain rates for each and are based on the following relations:

$$\dot{\varepsilon_c} = \frac{0.002}{t_E} \quad \textbf{(4-26)}$$

$$\dot{\varepsilon_s} = \frac{f_{yd}}{E_s\, t_E} \quad \textbf{(4-27)}$$

$$f_{yd} = 1 + \left(\frac{\dot{\varepsilon_s}}{c}\right)^{\frac{1}{p}} \quad \textbf{(4-28)}$$

In these equations, t_E is the time gap in seconds from first impact to peak response, E_s is the steel modulus, and f_{yd} is the dynamic reinforcing steel yield strength. The value of f_{yd} was computed using Equation (4-28). In Equation 4.31, c equals 40 and p equals 5. The procedure to calculate strain rate effects initiates by obtaining the time gap to peak response.

4.4.1. Time Gap to Peak Response

Time gap to peak response, t_E, was obtained by solving the equation of motion of a single degree of freedom system as expressed in Section 2.5.1 and using the applied forcing function depicted

in Figure 2-13 and Equations (4-8), (4-9), and (4-10). The time gap, t_E, can also be obtained directly from evaluating a bridge response under impact loads.

In Equations (4-8), (4-9), and (4-10), $F_i(t)$ represents the loading function branches depicted in Figure 2-13. These loading branches were evaluated for truck velocities and weight ranges, respectively, of V= [24–80] mph and W= [10–40] kips, and pier width between the ranges of b = [24–48] inches. Also in these equations, ω_{eff} and ξ_{eff} are, respectively, the effective natural frequency and effective damping ratios for a given performance limit state (Hose et al. 2000, Lu and Silva 2006, Silva et al. 2009).

Structural properties were evaluated using an applied axial and inertia load of 150 kips. For a concrete compressive strength of 6 ksi, this axial load ratio represents nearly a 7 percent axial load ratio. In the analysis the column length was 16 ft, and the impulse forces, $F_i(t)$, were applied at 5 feet above ground level.

Reinforcement layout for the prototype column is shown in Figure 4-41. As shown, the longitudinal reinforcement consisted of twelve #8 bars, which corresponds to a longitudinal reinforcement ratio of 2.73 percent. The yield and ultimate strength, ultimate strain, and modulus of elasticity for the #8 bars were, respectively, 60 ksi, 100 ksi, 0.20 inch/inch, and 29,000 ksi. Likewise, the transverse reinforcement consisted of #4 spirals at 2.75 inches, which corresponds to a volumetric reinforcement ratio of 1.32 percent. The yield strength for the #4 spirals bars was 66 ksi.

Using these columns material properties and geometry, the evaluated moment-curvature response is presented in Figure 4-42, and the load-deformation response is presented in Figure 4-43. Table 4-9 lists prototype column main structural properties obtained from Figure 4-43 as a function of three specified damage levels. Finally, solving Equations (4-8), (4-9), and (4-10), t_E for the three different damage levels are computed and used in Equations (4-26) and (4-27) in calculating the strain rate in steel and concrete, respectively.

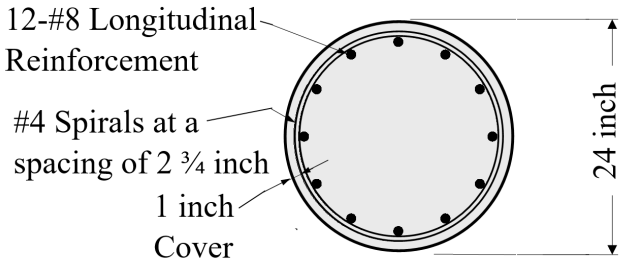

Figure 4-41. Illustration. Prototype column section.

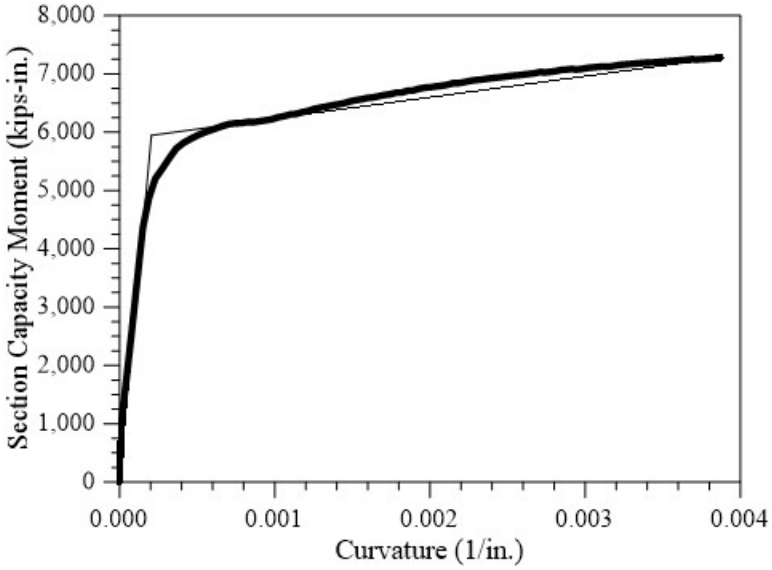

Figure 4-42. Graphs. Example of prototype column moment-curvature response.

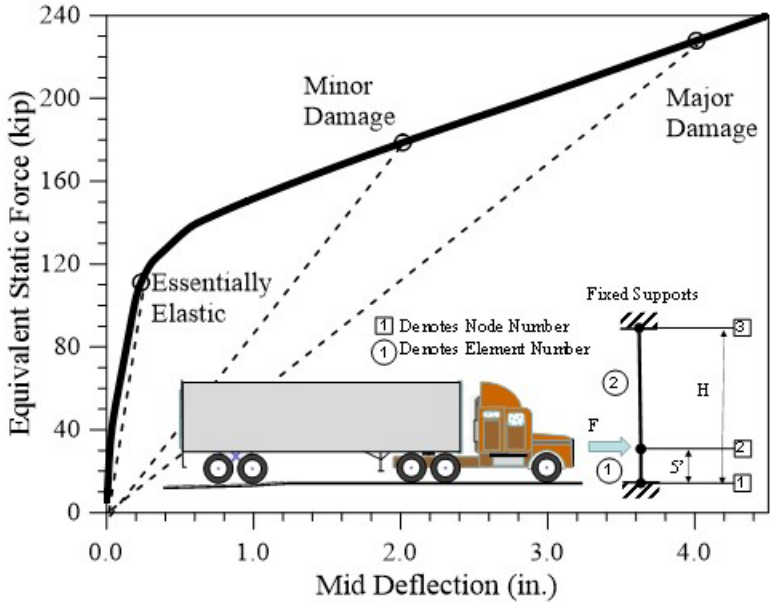

Figure 4-43. Graphs. Example of Prototype column load-deformation response.

Table 4-9. Prototype column main structural properties.

Performance Damage Limit State	Ductility [(1)]	Effective Damping Ratio, ξ_{eff}	Effective Stiffness (kip/in.)	Effective Frequency, ω_{eff} (rad/sec)	Effective Period, T_{eff} (sec)
Essentially Elastic	1	0.05	480	35.16	0.18
Minor Damage	3	0.10	95	15.64	0.41
Major Damage	5	0.20	58	12.22	0.52

Note: (1) Ductility as expressed in the table above is an indicator of the expected level damage level in pier concrete columns (Hose et al. 2000). These ductility levels correspond to the performance damage limit states: "essentially elastic", "minor damage", and "major damage" (Hose et al. 2000).

4.4.2. Average Strain Rate for Steel and Concrete

Considering the time gap to peak responses described in the previous section, the average strain rate for the reinforcing steel was calculated using Equation (4-27). Likewise, using the time gap to peak responses, the average concrete strain rates was calculated using Equation (4-26). Results of these analysis show that strain rate effects in concrete are significantly higher than those for steel, which suggests that concrete average stain rates are likely to contribute significantly more to any increase in the section capacities.

4.4.3. Dynamic Increase Factors for Reinforcing Steel Yield and Ultimate Strength

Reinforcing steel properties are affected by strain rate effects. Strain rate effect were evaluated for different models by Malvar (1998), and the adopted relations in Malvar's work were also adopted in this work. The dynamic increase factor (DIF_y) for the yield strength of reinforcing steel is computed using the following equation and results are presented in Figure 4-44:

$$DIF_y = \left(\frac{\dot{\varepsilon}_s}{10^{-4}}\right)^{\left(0.074-0.040\frac{f_y}{60}\right)} \quad \textbf{(4-29)}$$

The dynamic increase factor (DIF_u) for the ultimate strength of reinforcing steel is computed using the following equation and results are presented in Figure 4-45.

$$DIF_u = \left(\frac{\dot{\varepsilon}_s}{10^{-4}}\right)^{\left(0.019-0.009\frac{f_y}{60}\right)} \quad \textbf{(4-30)}$$

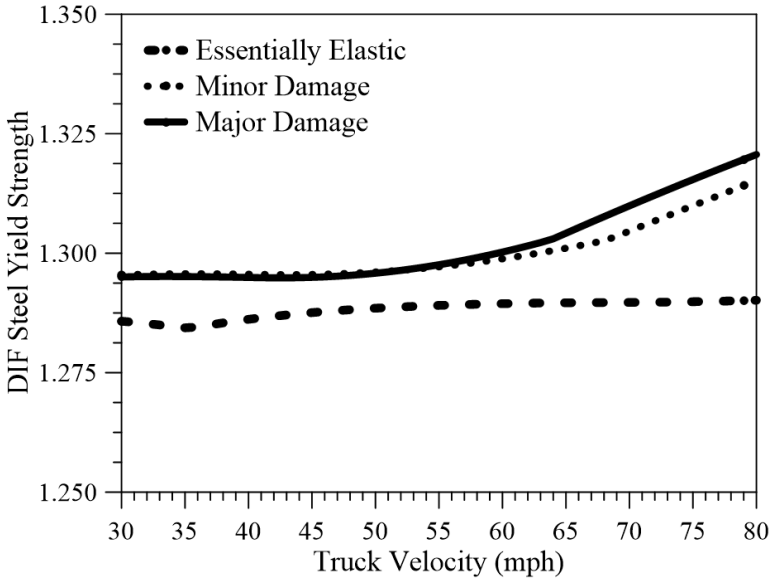

A. Results as a function of impact velocity for a truck weight of 20 tons.

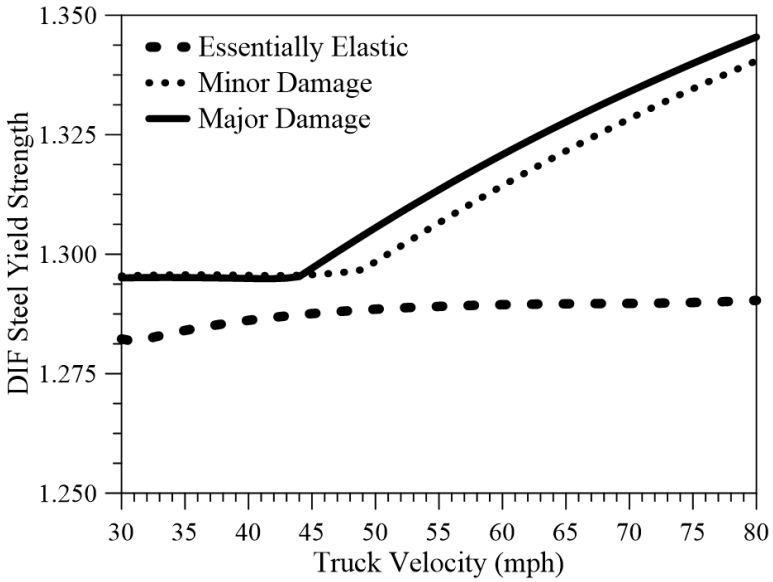

B. Results as a function of impact velocity for a truck weight of 48 tons.

Figure 4-44. Graphs. DIF reinforcing steel yield strength on a pier width of 36 inches.

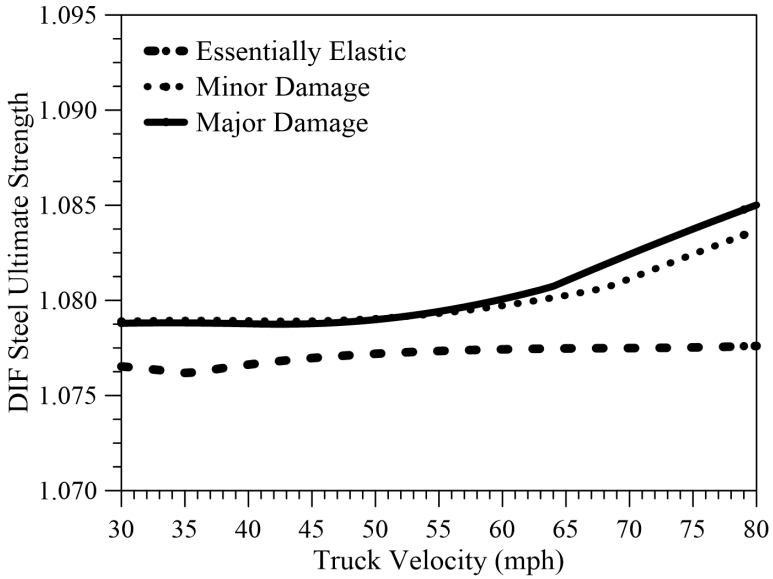

A. Results as a function of impact velocity for a truck weight of 20 tons.

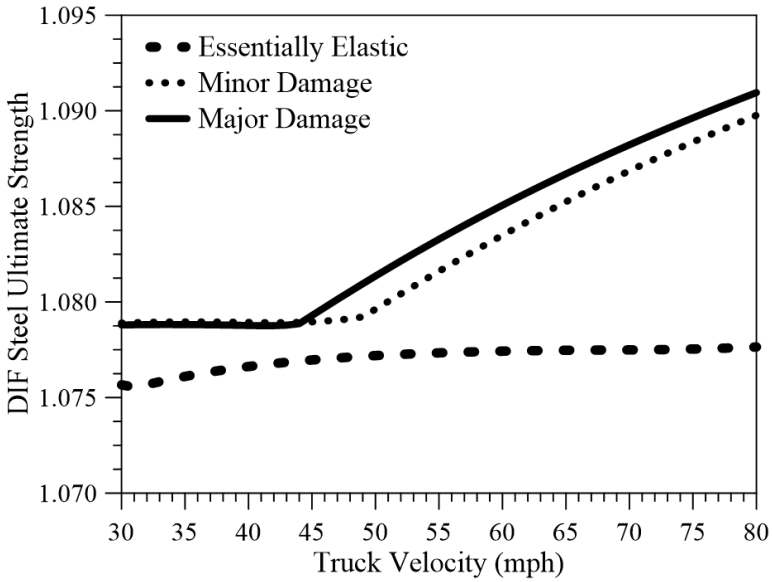

B. Results as a function of impact velocity for a truck weight of 48 tons.

Figure 4-45. Graphs. DIF reinforcing steel ultimate strength on a pier width of 36 inches.

4.4.4. Dynamic Increase Factors for Concrete Compressive Strength

The CEB-FIP90 (1993) model was used to evaluate concrete compression strength properties for different strain rates. The dynamic increase factor (*DIF*) for the concrete compression strength of confined and unconfined concrete were computed using the following equation (CEB-FIP90 1993):

$$DIF_{cc} = \left(\frac{\dot{\varepsilon}_c}{30 \times 10^{-6}}\right)^{1.026\left[1/\left(5+\frac{9f_c'}{1{,}450}\right)\right]} \quad \textbf{(4-31)}$$

Where $\dot{\varepsilon}_c$ is the strain rate for concrete in compression and was computed using Equation (4-26), and f_c' is the 28-day unconfined concrete compressive strength in psi. In Equation (4-31), $\dot{\varepsilon}_c$ is limited to less than 30 per second. Dynamic increase factors were then computed using Equation (4-31) and results are presented in Figure 4-46.

4.4.5. Dynamic Increase Factors for Concrete Tensile Strength

The CEB-FIP90 (1993) model was used to evaluate the concrete tensile strength properties for different strain rates using the following equation (CEB-FIP90 1993):

$$DIF_{ct} = \left(\frac{\dot{\varepsilon}_c}{30 \times 10^{-6}}\right)^{1.016\left[1/\left(10+\frac{6f_c'}{1{,}450}\right)\right]} \quad \textbf{(4-32)}$$

Where $\dot{\varepsilon}_c$ is the strain rate for concrete in compression and was obtained using Equation (4-26), and f_c' is in psi. In the form presented in Equation (4-32), $\dot{\varepsilon}_c$ is less than 30 per second. Dynamic increase factors for the tensile strength of concrete are presented in Figure 4-46.

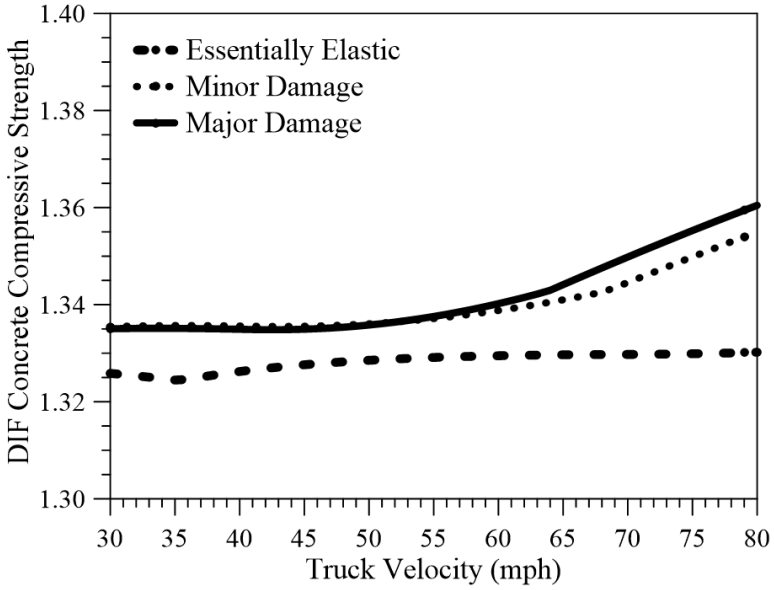

A. Results as a function of impact velocity for a truck weight of 20 tons.

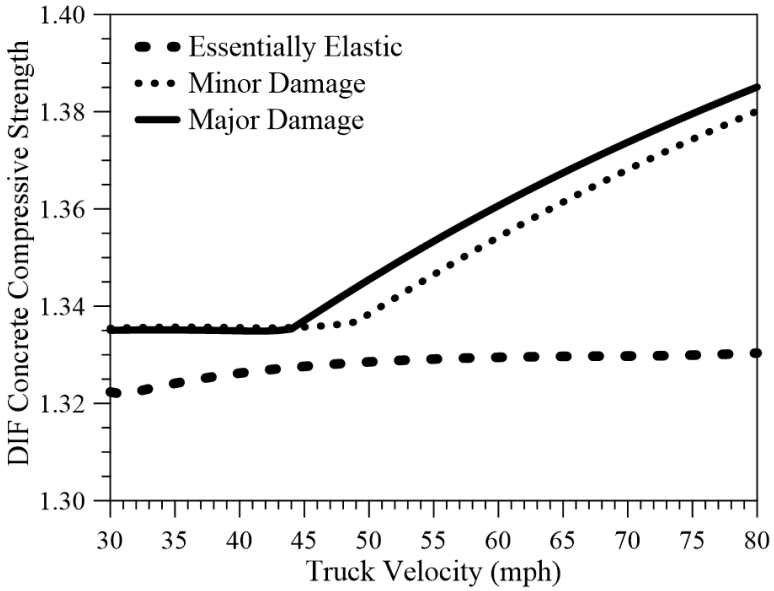

B. Results as a function of impact velocity for a truck weight of 48 tons.

Figure 4-46. Graphs. DIF concrete compressive strength on a pier width of 36 inches.

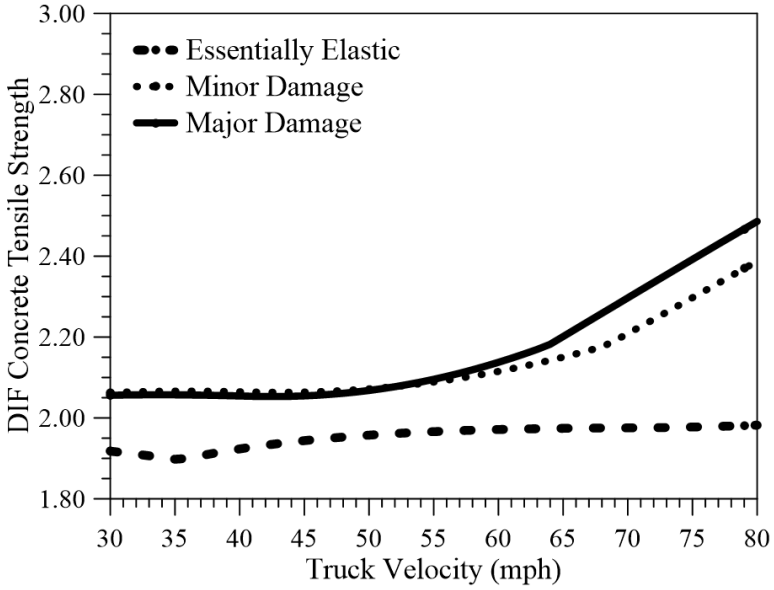

A. Results as a function of impact velocity for a truck weight of 20 tons.

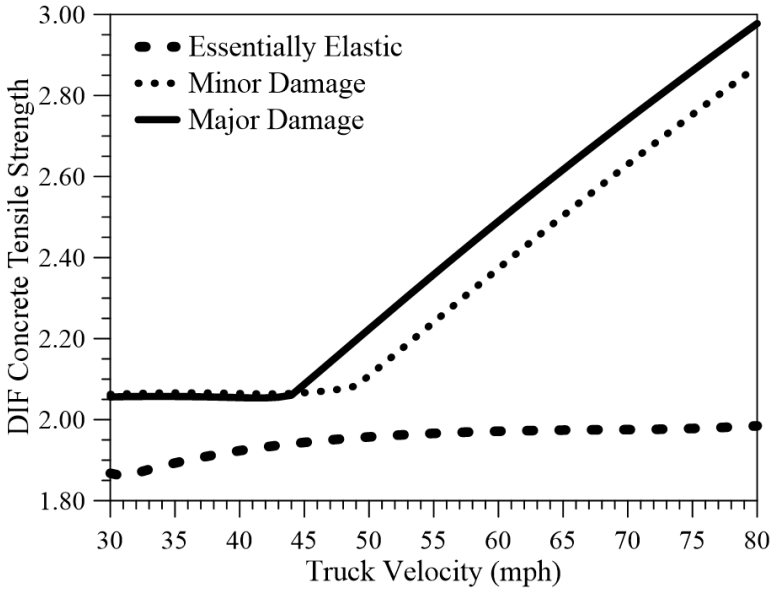

B. Results as a function of impact velocity for a truck weight of 48 tons.

Figure 4-47. Graphs. DIF concrete tensile strength on a pier width of 36 inches.

4.4.6. Concrete Compressive Stress–Strain Relations under Strain Rate Effects

Strain rate effects for the concrete compression strength for confined and unconfined concrete are presented in Figure 4-48. The effects of strain rate on the cyclic loading reversal of confined and unconfined concrete are presented in Figure 4-49 and Figure 4-50, respectively. These material properties are used in evaluating bridges pier column resistance as a function of the dynamic effects from heavy truck collisions.

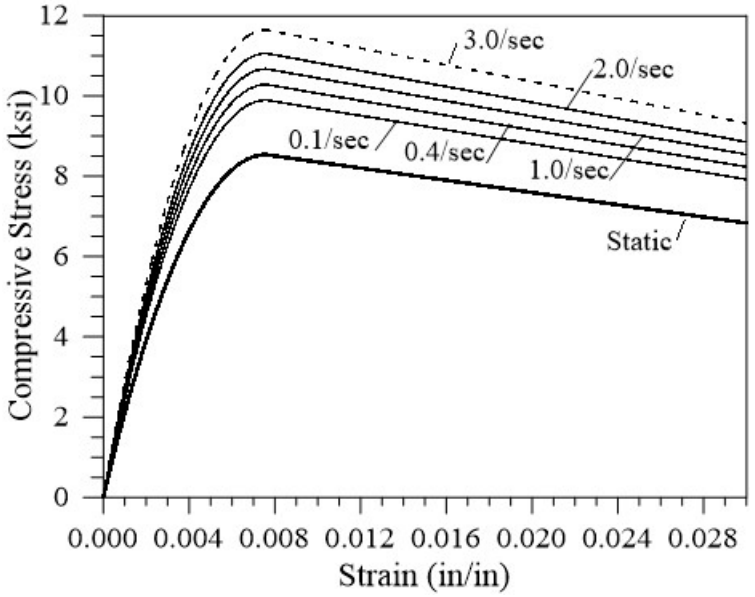

A. Confined Concrete.

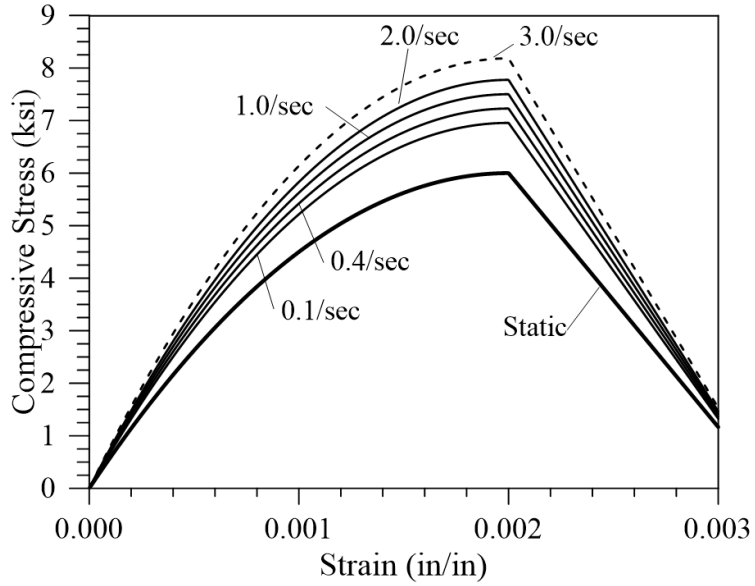

B. Unconfined Concrete.

Figure 4-48. Graph. Concrete strain rate effects under monotonic loadings.

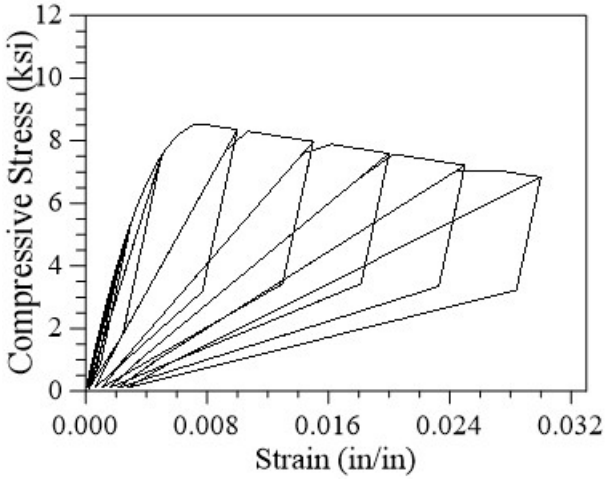

A. Static Load or strain rate of 0.0/sec.

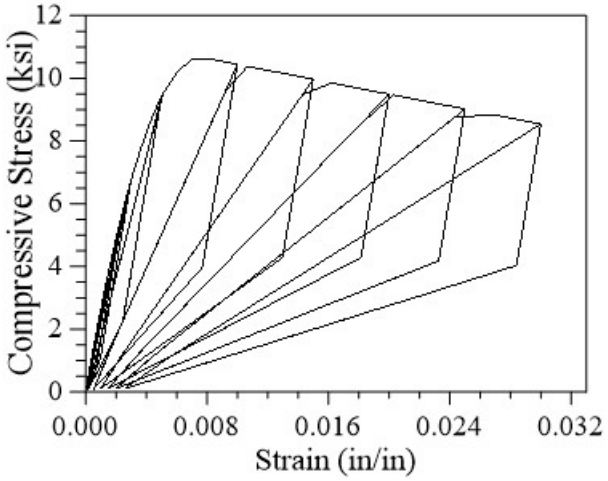

B. Strain Rate of 1.0/sec.

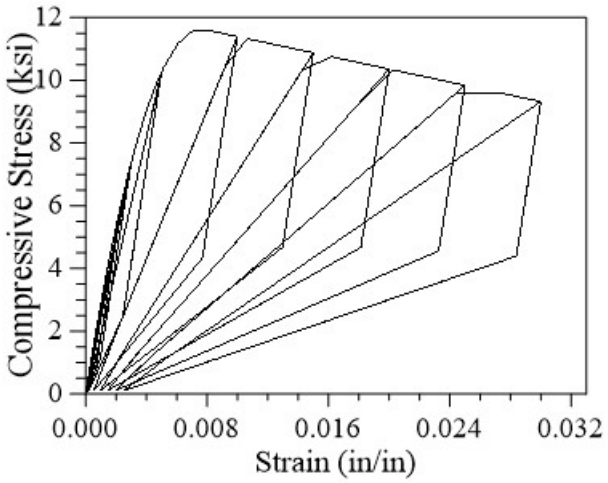

C. Strain Rate of 3.0/sec.

Figure 4-49. Graphs. Confined concrete strain rate effects under cyclic loadings.

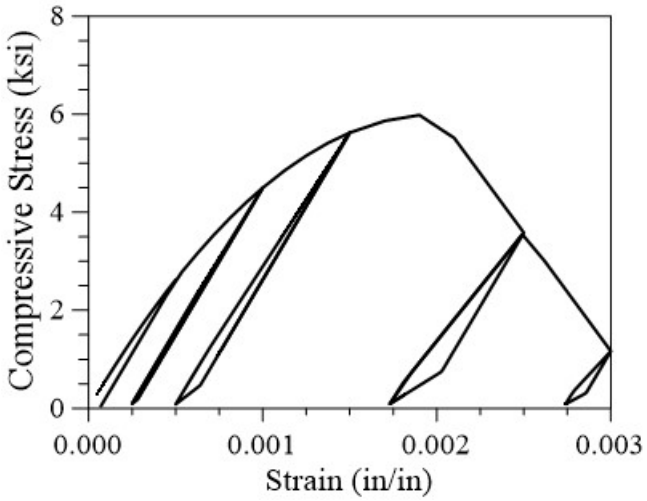

A. Static Load or strain rate of 0.0/sec.

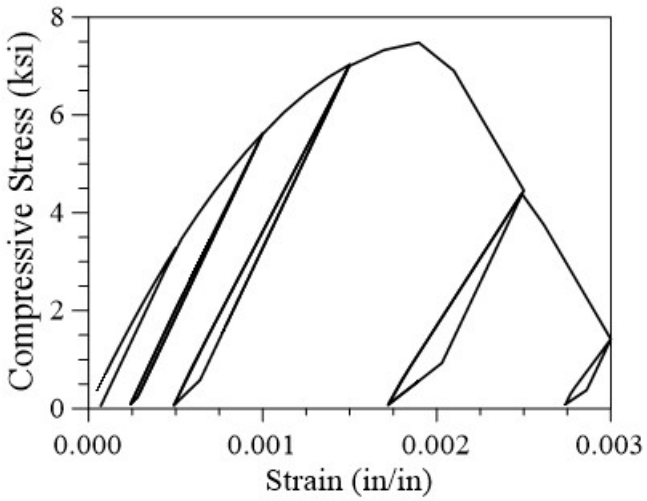

B. Strain Rate of 1.0/sec.

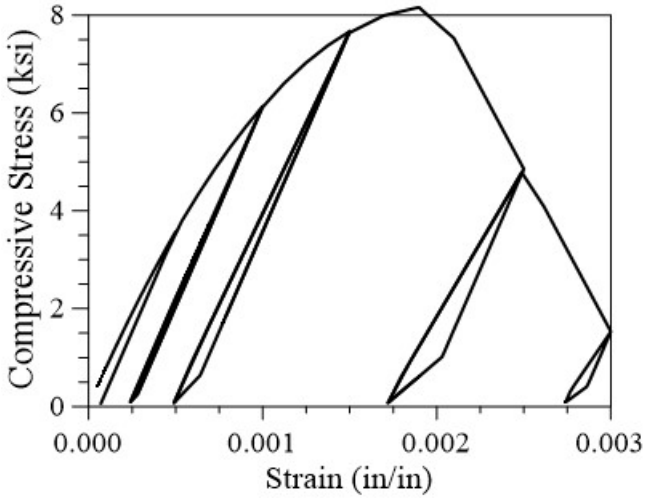

C. Strain Rate of 3.0/sec.

Figure 4-50. Graphs. Unconfined concrete strain rate effects under cyclic loadings.

4.4.7. Concrete Tensile Stress–Strain Relations under Strain Rate Effects

Strain rate effects for the tensile strength of concrete are presented in Figure 4-51. The effects of strain rate on the cyclic loading reversal of concrete in tension and under different strain rates are presented in Figure 4-52.

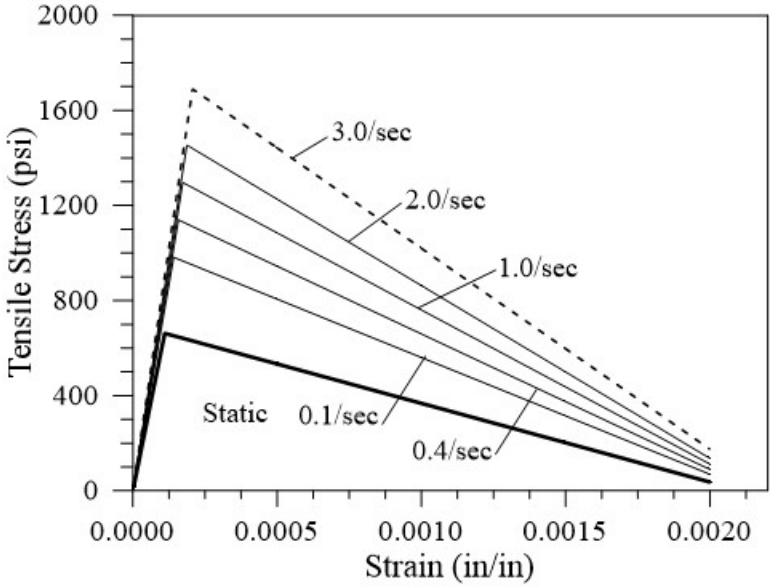

Figure 4-51. Graph. Concrete tensile strain rate effects under monotonic loadings.

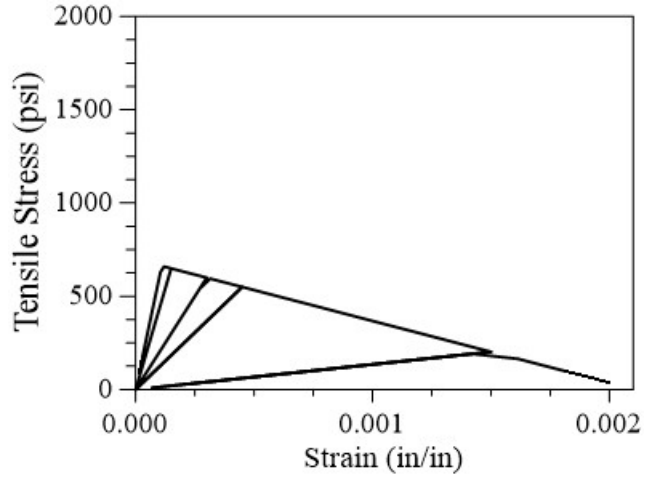

A. Static Load or strain rate of 0.0/sec.

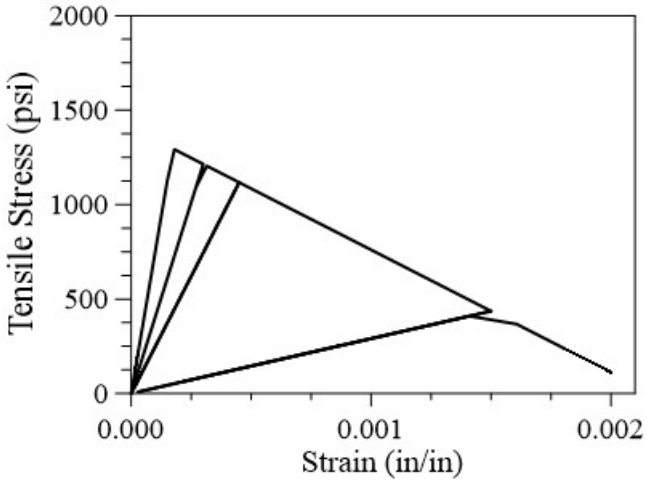

B. Strain Rate of 1.0/sec.

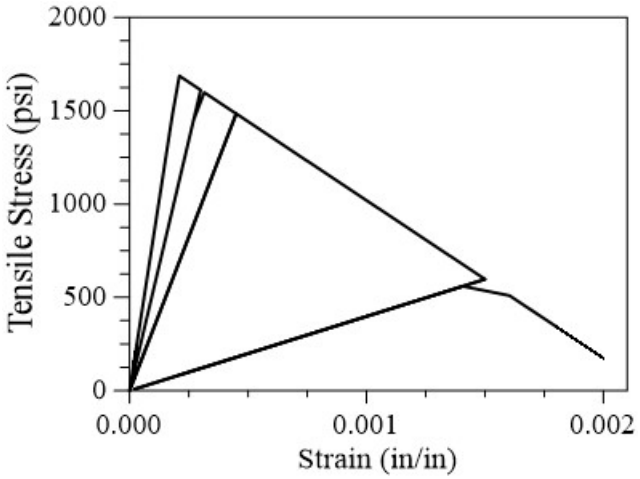

C. Strain Rate of 3.0/sec.

Figure 4-52. Graphs. Concrete tensile strain rate effects under cyclic loadings.

4.4.8. Reinforcing Steel Stress–Strain Relations under Strain Rate Effects

Strain rate effects on the tensile strength of reinforcing steel is presented in Figure 4-53. Reverse cyclic loading of reinforcing steel under different strain rates are presented in Figure 4-54.

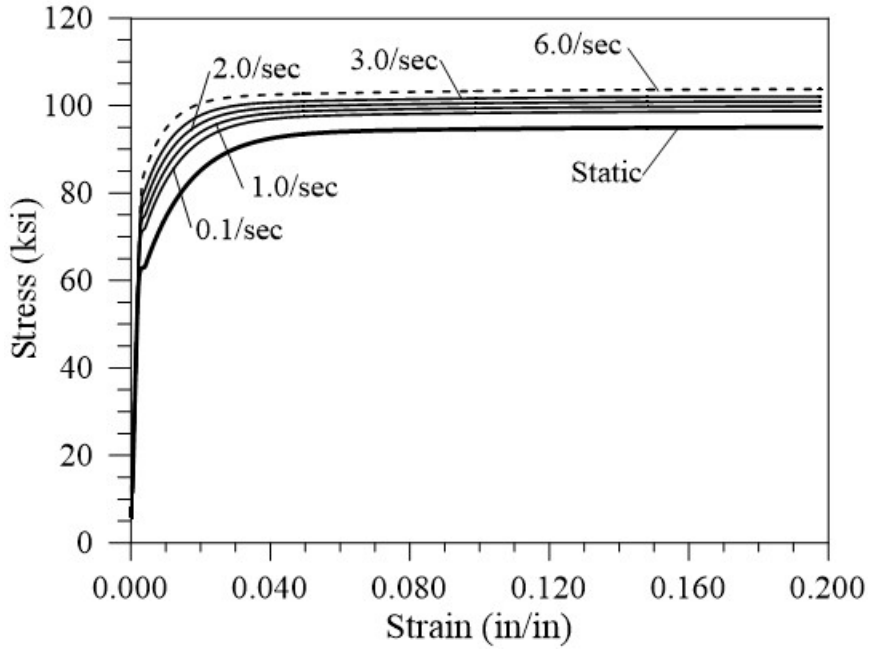

Figure 4-53. Graph. Reinforcing steel strain rate effects under monotonic loadings.

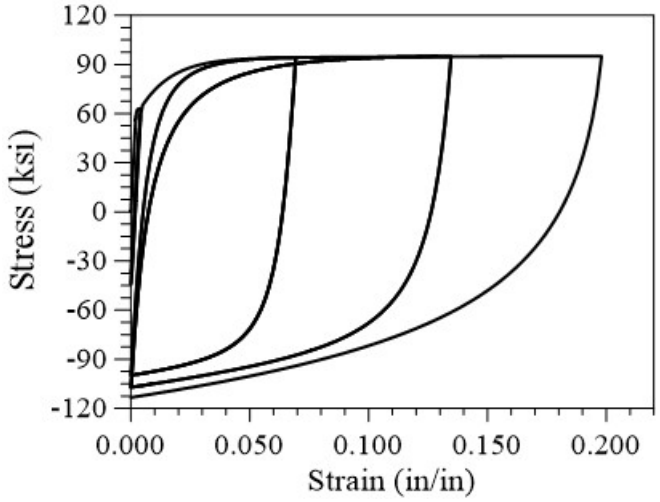

A. Static Load or strain rate of 0.0/sec.

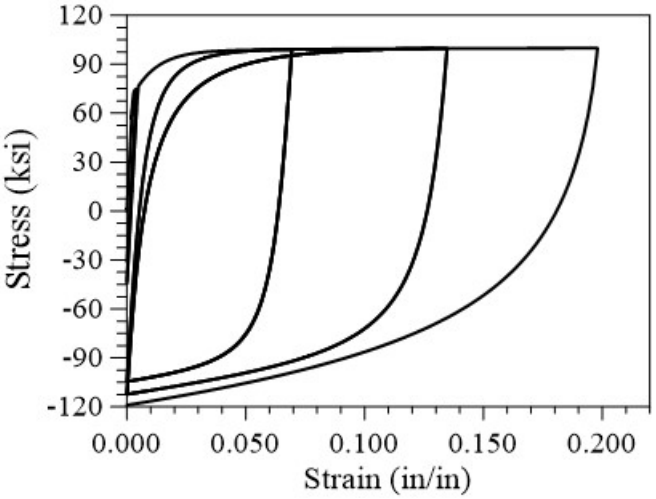

B. Strain Rate of 3.0/sec.

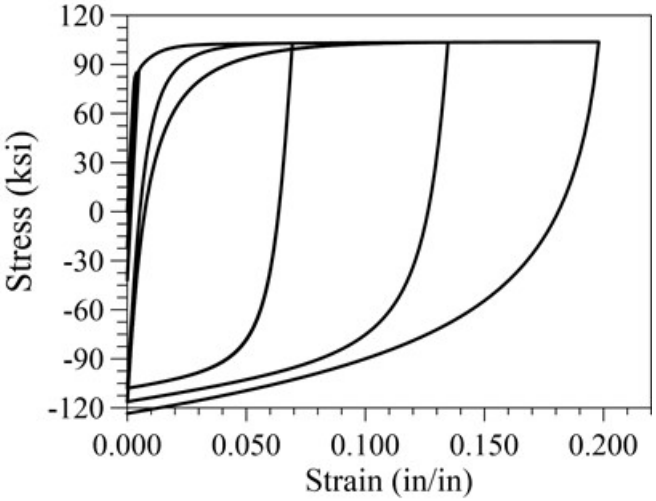

C. Strain Rate of 6.0/sec.

Figure 4-54. Graphs. Reinforcing steel strain rate effects under cyclic loadings.

4.5. STOCHASTIC SYSTEM PARAMETERS

This section presents stochastic models for these variables: material properties, element level dimensions for reinforcing bar, members, and bridge layout dimensions. These variables were established according to system parameters investigation carried by Mirza and MacGregor (1979). Figure 4-55 shows one of 17 bridges outlined in Table 4-1, which comprise the test bed study site. Common to all bridge configurations the impact loading is applied in a horizontal plane at 5.0 feet above the ground level. In computing the governing condition, this force should be considered within a range of 0 to 15 degrees.

A. Sample bridge isometric view.

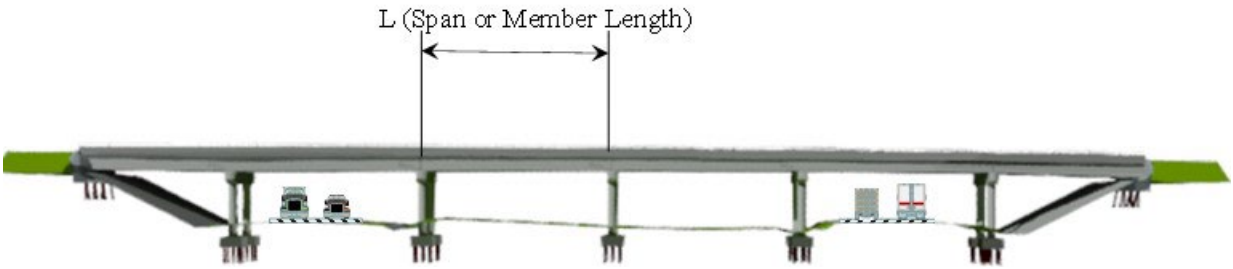

B. Sample bridge frontal elevation.

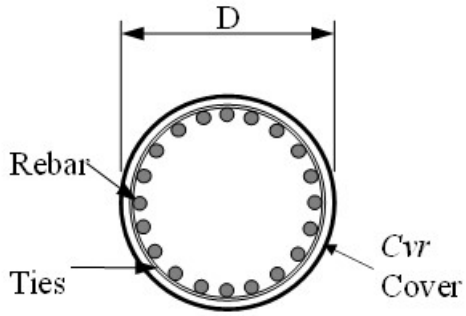

C. Sample bridge pier cross section.

Note: The sample bridge depicted in these drawings is Test Bed Study Site Bridge No. 7, see Section 4.1.7

Figure 4-55. Illustrations. Sample bridge structure.

4.5.1. Uncertainty in Geometric Dimensions

Mirza and MacGregor (1979) suggested using normal distribution models for all geometric uncertainties. A combination of the data from Nowak and Collins (2012) and Lu et al. (1994) was used to define bias factors and coefficient of variables for dimension variables. Probability distribution and dimension variables are defined in Table 4-10. The variations and uncertainties

in the dimensions are not expected to significantly impact the probability of failure of the system under heavy vehicle collisions.

Table 4-10. Bridge dimensions random variables values.

Variable	Distribution	$\hat{\lambda}$, Bias factor	Ω	Reference
ds	Normal	1.00	0.07	Lu et al. (1994)
b	Normal	1.01	0.02	Lu et al. (1994)
h	Normal	1.01	0.04	Lu et al. (1994)
D	Normal	1.01	0.04	Nowak and Collins (2012)
ht	Normal	0.99	0.04	Nowak and Collins (2012)
cvr	Normal	0.99	0.04	Nowak and Collins (2012)
s	Normal	0.99	0.041	Nowak and Collins (2012)
w	Normal	1.00	0.02	Nowak and Collins (2012)
L	Normal	0.99	0.042	Nowak and Collins (2012)
S	Normal	1.01	0.02	Nowak and Collins (2012)

Where $\hat{\lambda}$ is the bias factor, Ω is the coefficient of variation, *ds* is the bar diameter, *b* and *h* are member section width and depth for rectangular sections, *D* is the diameter of circular sections, *ht* is the bridge deck thickness, *w* is the bridge deck total width, *cvr* is the concrete cover, *s* is the stirrup spacing or spiral pitch, *L* is the member length or span length, and *S* is the spacing between members (such as bridge girders or bent columns). The mean value of any variable, μ_i, is calculated using the given nominal values, $\widetilde{N}_i$, and the following equation, which includes the bias factor:

$$\mu_i = \widetilde{N}_i \hat{\lambda} \qquad \textbf{(4-33)}$$

Using the mean value and the standard deviation any random variable is sampled several times to represent the underlying probabilistic characteristics of these variables.

4.5.2. Uncertainty in Concrete Material Properties

Concrete material properties are defined for normal concrete strength with random variables presented in Table 4-11. According to Nowak and Collins (2012), the bias factor and coefficient of variation associated with the compressive strength of normal-weight concrete are 1.24 and 0.15 respectively. Expecting only minor variations in the strain variables of concrete, the bias factor and the coefficient of variation are assigned the values of 1.05 and 0.02, respectively.

Table 4-11. Concrete random variables values.

Variable	Distribution	Bias factor	Ω	Reference
ε_{co}	Normal	1.05	0.02	N/A
ε_{cu}	Normal	1.05	0.02	N/A
$f_c^{'}$	Normal	1.24	0.15	Nowak and Collins (2012)

4.5.3. Uncertainty in Reinforcing Steel Material Properties

According to Nowak and Collins (2012), the bias factor and coefficient of variation for the reinforcement bar area are 1.0 and 0.015, respectively (see Table 4-12). Other steel properties described by Nowak and Collins (2012) state that the yield strength of a #6 rebar has a bias factor and coefficient of variation of 1.12 and 0.02, respectively. The yield strength of a #7 rebar has a bias factor and coefficient of variation of 1.14 and 0.03, respectively. The modulus of elasticity has a bias factor and coefficient of variation of 1.00 and 0.033, respectively (Lu and Gu 2004). The parameters for the strain of steel will resemble that of concrete with a bias factor of 1.05 and a coefficient of variation of 0.02.

Table 4-12. Reinforcing steel random variables values.

Variable	Distribution	Bias factor	Ω	Reference
A_b	Normal	1.00	0.015	Nowak and Collins (2012)
ε_{su}	Normal	1.05	0.02	Nowak and Collins (2012)
E_s	Normal	1.00	0.033	Lu and Gu (2004)
f_y (#6)	Normal	1.12	0.02	Nowak and Collins (2012)
f_y (#7)	Normal	1.14	0.03	Nowak and Collins (2012)

CHAPTER 5 - CONCLUSIONS, LIMITATIONS AND FUTURE RESEARCH

5.1. SUMMARY AND CONCLUSIONS

This report includes a literature review of current state of design practice of bridges piers and girders against heavy truck collisions. This review also includes experimental and analytical research on bridge failures resulting from these types of collisions. Also, this review includes risk analysis for evaluating the vulnerability of bridge piers and girders against heavy truck collisions. Heavy truck collisions have resulted in the disproportionate collapse or reduction in the resiliency and safety of bridges around the world.

In this work, thirteen published studies were reviewed to extract 470 data points to assess peak dynamic forces resulting from heavy truck collisions. The calculated peak dynamic forces were calculated through parametric impulse loading functions, which are expressed as functions of weight and speed of a truck, and width of a bridge pier measured perpendicular to the impact direction. These three variables were obtained from reported values in the thirteen reference studies. Considering the stochasticity of the ratios between the reported and the calculated peak dynamic forces, along with the collision impact kinetic energy per width of bridge pier, these ratios were further sorted into five bins over the per pier width kinetic energy. Accordingly, for each defined peak dynamic force and for each bin, best-fit distribution functions (e.g., lognormal and kernel) and their associated upper- and lower-95 percent confidence intervals were utilized to characterize the variations of the ratios between the reported (i.e., actual) and the calculated (i.e., theoretical) forces.

Bridge inventory data, collision data, and traffic detector data from Virginia were analyzed to create a test bed study site consisting of seventeen representative bridges. The main criteria in selecting these bridges were their on-site data availability to conduct pilot studies, exposure to heavy truck collisions, and vulnerability to failure due to an ensuing collision. Results from the seventeen test bed study sites were used to characterize and validate these stochastic variables:

- *Truck weight as a function of bridge location.* Axle-based gross vehicle weight rating was adopted to transform axle information into vehicular weight data. Axle-based gross vehicle is collected by associated traffic detectors with vehicle classification based on the number of axles. Vehicular weight data was subsequently used in reproducing the stochastic weight of trucks traversing under a bridge.

- *Truck speed of as a function of bridge location.* Data analysis as shown truck velocity follows an Extreme Value Type I distribution, also referred to as the Gumbel distribution. Site-specific location and scale parameters necessary in developing the Gumbel distribution were derived from speed distribution data collected at the corresponding traffic detectors in proximity to a bridge site.

- *Frequency of heavy truck collisions as a function of bridge location*. Data analysis as shown the stochastic frequency of heavy truck collisions on bridge piers follows closely a Poisson distribution. This is a realistic assumption since heavy truck collisions at a given

bridge location tend to occur independently of time and at a constant rate. The Poisson distribution variables of time and constant rate were formulated as the multiplication of truck volume crossing under the bridge, the width of the bridge pier, and a representative collision involvement rate for truck-related collisions.

- *Equivalent static force resulting from frontal collisions*. Equivalent static forces were obtained for a range of truck weight and speed, and pier width using well-established parametric impulse loading functions available in the literature. Parametric impulse loads can be characterized by three well defined pulses. These pulses are associated with bumper, engine, and trailer impacts.

- *Strain rate effects from impact loads on material properties.* Material properties, including the strengths of concrete and reinforcing steel are influenced by strain rate effects. Average strain rates of concrete and reinforcing steel were mapped based on truck velocity and weight, and pier width perpendicular to the impact. Strain rates were further mapped in terms of performance limit states such as *Essentially Elastic*, *Minor Damage* and *Major Damage*.

- *Bridge system variables.* Bridge system stochastic variables are related to uncertainties in geometric dimensions and material properties. Following well established methodologies, uncertainties in system variables are often developed considering their corresponding bias factors and coefficients of variation. Geometric dimensions refer to variables such as rebar diameter, width and depth of rectangular pier section, diameter of circular pier section, and other variables such as member lengths. Material properties variables refer to properties of concrete and reinforcing steel such as compressive, tensile and yield strength.

These stochastic variables are then used in evaluating some of the design parameters listed below:

- Extreme Event II and specifically to this research vehicular collisions.

- Structural resistance of bridge girders and pier elements necessary to prevent collapse of bridges.

- Probability of failure of a bridge in one year or over a prolonged time duration, which may correspond to the service life of bridges.

5.2. LIMITATIONS OF TRAFFIC ANALYSIS AND REAL-TIME CONTROL

5.2.1. A Hazard-Based Model to Estimate Collision Events

Literature review shows vehicle collisions on bridges have occurred at an average rate of 15,000 annually in the United States. This translates in an expected 0.15 annual vehicular collisions per bridge, based on a total of 93,000 bridges in the United States with one or more traffic lanes under the structure. For this reason, these events have been designated as low-frequency high impact events. This has resulted in limited data availability to derive the corresponding stochastic

characteristics at a given bridge site. Accordingly, using traditional probabilistic approaches to estimate collisions occurrence at specific sites leads in significant challenges such as: data collection, estimation errors, and robustness. Furthermore, alternative modeling methodologies are needed to address limited data availability at a specific bridge site. In this work, collisions on bridge piers and girders were considered as a subset of all traffic collisions based on a truck-related collision involvement rate. Data collected from traffic detector stations with vehicle classification in Virginia were used in estimating an overall truck-related collision involvement rate and to classify collisions based on a set of exogenous factors such types of vehicles involved and their proximity to these bridges. (i.e., traffic anomalies associated with existing flow and speed trends)

A formulation that allows differentiation between events and incorporates the effects on exogenous characteristics on a given structure is the duration modeling formulation. According to this formulation, inter-event durations are modelled from bridge failure modes, traffic dynamics involving speed and vehicular type, and collision distributions as a function of space and time. The stochasticity of bridge failure is then associated with a hazard level where each event depends on the time elapsed since the latest event occurrence. This data driven approach assumes that collision occurrences associated with each site are relatively independent, which was the primary assumption outlined in this research project. Among many other factors, overlapping traffic data and collisions data from one end and data sets related to external geometric and weather data, fatigue data, heavy vehicle data, the inter-collision times may be identified with different types of parametric and semi-parametric hazard functions. This process differs significantly from existing static approaches since the extracted probabilities are time-dependent (i.e., dynamic) and can be simulated through different Monte-Carlo implementations and Bayesian prior and posterior probability functions while relying on data repositories such as those available in Virginia.

One of the main challenges in investigating heavy truck collisions is the lack of data on the behavioral reasons that may lead to collisions involving heavy vehicles in proximity to bridges. To overcome such challenge, driver behavioral studies may be performed by replicating the collision site in a Truck Simulator environment. Behavioral parameters such as distraction, reaction times, and task overload may be recorded and then incorporated in the duration modeling for added comprehensiveness and robustness in the estimation exercise. Such multifaceted research combines the microscopic driver-behavioral modeling approach with big-data macroscopic traffic flow simulations.

5.2.2. Test Bed Study Site for Future Research

Future research could refine the collision frequency under bridges to evaluate the extent at which bridges are exposed to truck-related collisions. Refined evaluation of these types of bridge collisions can be achieved by further multiplying the collision frequency by a conditional factor that reveals the likelihood of under-bridge truck-related collisions colliding into bridge piers. Such conditional probability may be estimated by a Monte Carlo simulation setup that considers various endogenous and exogenous variables. The endogenous variables are the weight and speed of trucks involved in collisions. The exogenous variables are the type of bridge pier protection and the roadway geometric alignment under bridges. In the above simulation method,

additional collision variables, such as the angles of trucks colliding into bridge piers and the applied deceleration before collisions, may also be captured to consolidate the estimation of bridge failure possibility.

Future research could consider finite element analysis of a sample population of seventeen bridges in the state of Virginia using the test bed study site developed in this report. The main objective of this future work could consider failure rate and investigate the expected annual frequency of bridge collapse. Future work could also include physical testing of bridge pier columns to investigate the response of bridge columns under a pulse generated force. Physical tests will provide data for element (local) behavior assessment and global behavior using finite element simulations. The former will provide fundamental information on disproportionate collapse behavior and failure mechanisms.

REFERENCES

Abdelkarim, O.I., and ElGawady, M.A. (2017), "Performance of Bridge Piers under Vehicle Collision," *Engineering Structures*, Vol. 140, No. 1, pp. 337-351.

Agrawal, A.K., El-Tawil, S., Cao, R., Xu, X., Chen, X. and Wong, W. (2018), "A Performance-Based Approach for Loading Definition of Heavy Vehicle Impact Events," Federal Highway Administration Report FHWA-HIF-18-062, 129 pp.

American Association of State Highway and Transportation Officials (AASHTO) (2008), "Chapter 3: States Respond Quickly to Bridge Disasters," *Bridging the Gap: Restoring and Rebuilding the Nation's Bridges*, Washington, DC, p.18.

American Association of State Highway and Transportation Officials (AASHTO Green Book), (2018), *A Policy on Geometric Design of Highways and Streets seventh edition*, January 2018, Washington, DC: AASHTO, 1098 pp.

American Association of State Highway and Transportation Officials (AASHTO), (2017), *AASHTO LRFD Bridge Design Specifications: 8th Edition*, Washington, DC: AASHTO (September 2017), 1781 pp. (23 CFR 625.4(d)(1)(v)).

American Association of State Highway and Transportation Officials (AASHTO), (2020), *AASHTO LRFD Bridge Design Specifications: 9th Edition*, Washington, DC: AASHTO (January 2020), 1914 pp.

American Association of State Highway and Transportation Officials (AASHTO) Manual for Assessing Safety Hardware (MASH), (2016), American Association of State Highway and Transportation Officials (AASHTO), Washington, D.C., 2016. 277 pp.

AuYeung, S. and Alipour, A. (2016), "Evaluation of AASHTO Suggested Design Values for Reinforced Concrete Bridge Piers Under Vehicle Collisions," *Journal of the Transportation Research Board*, No. 2592, Transportation Research Board, pp. 1–8. DOI: 10.3141/2592-01.

Berton, E., Bouaanani, N., Lamarche, C.P., and Roy, N. (2020), "Statistics and prediction of vehicle–bridge collisions in Quebec," *Canadian Journal of Civil Engineering*. https://doi.org/10.1139/cjce-2018-0785.

Bureau of Transportation Statistics (BTS) (2023), "National Transportation Statistics," U.S. Department of Transportation, Link at: https://www.bts.gov/topics/national-transportation-statistics.

Buth, C. E., W. F. Williams, M. S. Brackin, D. Lord, S. R. Geedipally, and A. Y. Abu-Odeh, (2010), "Analysis of Large Truck Collisions with Bridge Piers: Phase 1. Report of Guidelines for Designing Bridge Piers and Abutments for Vehicle Collisions," Research Report. Texas Transportation Institute, College Station, TX, http:// ntl.bts.gov/lib/33000/33100/33107/9-4973-1.pdf, 2010, 186 pp.

Buth, C. E., W. F. Williams, M. S. Brackin, D. Lord, S. R. Geedipally, and A. Y. Abu-Odeh, (2011), "Collision Loads on Bridge Piers: Phase 2. Report of Guidelines for Designing Bridge Piers and Abutments for Vehicle Collisions," Research Report. Texas Transportation Institute, College Station, TX, http://texashistory.unt.edu/ ark:/67531/metapth303536/m1/3, 2011.

Button, N.P. and Reilly, P.M. (2000), "Uncertainty in Incident Rates for Trucks Carrying Dangerous Goods," Journal of Accident Analysis and Prevention, Vol. 32, No. 6, Nov. 2000, pp. 797–804.

Caltrans Bridge Design Manual (BDM) (2014), "Section 3: Loads and Load Factors California Amendments to AASHTO LRFD Design Specifications – Sixth Edition," Department of Transportation. State of California, Sacramento, 34 pp.

Cao, R., Agrawal, A.K., El-Tawil, S., and Wong, W. (2020), "Performance-Based Framework for Evaluating Truck Collision Risk for Bridge Piers," *Journal of Bridge Engineering*, American Society of Civil Engineers, Vol. 25, No. 10, pp. 04020082-1:14.

CEB-FIP90 (1993), "*CEB-FIP Model Code 1990: Design Code*," Comite Euro-International du Beton, CEB-FIP Model Code," Thomas Telford, London, UK, 437 pp.

Chen, L., El-Tawil, S., and Xiao, Y. (2016), "Reduced Models for Simulating Collisions between Trucks and Bridge Piers," *Journal of Bridge Engineering*, Vol. 21, No. 6, 14 pp., 04016020 (1-14).

Chen, L., Wu, H., and Liu, T (2020), "Shear Performance Evaluation of Reinforced Concrete Piers Subjected to Vehicle Collision," *Journal of Structural Engineering*, Vol. 146, No. 4, pp 04020026-1-14.

Chen, L., Wu, H., and Liu, T. (2021), "Vehicle Collision with Bridge Piers: A State-of-the-art Review," *Advances in Structural Engineering*, Vol. 24, No. 2, pp. 385-400.

Cook, W., Barr, P.J., Halling, M.W. (2015), "Bridge failure rate," J*ournal of Performance of Constructed Facilities*, 29(3) 04014080.

Das, A., Abdel-Aty, M. and Pande, A. (2009), "Using conditional inference forests to identify the factors affecting crash severity on arterial corridors," *Journal of Safety Research*, 40 (2009), pp. 317-327, 10.1016/j.jsr.2009.05.003.

Davis, S.C. and Boundy, R.G., (2021), "Transportation Energy Data Book: Edition 39," Report No. ORNL/TM-2020/1770, Oak Ridge National Lab. (ORNL), Oak Ridge, TN, 459 pp.

Deng, L., and Cai. C. S. (2010) "Development of dynamic impact factor for performance evaluation of existing multi-girder concrete bridges." *Engineering Structures,* 32 (1): 21–31.

Deng, Lu, Wang, W., and Yu, Y. (2016), "State-of-the-Art Review on the Causes and Mechanisms of Bridge Collapse," Journal of Performance of Constructed Facilities, 10.1061/(ASCE) 04015005-1 (2016) 30(2), pp. 1–13.

Do, T.V., Pham, T.M., and Hao, H., (2019), "Proposed Design Procedure for Reinforced Concrete Bridge Columns Subjected to Vehicle Collisions," *Structures*, Vol. 22, No. 1, pp. 213-229.

Dunne, R., and Thorkildsen, E. (2020), "*Case Study: Response to Bridge Impacts – An Overview of State Practices*," Federal Highway Administration, FHWA-HIF-20-087, 24pp.El-Tawil, S., Severino, E., Fonseca, P. (2005), "Vehicle Collision with Bridge Piers," *ASCE Journal of Bridge Engineering*, Vol. 10, No. 3, pp.345–353.

Dusenberry, D.O. (2022), "New SEI/ASCE Disproportionate Collapse Mitigation Standard," *ASCE Journal of Structural Engineering*, Vol. 148, No. 4, 04022014, 6 pp.

EN 1991-1-7 (2006), *Eurocode 1 - Actions on structures - Part 1-7: General actions - Accidental actions,* This European Standard was approved by CEN on 9 January 2006, 69 pp.

The Bridge Portal Federal Highway Administration (FHWA- LTBP) (2021), The LTBP Bridge portal is the new bridge analysis site, with improved performance and experience. Link at: https://infobridge.fhwa.dot.gov/Data

Federal Highway Administration (FHWA) (2022), "KABCO Injury Classification Scale and Definitions," Link at: https://safety.fhwa.dot.gov/hsip/spm/conversion_tbl/pdfs/kabco_ctable_by_state.pdf

Federal Highway Administration (FHWA) (2016), "Joint Implementation Agreement for Manual for Assessing Safety Hardware (MASH)," Office of Program Administration and Office of Safety Technologies

Federal Highway Administration (FHWA) (2015), "Federal-aid Reimbursement Eligibility Process For Safety Hardware Devices", Office of Safety Technologies Memorandum, Link at: https://highways.dot.gov/sites/fhwa.dot.gov/files/2022-06/memo111215.pdf

Federal Highway Administration (FHWA) (2006), *Highway statistics 2004*, Washington, DC: US Department of Transportation. Link at: https://www.fhwa.dot.gov/policy/ohim/hs04/

Federal Highway Administration (FHWA) (2000), ''National Bridge Inventory Record Count 1998–2000,'' Link at: http://www.fhwa.dot.gov/bridge/Feldman, L.R., Jirsa, J.O. and Kowal, E.S. (1998), "Repair of Bridge Impact Damage," *Concrete International*, Vol. 20, No. 2, pp 61-66.

Fu, C.C. (2001), "Maryland Study, Vehicle Collisions with Highway Bridges," Contract No. SP907B1, Maryland State Highway Administration, The Bridge Engineering Software and Technology Center, Department of Civil Engineering, University of Maryland.

Garlock, M. E., Paya-Zaforteza, I., Gu, L., and Kodur, V. (2012). "Fire Hazard in Bridges: Review, Assessment and Repair Strategies." *Engineering Structures*, Vol. 35, pp. 89–98.

Gomez, N.L. (2014), "Performance of Circular Reinforced Concrete Bridge Piers Subjected to Vehicular Collisions," Masters Thesis, University of Massachusetts, https://doi.org/10.7275/5563363 https://scholarworks.umass.edu/masters_theses_2/20, 158 pp.

Hanchey, C.M. and Exley, S.F. (1990), "Overheight Vehicle Warning Systems in Mississippi," *ITE Journal, Vol.* 60, No. 6, pp 24-29.

Harik, I.E., Shaaban, A.M., Gesund, H., Valli, Y.S. and Wang. S.T. (1990), "United States Bridge Failures 1951-1988," J*ournal of Performance of Constructed Facilities*, Vol. 4, No. 4, pp 272-277.

Harries, K. A., Kasan, J., Miller, R., and Brinkman, R. (2012), *Updated Research for Collision Damage and Repair of Prestressed Concrete Beams*, NCHRP Project 20-07, Task 307, National Cooperative Highway Research Program, Transportation Research Board, Washington, D.C., 228 pp.

Heng, K., Jia, P., Xu, J., Li, R., and Wu, H. (2022), "Vehicular Impact Resistance of Highway Bridge with Seismically-Designed UHPC Pier," Engineering Structures, Vol. 252, No. 1, 17 pp., https://doi.org/10.1016/j.engstruct.2021.113635.

Heng, K., Li, R., Li, Z., Wu, H. (2021), "Dynamic Responses of Highway Bridge Subjected to Heavy Truck Impact," Engineering Structures, Vol. 232, No. 1, 22 pp., https://doi.org/10.1016/j.engstruct.2020.111828

Highway Safety Information System (HSIS) (2021), Turner-Fairbank Highway Research Center, Link at: https://www.hsisinfo.org/

Hose, Y. D., Silva, P. F., and Seible, F. (2000), "Performance Evaluation of Concrete Bridge Components and Systems under Simulated Seismic Loads," *EERI Earthquake Spectra*, May 2000, Vol. 16, No. 2, pp. 413–442.

Hong, F. Prozzi, J.P. and Prozzi, J.A. (2007), "Characterizing Truck Traffic in the U.S.-Mexico Highway Trade Corridor and the Load Associated Pavement Damage," Center for Transportation Research University of Texas at Austin, Report No. 167555-1, April 2007, 58 pp.

Hosseinzadeh, A., Moeinaddini, A., Ghasemzadeh, A. (2021), "Investigating factors affecting severity of large truck-involved crashes: Comparison of the SVM and random parameter logit model," Journal of Safety Research, Volume 77, Pages 151-160

Lee, G.C., Mohan, S.B., Chao, H., Fard, B.N. (2013)' "A Study of U.S. Bridge Failures (1980-2012)", *Technical Report MCEER-13-0008*, State University of New York, Buffalo, NY, 148 pp.

Li, R.W., Cao, D.S., Wu, H., and Wang, D.F. (2021), "Collapse Analysis and Damage Evaluation of Typical Simply Supported Double-Pier RC Bridge under Truck Collision," *Structures*, Vol. 33, pp. 3222-3238.

Li, R.W., Zhou, D.Y., and Wu, H. (2020), "Experimental and Numerical Study on Impact Resistance of RC Bridge Piers under Lateral Impact Loading," Engineering Failure Analysis, Vol. 109, No. 1, 19 PP., https://doi.org/10.1016/j.engfailanal.2019.104319

Lu, B., and Silva, P. F. (2006), "Estimating Equivalent Viscous Damping Ratio for RC Members under seismic and Blast Loadings," Elsevier *International Journal of Mechanics Research Communications*, Dec. 2006, 33(6).

Lu, R., Luo, Y., and Conte, J.P. (1994), "Reliability Evaluation of Reinforced Concrete Beams," Structural Safety, Vol. 14, No. 4, pp. 277-298.

Ma, X., Xing, Y., and Lu, J. (2018), "Causation Analysis of Hazardous Material road Transportation Accidents by Bayesian Network Using Genie," *Journal of Advanced Transportation*, 2018 (2018), pp. 1-12, 10.1155/2018/6248105

Ma, Z., Mei, G., Cuomo, S. (2021). An analytic framework using deep learning for prediction of traffic accident injury severity based on contributing factors. Accident Analysis and Prevention, 160 (2021).

McKinley, J., and Marshall, C. (2007), *Tanker Truck Fire Collapses Bay Area Overpass*, New York Times, Link at: https://www.nytimes.com/2007/04/30/us/30collapse.html

Maghiar, M., Jackson, M., and Maldonado, G. (2017), "*Warning Systems Evaluation for Overhead Clearance Detection*," Report No. FHWAGA-16-1521, Georgia Department of Transportation, 115 pp.

Mallet, W., Schmitt, B. R., and Sedor, J. (2005), "Freight Facts and Figures 2005," Report No. FHWA-HOP-05-071, U.S. Department of Transportation, FHWA, Office of Freight Management and Operations, 57 pp.

Malvar, J. and Ross C.A. (1998), "Review of Strain Rate Effects for Concrete in Tension," *ACI Materials Journal*, pp. 735-739.

Malvar, J (1998), "Review of Static and Dynamic Properties of Steel Reinforcing Bars," *ACI Materials Journal*, Vol. 5, No. 5, pp. 609-614.

McCartt, A.T., Hellinga L.A., and Solomon, M.G. (2008), "Work schedules of long-distance truck drivers before and after 2004 hours-of-service rule change," *Traffic Injury Prevention*, 9:201-10. DOI: 0.1080/15389580802040287

Michigan Roads and Construction, MRC (1988), "5 Span Damage Rate Rising," Michigan Roads and Construction, Vol. 85, No.50, 3pp.

Milton, J.C., Shankar, V.N., and Mannering, F.L. (2008). Highway accident severities and the mixed logit model: an exploratory empirical analysis. *Accident Analysis and Prevention*, 40 (2008), pp. 260-268

Mirza, S.A., and MacGregor, J.G., (1979), "Variations in Dimensions of Reinforced Concrete Members," *ASCE Journal of the Structural Division,* Vol. 105, No. 4, pp. 751-766.

National Bridge Inventory (NBI) (2021) Bridge Inspection - Safety - Bridges & Structures - Federal Highway Administration (dot.gov). Link at: National Bridge Inventory - Management and Preservation - Bridges & Structures - Federal Highway Administration (dot.gov)National Bridge Inventory (NBI) - Data Dictionary (2023), "NBI Elements," Federal Highway Administration. Link at: https://nationalbridges.com/nbiDesc.html

National Highway Traffic Safety Administration, U.S. Department of Transportation (NHTSA) (2021), Link at: Traffic Safety Facts 2019: A Compilation of Motor Vehicle Crash Data (dot.gov)

National Highway Traffic Safety Administration (2021), "*Traffic Safety Facts Annual Report Tables*," Available at: https://cdan.dot.gov/tsftables/tsfar.htm#

National Highway Traffic Safety Administration (NHTSA) (2021), 2019 Traffic Safety Facts Annual Report, Link at: https://crashstats.nhtsa.dot.gov/Api/Public/ViewPublication/813141.

National Highway Traffic Safety Administration (NHTSA) (2022), 2020 Traffic Safety Facts Annual Report, Link at: https://crashstats.nhtsa.dot.gov/Api/Public/ViewPublication/813375National Highway Traffic Safety Administration (NHTSA) (2015), "Traffic Safety Facts 2013," Available at: http://www-nrd.nhtsa.dot.gov/Pubs/812139.pdf.

National Highway Traffic Safety Administration (NHTSA) (2015), "The Economic and Societal Impact of Motor Vehicle Crashes, 2010 (Revised)" Washington, DC: U.S. Department of Transportation, Available at: https://crashstats.nhtsa.dot.gov/Api/Public/ViewPublication/812013

National Highway Traffic Safety Administration (NHTSA) (2021a), "2020 Fatality Data Show Increased Traffic Fatalities During Pandemic," Available at: https://www.nhtsa.gov/press-releases/2020-fatality-data-show-increased-traffic-fatalities-during-pandemic

National Highway Traffic Safety Administration (2021b). Early Estimate of Motor Vehicle Traffic Fatalities for the First Quarter of 2021. Washington, DC: US Department of Transportation. Available at: https://www.nhtsa.gov/sites/nhtsa.gov/files/2021-09/Early-Estimate-Motor-Vehicle-Traffic-Fatalities-Q1-2021.pdf

National Research Council (NRC) (1995), *Protecting Buildings from Bomb Damage,* National Academy Press, Washington, D.C., 1995.

Nebraska Department of Roads (NDOR) (2003), "I-80 Overpass Collapse & Repair Near Big Springs, NE May 23-25, 2003, Available at: http://www.nebraskatransportation.org/big-springs/

New Hampshire Bridge Design Manual (BDM) (2016), "*Bridge Design Manual Chapter 4 Load and Load Factors*," New Hampshire Department of Transportation, Revised March 2016, 36pp.

New York City OpenData (NYC WIM) (2024), "NYC OpenData Weight in Motion (WIM)," Date of last update February 2024, Available at: https://data.cityofnewyork.us/Transportation/Weigh-in-Motion/4fwc-j3vn/about_data.

Nowak, A.S., and Collins, K.R., (2012) *Reliability of Structures*, CRC press, Taylor and Francis Group, Second Edition, 391 pp.

Peris-Sayol, G, Payá-Zaforteza, I., and Moya, J.A., (2016), "Detailed Analysis of the Causes of Bridge Fires and Their Associated Damage Levels," Journal of Performance of Constructed Facilities, American Society of Civil Engineers, Nov. 2016, Vol. 31, No. 3, 10.1061/(ASCE)CF.1943-5509.0000977, pp. 04016108:1-9.

Plaxico, C.A (2016), "MASH TL5 Evaluation of the Proposed Three Rail Barrier," New NY Bridge (Tappan Zee Bridge Replacement) New York State Thruway Authority, Final Report, 2016, 110 pp.

Ross, H.E., Sicking, D.L., Zimmer, R.A., and Michie, J.D., (1993) *Recommended Procedures for the Safety Performance Evaluation of Highway Features*, NCHRP Research Report 350, NCHRP Project 22-7 FY'89, National Cooperative Highway Research Program, Transportation Research Board, Washington, D.C. Transportation Research Board of the National Academies, Washington, D.C., 1993, 74 pp.

Shanafelt, G.O., and Horn, W.B. (1984)' "Guidelines for Evaluation and Repair of Damaged Steel Bridge Members," Washington, D.C.: Transportation Research Board, National Cooperative Highway Research Program Report 271, 73 pp.

Silva, P. F., Mesia, W. D., Marzougui, D., and Badie, S. S. (2009), "Performance Evaluation of the Impact Resistance Capacity of RC Members," *ACI Structural Journal*, Sep. 2009, Vol. 106, No. 5, pp. 726–736.

Sparks, J., Shuh, J. and Smith, A.T. (2009), "Field Operations Guide for Safety/Service Patrols," Report No. FHWA-HOP-10-014, Office of Operations, Federal Highway Administration, Washington, DC. 48 pp.

Texas Bridge Design Manual (BDM) (2020), "Bridge Design Manual – LRFD," Texas Department of Transportation, Revised 2020, 90pp.

United States Department of Transportation Bureau of Transportation Statistics (BTS) (2019a), *Freight Facts and Figures: Freight Transportation & the Economy*. Available at: https://data.bts.gov/stories/s/Freight-Transportation-the-Economy/6ix2-c8dn

U.S. Department of Transportation, Bureau of Transportation Statistics (BTS), (2019b), *Freight Facts and Figures: Moving Goods in the United States*. Available at: https://data.bts.gov/stories/s/Moving-Goods-in-the-United-States/bcyt-rqmu

Virginia DMV (2022), "Highway Safety Traffic Records Information System," Link at: https://www.dmv.virginia.gov/general/#records/accident.asp

Virginia Department of Transportations (VDOT) (2022), "Official AADT and VMT Publications," Link at: https://www.virginiadot.org/info/ct-TrafficCounts.asp

Wang, W., Deng, L., and Shao, X. (2016), "Fatigue Design of Steel Bridges Considering the Effect of Dynamic Vehicle Loading and Overloaded Trucks." ASCE Journal of Bridge Engineering, Vol. 21, No. 9, 04016048.

Wardhana, K., and Hadipriono, F. (2003) "Analysis of Recent Bridge Failures in the United States." *Journal of Performance of Constructed Facilities*, 10.1061/(ASCE) 0887-3828(2003)17:3(144), 144–150.

Washington State Department of Transportation (WSDOT) (2020), *Bridge Design Manual*, Engineering and Regional Operations Bridge and Structures Office, September 2020, 1310 pp.

Wehbe, N. I., Qin, X., Tigges, B., Shen, Z., & Boudaqa, A. (2017), *Evaluation and Mitigation of Vehicle Impact Hazard for Overpasses*, Project No. SD2012-02-F South Dakota State University, 152 pp.

Wipf, T. J., Klaiber, F. W., Rhodes, J. D., Kempers, B. J. (2004), "Effective Structural Concrete Repair Volume 1 of 3 Repair of Impact Damaged Prestressed Concrete Beams with CFRP," March 2004, *Sponsored by the Iowa Department of Transportation Highway Division and the Iowa Highway Research Board Iowa*, DOT Project TR – 428, 195 pp.

Wright, W., Lattimer, B., Woodworth, M., Nahid, M., and Sotelino, E. (2013). "Highway Bridge Fire Assessment, Guide Specification for Fire Damage Evaluation in Steel Bridges," Project NCHRP 12-85 Program Transportation Research Board of the National Academies, Virginia Polytechnic Institute and State Univ., Blacksburg, VA. 75 pp.

World Health Organization (WHO) (2021), "Road Traffic Injuries," Link at: https://www.who.int/news-room/fact-sheets/detail/road-traffic-injuries

Wu, M., Jin, L., and Du, X. (2020), "Dynamic Responses and Reliability Analysis of Bridge Double-Column under Vehicle Collision," *Engineering Structures*, Vol. 221, 13 pp., https://doi.org/10.1016/j.engstruct.2020.111035

Yu, R. and Abdel-Aty, M. (2014), "Analyzing Crash Injury Severity for a Mountainous Freeway Incorporating Real-Time Traffic and Weather Data," Safety Science, 63 (2014), pp. 50-56, 10.1016/j.ssci.2013.10.012

Zhao, W., Ye, J., and Qian, J. (2021), "Dynamic Behavior and Damage Mechanisms of Reinforced Concrete Piers Subjected to Truck Impact," *Engineering Failure Analysis*, Vol. 121, 105158, 21pp.

Zhou, D., Li, R.,Wang, J., Guo, C., (2017) “Study on Impact Behavior and Impact Force of Bridge Pier Subjected to Vehicle Collision,” *Journal of Shock and Vibration*, Article ID 7085392, https://doi.org/10.1155/2017/7085392, 12 pp.

Zhou, X., Zhou, M., Luo, D., Wu, B., and Liu, L. (2021),” Study on the Nonlinear Response and Shear Behavior of RC Columns under Lateral Impact,” Structures, Vol. 34, No. 1, pp. 3834-3850.